UC Berkeley
UC Berkeley Electronic Theses and Dissertations

Title
Controllers for an Autonomous Vehicle Treating Uncertainties as Deterministic Values

Permalink
https://escholarship.org/uc/item/95f6m1cn

Author
Lee, Chan Kyu

Publication Date
2016

Peer reviewed|Thesis/dissertation

eScholarship.org Powered by the California Digital Library
University of California

Controllers for an Autonomous Vehicle Treating Uncertainties as Deterministic Values

by

Chan Kyu Lee

A dissertation submitted in partial satisfaction of the

requirements for the degree of

Doctor of Philosophy

in

Engineering - Mechanical Engineering

in the

Graduate Division

of the

University of California, Berkeley

Committee in charge:

Professor J. Karl Hedrick, Chair
Professor Francesco Borrelli
Professor Samer M. Madanat

Spring 2016

Controllers for an Autonomous Vehicle Treating Uncertainties as Deterministic Values

Copyright 2016
by
Chan Kyu Lee

Abstract

Controllers for an Autonomous Vehicle Treating Uncertainties as Deterministic Values

by

Chan Kyu Lee

Doctor of Philosophy in Engineering - Mechanical Engineering

University of California, Berkeley

Professor J. Karl Hedrick, Chair

This thesis presents disturbance estimators and controllers for autonomous vehicles. In particular, it focuses on a longitudinal distance controller and a lateral lane keeping controller. First, in order to estimate road bank angle as a disturbance term in the lane keeping controller, a kinematic relationship between road shape and sensor measurements was proposed. Utilizing longitudinal and lateral vehicle dynamics, longitudinal road gradient and lateral road bank angle were estimated simultaneously using the Unscented Kalman Filter (UKF) approach. Second, a lane keeping controller associated with the road bank angle estimator was proposed. For the controller, a steady state dynamic vehicle model was derived to describe lateral vehicle dynamics. A Receding Horizon Sliding Control (RHSC) approach was implemented to guarantee simple formulation and easy constraint consideration for the receding horizon technique.

For the longitudinal control systems, the front vehicle's future motion was considered as a disturbance term in a longitudinal distance controller for the ego vehicle. To predict the motion, a new car-following model was proposed. To extract the current front vehicle driver's driving style, a driver aggressivity factor was derived and estimated in real-time through the UKF approach. Adopting a base car-following model and an aggressivity factor estimator on the front vehicle, the front vehicle's future motion sequence was propagated. Furthermore, as a distance controller associated with the front vehicle's future motion, a Fuel Efficiency Adaptive Cruise Control (ACC) was presented. A new fuel consumption model was included in the optimization problem in order to improve fuel efficiency. The nonlinear Model Predictive Control approach was applied to the controller, and the front vehicle's future motion was considered in the prediction horizon.

Two disturbance estimators for longitudinal and lateral motion were verified under simulation and real vehicle tests in real-time. The lane keeping controller was proven to have better performance with the bank angle estimator on public roads. Furthermore, for a distance controller, fuel economy using a Fuel Efficiency ACC has been verified in simulation.

Contents

Contents **i**

List of Figures **iv**

List of Tables **vii**

1 Introduction **1**
1.1 Driver Assistance System and Self Driving Vehicle 1
1.2 Lateral Vehicle Control 3
1.2.1 Disturbance of Lateral Vehicle Control 3
1.2.2 Lane Keeping Control 4
1.3 Longitudinal Vehicle Control 5
1.3.1 Disturbance of Longitudinal Vehicle Control 5
1.3.2 Distance Control 6
1.4 Contributions and Outlines 7

2 Lateral Disturbance Estimation : Road Gradient Estimator **9**
2.1 Introduction 9
2.2 Framework for a Disturbance Estimator Design using Dual Unscented Kalman Filter 12
2.3 Vehicle Kinematics 13
2.3.1 Step 1 : Motion in *Vehicle-Frame-Fixed Coordinate* with respect to *Inertial Coordinate* 15
2.3.2 Step 2 : Motion in *Vehicle-Frame-Fixed Coordinate* with respect to *Intermediate Coordinate1* 15
2.3.3 Step 3 : Motion in *Vehicle-Body-Fixed Coordinate* with respect to *Vehicle-Frame-Fixed Coordinate* 16
2.4 Vehicle Dynamics 17
2.4.1 Longitudinal Vehicle Dynamics 17
2.4.2 Lateral Vehicle Dynamics 17
2.4.3 State Definition and Measurement 18
2.5 Estimator Design 21

2.5.1 Dual Unscented Kalman Filter Approach . . . 22
2.5.2 Observability Analysis . . . 22
2.6 Vehicle Model Validation . . . 24
2.6.1 Longitudinal Vehicle Model Validation . . . 24
2.6.2 Lateral Vehicle Model Validation . . . 27
2.7 Vehicle Test Results . . . 29
2.7.1 Essential Vehicle State Estimation Validation . . . 29
2.7.2 Vehicle Test on a Public Road . . . 31
2.8 Conclusion . . . 36

3 Lateral Motion Controller : Lane Keeping Controller associated with Road Disturbance Estimator 37
3.1 Introduction . . . 37
3.1.1 Motivation for a New Vehicle Dynamics Model . . . 37
3.1.2 Motivation for a New Control Law . . . 38
3.2 New Lateral Vehicle Dynamics Model . . . 40
3.2.1 Current Vehicle Model of Lateral Vehicle Motion and Its Limitation . 40
3.2.2 Steady State Dynamic Model . . . 42
3.2.3 Simulation and Vehicle Test for Steady State Dynamic Model Validation 46
3.2.4 Error Dynamics . . . 49
3.3 Lane Keeping Controller . . . 50
3.3.1 Control Law Design . . . 50
3.3.2 Lane Keeping Controller . . . 51
3.3.2.1 Controller Setup . . . 51
3.3.2.2 Stability of the Controller . . . 54
3.4 Simulation Results . . . 55
3.4.1 Basic Control Performance . . . 55
3.4.2 Bank Angle Effect Simulation . . . 56
3.5 Vehicle Test Results . . . 59
3.5.1 Vehicle Test on the Public Roads . . . 59
3.5.2 Bank angle Effect . . . 60
3.6 Conclusion . . . 66

4 Longitudinal Disturbance Estimation : Front Vehicle's Future Motion 67
4.1 Introduction . . . 67
4.1.1 Motivation . . . 67
4.1.2 Method for Prediction of the Front Vehicle's Motion . . . 68
4.2 Step 1 : Base Car-Following Model . . . 70
4.2.1 Literature Review . . . 70
4.2.2 New Car Following Model . . . 72
4.3 Step 2 : Aggressivity Factor Estimation . . . 75
4.4 Step 3 : Front Vehicle's Future Motion Estimation . . . 78

4.5 Vehicle Test Results 79
4.6 Conclusion 86

5 Longitudinal Motion Controller : Fuel Efficiency ACC associated with Front Vehicle's Future Motion 87
5.1 Introduction 87
5.1.1 Motivation 87
5.1.2 Framework of Fuel Efficiency ACC Controller 88
5.2 Modeling 89
5.2.1 Fuel Consumption and Vehicle Model 89
5.2.2 Plant and Distance Dynamics 92
5.3 Distance Controller 93
5.3.1 Control Law Design : Nonlinear Model Predictive Control 93
5.3.2 Controller without Optimal Gear Selection 94
5.3.2.1 Control Goal 94
5.3.2.2 State Definition and System Dynamics 94
5.3.2.3 Nonlinear MPC 95
5.3.3 Controller with Optimal Gear Selection 96
5.4 Simulation Results Using Real Traffic Data 98
5.4.1 Distance Controller Validation under Normal Scenarios 98
5.4.2 Distance Controller without Optimal Gear Selection Using Real Traffic Data 100
5.4.3 Basic Distance Controller with Optimal Gear Selection Using Real Traffic Data 102
5.5 Conclusion 106

6 Conclusions and Future Work 109
6.1 Conclusions 109
6.2 Future Work 112

Bibliography 115

List of Figures

1.1 Autonomous Vehicle Subsystems and Components 2
1.2 Source of Disturbance 3

2.1 Bank Angle Effect of Lane Keeping Control 11
2.2 Framework for the Dual Unscented Kalman Filter 11
2.3 Kinematics - Vehicle Side View 13
2.4 Kinematics - Vehicle Rear View 14
2.5 Kinematics - Euler Angle Definition 14
2.6 Lateral Vehicle Dynamics - Bicycle Model 18
2.7 Lateral Vehicle Roll Dynamics 19
2.8 Test Vehicle(Hyundai AZERA) 24
2.9 Reference Measurement Unit - GPS/IMU 25
2.10 Vehicle Model Validation - Mechanical Efficiency 26
2.11 Vehicle Model Validation - Air Drag Force and Rolling Resistance 26
2.12 Vehicle Model Validation - Brake Gain 27
2.13 Vehicle Model Validation - Combined Longitudinal Dynamics 28
2.14 Vehicle Model Validation - Lateral Dynamics 28
2.15 Vehicle Test Facility - Hyundai California Proving Ground 29
2.16 Vehicle State Estimation Results 30
2.17 dSpace Microautobox 31
2.18 Vehicle Test Route 32
2.19 Vehicle Test Route - Road Shape 32
2.20 Vehicle Test Results - Road Gradient 34
2.21 Vehicle Test Results - Bank Angle 35

3.1 Kinematic Model of Lateral Vehicle Motion 40
3.2 Vehicle Model Limitation - 20km/h 42
3.3 Vehicle Model Limitation - 60km/h 43
3.4 Vehicle Model Limitation - 120km/h 43
3.5 New Vehicle Model Validation - 20km/h 46
3.6 New Vehicle Model Validation - 60km/h 47
3.7 New Vehicle Model Validation - 120km/h 47

3.8 New Vehicle Model Validation Test - 60km/h . . . 48
3.9 Error Dynamics of Path Following or Lane Keeping . . . 49
3.10 Steering Actuator Delay . . . 52
3.11 Simulation Results - Lane Keeping Control with Initial Offset Error . . . 55
3.12 Simulation Results - Closed-loop vs. Open-loop . . . 56
3.13 Simulation Results - On the curved road . . . 57
3.14 Simulation Results - Shortest path On the curved road . . . 57
3.15 Simulation Results - Bank Angle Effect . . . 58
3.16 Test Vehicle equipped with a Forward Looking Camera . . . 59
3.17 Road Gradient Estimation in Real Time . . . 60
3.18 Lane Keeping Control Results on a Public Road . . . 61
3.19 Bank Angle Effect - Low Offset Error Gain . . . 62
3.20 Bank Angle Effect - High Offset Error Gain . . . 63
3.21 Controller with Bank Angle Estimator . . . 64
3.22 Controller without Bank Angle Estimator . . . 65

4.1 Advantage of the Front Vehicle's Future Motion Prediction - Early Braking . . . 68
4.2 Advantage of the Front Vehicle's Future Motion Prediction - Smooth Velocity Profile . . . 68
4.3 Definition of Control Variable for the Ego Vehicle . . . 73
4.4 Gain Scheduling of an ACC controller depending on Vehicle Speed . . . 73
4.5 Definition of Control Variable for the Front Vehicle . . . 75
4.6 Concept of Front Vehicle's Future Motion Prediction . . . 78
4.7 Radar and its detection Coverage . . . 79
4.8 Vehicle Test Route . . . 80
4.9 State Estimation Results . . . 81
4.10 Aggressivity Factor Estimation Results . . . 82
4.11 Future Motion Prediction(0-250 sec) . . . 82
4.12 Future Motion Prediction(40-100 sec) . . . 83
4.13 Future Motion Prediction Error . . . 83
4.14 Future Motion Prediction Error Analysis . . . 84
4.15 Future Motion Prediction Error Rate - Constant Acceleration Model vs. Car Following Model . . . 84

5.1 Framework of Fuel Efficiency ACC Controller . . . 89
5.2 Engine Fuel Consumption Map . . . 90
5.3 Negative Fuel Consumption Avoiding . . . 91
5.4 Framework of Optimal Gear Selection . . . 97
5.5 Example of Optimal Gear Selection . . . 97
5.6 Scenario 1 - Positive Distance Error . . . 99
5.7 Scenario 2 - Accelerating and Braking . . . 99
5.8 Scenario 3 - Slow Moving Front Vehicle . . . 101

5.9 Distance Control Using LQ Controller 103
5.10 Distance Control Using MPC Controller 104
5.11 Distance Control Results Comparison - Velocity Profile for Braking Timing . . . 105
5.12 Distance Control Results Comparison - Velocity Profile for Fuel Saving 105
5.13 Distance Control Results Comparison - Fuel Consumption 106
5.14 Distance Control Considering Optimal Gear Selection 107
5.15 Distance Control Considering Optimal Gear Selection - Gear Stage 108
5.16 Distance Control Considering Optimal Gear Selection - Velocity Profile 108

6.1 Timegap Variation 112
6.2 Interested Vehicles for Lane Change 113

List of Tables

1.1 Related Factors for Drivers and Motorcycle Riders Involved in Fatal Crashes [49] 1

2.1 Scaling Factors and Weights 22

5.1 Simulation Setting of Scenario 1 98
5.2 Simulation Setting of Scenario 2 100
5.3 Simulation Setting of Scenario 3 100
5.4 Fuel Consumption Improvement of MPC Controller 102
5.5 Fuel Consumption Improvement of MPC Controller with Optimal Gear Selection 102

Acknowledgments

I would like to express sincere thanks to my advisor, Prof. J. Karl Hedrick, for his insightful guidance and continuous support while conducting my doctoral study. I also would like to thank Prof. Francesco Borrelli for his invaluable advice and support on the findings presented in this thesis. Further, I would like to thank Prof. Andrew Packard, Prof. Fai Ma and Prof. Samer Madanat for serving as committee members in my qualifying examination. I would also like to thank Prof. Samer Madanat for serving as a dissertation committee member.

In addition, I would like to acknowledge all of my friends and colleagues in the Vehicle Dynamics & Control Laboratory and the Model Predictive Control Laboratory. Namely, Sanghyun Hong, Chang Liu, Andreas Hansen, Yi-Wen Liao, Yujia Wu, Donghan Lee, Yongkeun Choi, Jungeun Choi, Emmanuel Sin and Ashwin Carvalho. They have provided great support in my academic career and shared invaluable life experiences in Berkeley.

I also want to express my gratitude to Hyundai Motor Company for their support of my research.

Finally, I owe thanks to my wife, Seon Ji and my daughter, Onyu for being solid foundation while overcoming hardships during graduate study.

Chapter 1

Introduction

1.1 Driver Assistance System and Self Driving Vehicle

In recent years, the automotive industry has made significant leaps in bringing new features for Advanced Driver Assist System (ADAS) and Active Safety System (ASV) to market. Some well known examples of ADAS include Adaptive Cruise Control (ACC), that controls speed and safe distance, and Lane Keeping Assist (LKA), that allows cars to steer themselves to maintain the lane. Furthermore, Forward Collision Warning (FCW) and Blind Spot Detection(BSD) have been developed to support safe driving. These systems are very efficient in improving driver's convenience and safety by assisting the driver's control efforts and correction decisions. Considering that most fatal crashes are generated from human error, as shown in Table 1.1, these systems have become very important features of the automobile.

Table 1.1: Related Factors for Drivers and Motorcycle Riders Involved in Fatal Crashes [49]

Factors	Percent
Driving too fast	19.9
Under the influence of alcohol, drugs or medication	13.5
Failure to keep in proper lane or running off road	8.3
Failure to yield right of way	7.1
Distracted (phone, talking, eating, object, etc)	6.6
Operating vehicle in a careless manner	4.7
Overcorrecting/oversteering	4.5
Failure to obey traffic signs, signals, or officer	4.0
Swerving or avoiding due to wind, slippery surface, etc	3.7
Operating vehicle in erratic, reckless, or negligent manner	3.3



Figure 1.1: Autonomous Vehicle Subsystems and Components

By combining such ADAS features, many automotive manufactures and suppliers are developing Autonomous Vehicles (AV, also called automated or self-driving vehicles) that can drive by themselves, taking into account environmental data, including traffic conditions and regulations. The AV consists of several subsystems and components, such as a digital map, sensors, controllers and actuators as shown in Figure 1.1. This thesis mainly focuses on the controller aspect of the AV, and suggests some approaches to improve control performance.

In the real world, autonomous vehicle control, performance can be affected by several factors called external uncertainties or disturbances. There are various sources of uncertainty for the autonomous vehicle, such as neighboring traffic, road, the vehicle itself, and the weather, as shown in Figure 1.2. Under these uncertainties, it can be difficult to obtain good control performance, which can lead to dangerous situations for the occupants. Therefore, developing an uncertainty estimator and adopting its value in the controller to compensate for the uncertainties, is valuable to obtain good control performance. This research suggests new algorithms to estimate the future motion of neighboring vehicles and the road geometry, treating them as longitudinal and lateral disturbances, respectively.



Figure 1.2: Source of Disturbance

1.2 Lateral Vehicle Control

1.2.1 Disturbance of Lateral Vehicle Control

Prior research highlights that detection of the road bank angle and vehicle's body roll is necessary for the satisfactory performance of lateral vehicle dynamics control systems [2][9][15]. This is because the disturbances give additional lateral force to the vehicle. Although several methods to estimate the road bank angle have been proposed, the vehicle roll was either neglected or lumped with the road bank angle [16][17].

However, it is difficult to differentiate between the road bank angle and the vehicle body roll angle by using typical roll related measurements, such as a lateral acceleration sensors and a roll rate sensor. Since these sensors are usually attached to the vehicle body, road geometry and body motion both have the same effect on sensor readings. Therefore, road bank angle and body roll cannot be separated directly using a kinematic relationship of the roll. While the road bank angle can be treated as a disturbance to the vehicle dynamics, the vehicle body roll angle is a state governed by lateral vehicle dynamics resulting from the road bank angle and steering angle input. A parameterized vehicle dynamics model can be used to separate the vehicle's body roll and road bank angle using additional measurements from Global Positioning System (GPS) and Inertial Navigation System (INS) [17][18].

Although this research starts from a proposed method in Ryu [17][18], the author did not consider the longitudinal road gradient term which could affect the lateral force. Therefore, in this research, an estimator that can simultaneously estimate the road bank angle, road gradient, and vehicle body roll, is introduced in order to determine the additional lateral force on the vehicle.

In addition, since GPS and INS, used in the prior research of [17][18], are not typically used in mass production vehicles. this study aims to use only conventional sensors, such as wheel speed sensors, yaw rate sensor, longitudinal and lateral acceleration sensors. This thesis

presents a novel approach to estimate road bank angle, road gradient and vehicle body roll simultaneously using only these sensors.

1.2.2 Lane Keeping Control

The lane keeping control system is an example of a lateral vehicular motion control system and is a very basic function of autonomous vehicles and driver assist systems. In order to improve control performance of this system, disturbance terms such as the road gradient should be considered in the controller. For this purpose, a model based controller can easily take into account such disturbance values. A vehicle dynamics model including a disturbance term should be included in the controller.
A dynamic vehicle model, derived from Newton's laws of motion, is typically used for the lateral control of autonomous vehicles and driver assist systems [55][65]. Due to the occurrence of a singularity at low speeds, the model is used only at high speeds over 40km/h.
In addition, a kinematic vehicle model is derived from Ackermann steering geometry. Since the kinematic model is derived from the assumption that there is no tire side-slip angle, it is reliable under low speed situations such as those encountered by a smart parking assist system under limited tire side slip. However, at higher speeds, vehicle side-slip easily occurs and this phenomenon violates the assumption of no tire side-slip.
For these reasons, prior research conventionally used a kinematic vehicle model at low speeds and a dynamic vehicle model at high speeds. For an autonomous vehicle, two separate controllers, one at low and the other at high speeds, should be used and tuned. A comparison between these two models is rarely found in prior research [6][37]. This thesis proposes a new vehicle model for use over all speed ranges.
As a control method for the lane keeping control system, a conventional PID control approach and simple state feedback control law are usually adopted. Using the Model Predictive Control (MPC) approach, an iterative linearized model from nonlinear system dynamics, is used for the control law [10][21]. But, in order to keep nonlinear system dynamics, Sliding Mode Control(SMC) can be considered for the control law.
From the perspective of calculation cost, since the MPC approach requires very expensive calculation costs, some research results [7][56] suggested computationally efficient method, such as Explicit MPC. In order to include the disturbance term in the controller, some methods based on SMC and MPC are suggested. In the Sliding Mode Controller, a Disturbance Observer can be included to reject not only mismatched disturbances but also other disturbances [39]. Specially, in the MPC formulation, the disturbance can be considered as a stochastic term [11] or a band [22] to guarantee robustness of the control performance, depending on the disturbance.
In order to satisfy criteria such as low computational cost, nonlinear dynamics over receding horizon, disturbance rejection, and consideration of constraints, a combination logic between sliding mode control and model predictive control is suggested [36]. Also, in A. Hansen and K. Hedrick [27], a discrete difference operator is used to adopt Receding Horizon Sliding

Control (RHSC) algorithm on a discrete time case. This thesis adopts the discrete RHSC approach using a proposed vehicle dynamics model.

1.3 Longitudinal Vehicle Control

1.3.1 Disturbance of Longitudinal Vehicle Control

An Adaptive Cruise Control (ACC) system is a well known driver assist system for longitudinal position and speed control. It maintains the speed set by the driver and if there exists a front vehicle, the system maintains a safe distance from the vehicle automatically. In order to detect the front vehicle, the system usually uses a forward looking radar. From the radar, current relative distance and velocity between the controlled ego vehicle and the front vehicle can be measured. Therefore, depending on the current motions of the vehicles, the ego vehicle can be controlled by the desired acceleration control input from the ACC algorithm. The front vehicle's future motion is one of the main disturbance terms for the system. This research uses a car-following model of the front vehicle to predict its future motion.

Various simplified car-following models are proposed to describe a vehicle's car following motion [5][8][28][45]. The method in [46] suggests the car-following model as a kind of controller or adaptive filter. In this approach, all parameters for each model were extracted from real car-following data, and a representative equation was chosen.

Recently, non-parametric approaches have been suggested for the car-following model. The method does not have any fixed equation at the beginning. But, using several sets of real data, called training data sets, probability parameters are defined. In addition to the non-parametric model, combining probabilistic models under various situations using a hybrid dynamical model was also suggested [19]. This approach is significant because the driver's behavior can be affected by various traffic situations. Furthermore, Artificial Neural Networks [54], Gaussian Mixture Regression and Hidden Markov Models are alternative methods for stochastic representation of a vehicle's motion.

A number of research results compare the performance of the car-following models. Some research focus on parametric benchmarking [26][52][53]. For the non-parametric model comparison, Angkititrakul [50] concluded that both approaches are very dependent on the situation, and may not be feasible under heavy traffic conditions. Recently, Stéphanie [63] compared the performance of both parametric and non-parametric approaches to predict the following vehicle's future movement. The results showed that the parametric models' performance was better than that of non-parametric models for short-term prediction under 3 seconds. But, for long-term prediction, non-parametric models and advanced parametric models prove to be quite better than simple parametric approaches.

This thesis introduces a new car-following model to describe the front vehicle's car-following motion. Additionally, since the car-following model should be parameterized depending on the current front vehicle driver, this thesis suggests a novel method to extract the current

vehicle driver's driving style using an aggressivity factor. Finally, the front vehicle's future velocity sequence is derived for a short time horizon within 2 seconds.

1.3.2 Distance Control

A conventional ACC System only ensures that the relative speed(preceding vehicle speed - ego vehicle speed) and relative distance error (relative distance - desired distance) converge to zero. However, this thesis introduces another feature of ACC - how the system can improve fuel efficiency while maintaining good control performance.

For vehicles equipped with automatic speed and distance control functions, there are several methods to improve the ego (controlled) vehicle's fuel consumption. First, if we know the traffic signal and traffic conditions in advance, an optimal velocity profile can be generated to minimize waiting time at stop lights and total fuel consumption [4][61]. The second method considers road slopes [13][25][44]. This is reasonable because longitudinal traction force and fuel consumption are related to the incline-decline slope of the road profile. This method is especially useful for heavy truck applications. Third, Vehicle to Vehicle (V2V) communication can be adopted for a platoon control system [23][41][68]. A platoon with communication can improve traffic efficiency and decrease vehicle to vehicle distance to reduce air drag force. Also, optimal gear shift selection considering fuel consumption, is another approach for controlling vehicle speed [38].

This research focuses only on the distance control scenario with preceding vehicle information using conventional sensors, such as a radar. Special information such as look-ahead traffic signal and road shape were not considered in this research. Also, in order to focus on a conventional ACC systems, platoon and V2V communication were not explored. Therefore, we only have the current ego vehicle's information, current relative distance and velocity to the front vehicle. Since Jonathan [62] shows that fuel economy is highly related to driver aggressivity, a smooth car-following distance controller is desired. Also, in Lang's research [42], the prediction of preceding driver behavior improved fuel efficiency for cooperative adaptive cruise control systems. If the front vehicle's future motions can be predicted, an optimal distance and gear selection with smooth movement can be constructed.

Therefore, this paper proposes an MPC approach, considering the front vehicle's future motions and fuel efficiency.

1.4 Contributions and Outlines

In chapter 2, a road geometry estimator as a lateral disturbance estimator is developed based on road-vehicle kinematics and lateral vehicle dynamics. The estimation algorithm:

- Proposes a kinematic relationship between the road shape and the sensor measurements using several coordinate systems. All measurements are gathered at the vehicle body using only conventional vehicle sensors.
- Utilizes a lateral and a longitudinal vehicle dynamics model to describe vehicle's motion. In addition, vehicle body's roll dynamics is included.
- Validates vehicle parameters for the dynamics equations using a test vehicle.
- Suggests a Dual Unscented Kalman Filter algorithm to estimate the longitudinal road gradient, the lateral road bank angle, and the vehicle body's roll angle simultaneously.
- Verifies the suggested algorithms on a real vehicle on a test track.
- Experimentally validates the performance of the proposed algorithms on public roads in real-time.

In chapter 3, a lane keeping controller associated with the road disturbance estimator is presented. The control algorithm:

- Proposes a steady state dynamics model to describe lateral vehicle dynamics over all speed ranges, which is also useful to consider bank angle effect.
- Verifies the new lateral vehicle dynamics model using a simulation tool and real vehicle test. The results conclude that the proposed model is reasonable and accurate.
- Derives an error dynamics model of offset and heading errors for lane keeping and path following.
- Constructs a discrete Receding Horizon Sliding Control approach using a proposed lateral vehicle dynamics and error dynamics model. This control approach is simple to formulate and easy to add constraints to for using the receding horizon technique.
- Verifies the suggested controller using a simulation tool and a real vehicle on a test track.
- Implements the controller on a real vehicle on public roads. Road bank angle estimation results are fed to the lane keeping controller to compensate for the lateral force disturbance effect. The proposed control logic is very effective to maintain the vehicle's position within a lane.

In chapter 4, the front vehicle's future motion prediction algorithm as a longitudinal disturbance estimator is developed. The algorithm:

- Proposes a new car-following model to describe the front vehicle's longitudinal speed control motion. It is a deterministic and parametric model, based on a well-tuned ACC system.
- Suggests a method for extracting the driver's aggressivity factor. This method is significant because each vehicle driver has a different driving style.
- Utilizes the UKF approach to extract the aggressivity factor in real time by comparing measurements and newly updated system states.
- Propagates the front vehicle's future motion sequence using the new car following model and the aggressivity factor.
- Validates the proposed algorithm on a real vehicle on public roads in real-time. The algorithm demonstrates good prediction performance for the next 2 seconds.

In chapter 5, a fuel efficiency ACC controller associated with the front vehicle's future motion, is developed. The control algorithm:

- Utilizes a Nonlinear Model Predictive Control approach for a basic distance controller with fuel consumption model to improve fuel efficiency.
- Suggests a new fuel consumption model, derived from a real engine's fuel consumption map.
- Verifies the logic with simulation. A sequence of the front vehicle's future motion is fed to the distance controller. By considering the future motion in the optimization problem, the fuel efficiency ACC logic improved fuel economy by 3.67% under real traffic data.
- Proposes a simple transmission gear selection logic to minimize fuel consumption. The logic compares shift-up and shift-down case costs in the optimization problem.
- Verifies the proposed logic. However,the optimal solution is unable to improve the fuel economy as much as anticipated.

Chapter 2

Lateral Disturbance Estimation : Road Gradient Estimator

2.1 Introduction

For vehicle control systems, various states and environmental conditions should be considered to guarantee desirable control performance. Effective operation of each control system should depend on accurate information of both the vehicle states and the vehicle parameters. Prior research focuses on estimating vehicle states such as side slip angle, longitudinal and lateral tire forces. Research has also been done on estimating parameters related to the vehicle and environmental conditions such as vehicle mass, tire-road friction, wind gust and road gradient. From the perspective of improving safety, these factors are considered especially significant for driver assistance systems and self driving vehicles. For example, vehicle side-slip angle is one of the most important states to consider in improving the performance of a control system designed to guarantee the stability of the vehicle lateral motion in emergency situations. The side-slip data should be considered to reduce accidents and improve driver's safety. Also, longitudinal and lateral road gradients generate additional longitudinal and lateral forces to the vehicle body. Such additional forces can be considered as disturbance terms of a controller for driver assistance systems such as Adaptive Cruise Control System (longitudinal controller) and Lane Keeping Assist System (lateral controller).
To estimate vehicle states and parameters, research has been conducted using various approaches. In this chapter, only the states and parameters related to lateral vehicle motion control are introduced. Side-slip angle describes lateral motion of the vehicle and it can be estimated using a lateral accelerometer or a yaw rate sensor. However, these measurements can easily be affected by disturbances such as road bank angle, road longitudinal gradient and vehicle roll induced by suspension deflection. Such inaccuracy in the measurements may result in false estimation of the vehicle states or misleading activation of the driver assistance control systems. Therefore, the information of road bank angle, road gradient and vehicle body roll are important for such systems.

Focusing only on the lateral disturbance term, numerous research results have pointed out that detection of the road bank angle and vehicle roll is necessary for the satisfactory performance of the driver assistance control systems [2][9][15]. Several methods are proposed to estimate the road bank angle, but the vehicle roll induced by suspension deflection is neglected or lumped with the road bank angle [16][17]. However, it is difficult to differentiate between the road bank angle and the vehicle roll angle by using typical roll related measurements, such as lateral acceleration and roll rate sensor. Since the lateral accelerometer and the roll rate sensors are usually attached at the vehicle body, the road bank angle and vehicle roll have the same effect on the lateral acceleration measurements. Therefore, road bank angle and body roll cannot be separated directly using kinematic relationships only. While the road bank angle can be treated as a disturbance term to the vehicle dynamics, the vehicle body roll angle is a state governed by lateral vehicle dynamics resulting from the road bank angle and steering angle input. A parameterized vehicle dynamics model can then be used to separate the vehicle roll from road bank angle using additional measurements from the Global Positioning System (GPS) and the Inertial Navigation System(INS) [17][18].
In Ryu [17][18], the results do not take into account the longitudinal road gradient term, which can affect lateral force with a cosine term multiplier, as shown in the following equation.

$$F_{road,y} = m \times g \times \sin\phi_r \times \cos\theta_r \tag{2.1}$$

$F_{road,y}$ is the lateral external force on the vehicle body due to vehicle mass(m), acceleration of gravity(g), road bank angle(ϕ_r) and road longitudinal gradient(θ_r). In this research, an estimator that can simultaneously estimate the road bank angle, road gradient and vehicle body roll is introduced in order to determine the additional lateral force on the vehicle. In addition, GPS and INS which have been used in prior research [17][18], are not the conventional vehicle sensors used for the estimators. Therefore, in order to guarantee implementation on a mass production vehicle, only conventional vehicle sensors such as wheel speed sensors, a yaw rate sensor and a longitudinal sensor should be used for the estimator. Figure 2.1 shows the bank angle effect of the lane keeping controller. On a curvy road, the road has a bank angle (especially with the longitudinal road gradient). While controlling a vehicle for lane keeping or path following, the road shape is a disturbance term for the controller, and the controller exhibits some oscillations on the curvy road as shown in Figure 2.1. With the road shape estimation results, a lane keeping controller is able to compensate for the lateral force due to bank angle and accurate control performance. As indicated above, road disturbance estimation is worthwhile for a lane keeping controller. This section focuses on estimation of $F_{road,y}$.
First, based on vehicle kinematics, angular motion between the road shape and measurement sensors is defined. After the effect of vehicle dynamics on measurement sensors is considered. Using kinematics and dynamics models, a dual Unscented Kalman Filter (UKF)-based estimator is developed. Before implementing the estimator on the real vehicle, vehicle model validation procedures are performed to determine vehicle parameters. Finally, vehicle test results are presented.



Figure 2.1: Bank Angle Effect of Lane Keeping Control

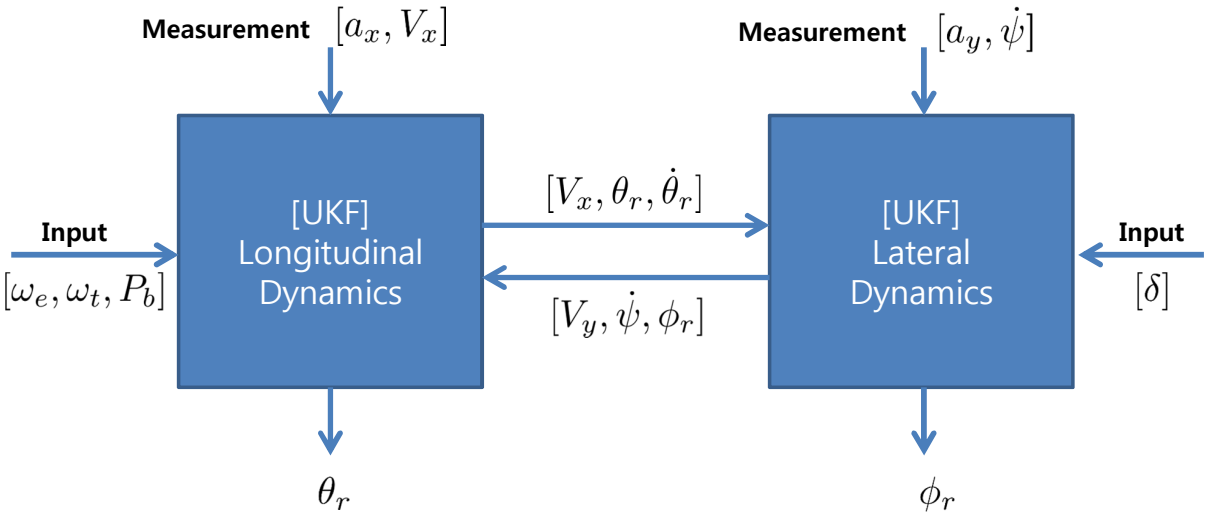

Figure 2.2: Framework for the Dual Unscented Kalman Filter

2.2 Framework for a Disturbance Estimator Design using Dual Unscented Kalman Filter

For estimating the exact lateral disturbance force, longitudinal and lateral road shapes should be considered simultaneously. Several approaches to the lateral disturbance estimation, such as road bank angle and vehicle roll estimation, use an unknown proportional integral observer, which is a generalized version of the Luenberger observer [43][59]. This method was developed for the reconstruction of vehicle lateral dynamics states while the road bank angle is considered as signal faults acting as unknown inputs. For the observer, some states should be measured. However, direct measurement of some variables requires the use of nonlinear equations and expensive sensors. To overcome difficulties in obtaining information with high accuracy and cost effectively, the Kalman Filter technique is commonly used. To adapt the Kalman Filter to a nonlinear system such as vehicle lateral dynamics, the Extended Kalman Filter (EKF) is used for estimation purposes [20]. However, since the model's behavior is strongly nonlinear and compromised of additive noise, a more accurate generalization approach, the UKF was developed [57][67]. This approach shows fast convergence and robustness in the presence of a noise term [12][47].
Longitudinal road gradient is generally considered as a driving load to the vehicle along with rolling resistance and aerodynamic drag forces. As a result, a very simple observer based on longitudinal vehicle dynamics is designed [33][35].
However, prior research has not considered combinational forces between longitudinal and lateral road gradient. A complete vehicle dynamics model considering both the longitudinal and the lateral motion should be considered for real time estimations. Such a model requires a higher order of states, and the respective UKF requires expensive calculation cost. In this paper, a dual-UKF approach adapted to be used in the estimators for longitudinal road gradient and lateral bank angle, as shown in Figure 2.2, is introduced. Each UKF algorithm uses prior information of the other UKF estimator's result for updating current state estimation. UKF for longitudinal dynamics requires measurements of longitudinal vehicle speed(V_x) and acceleration(a_x). Also, inputs of the estimator are engine speed(ω_e), transmission turbine speed(ω_t) and brake pressure(P_b). The estimator also requires lateral vehicle dynamics states from the lateral UKF. Lateral velocity(V_y), yaw rate(ψ) and road bank angle(ϕ_r) are fed to the longitudinal UKF module. Finally, the longitudinal UKF can estimate longitudinal road gradient(θ_r) in real-time. The lateral UKF module's framework is very similar to the longitudinal UKF. Measurements include lateral acceleration(a_y) and yaw rate(ψ), which are located at the vehicle body. From the longitudinal UKF module, longitudinal velocity(V_x), longitudinal road gradient and its rate($\theta_r, \dot{\theta}_r$) are delivered to the lateral module. Also, steering input(δ) is the main control input for the lateral vehicle dynamics. Then, current road bank angle(ϕ_r) can be estimated by the lateral UKF module. To guarantee the implementation of the dual UKF on the real vehicle, only widely-used sensors such as wheel speed sensors, accelerometers, and a yaw rate sensor are used.

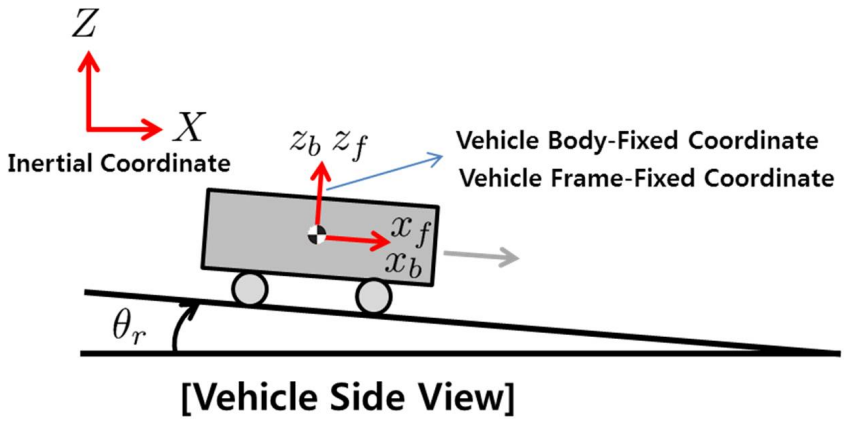

Figure 2.3: Kinematics - Vehicle Side View

2.3 Vehicle Kinematics

In this section, basic coordinates and the angular relationship between coordinates, based on the vehicle kinematics model, will be introduced. In order to estimate the longitudinal road gradient and lateral road bank angle, the relationship between the parameters and the measurement sensors should be derived. As the accelerometers and a yaw rate sensor are installed at the vehicle body, sensor measurements can be defined with respect to the road shape and vehicle motion. Figure 2.3 and Figure 2.4 show definitions of vehicle longitudinal motion and lateral motion. It neglects vehicle body's pitch motion, but roll motion is considered. Also, three types of coordinates are used: *Inertial Coordinate*, which is a base coordinate, *Vehicle-Frame-Fixed Coordinate*, which defines vehicle's basic motion with respect to the road shape under the assumption that the vehicle is attached on the road, and *Vehicle-Body-Fixed Coordinate*, which defines the vehicle roll motion. The 3-2-1 Euler Angle definition was derived for a more convenient method to describe angular change, as shown in Figure 2.5. Yaw, pitch and roll motions are essential motions using additional *Intermediate1* and *Intermediate2* coordinate systems. Furthermore, each motion can be transformed to the other coordinates' angles. Therefore, road shape and vehicle body's roll motion can be defined simultaneously with the coordinate definitions. We assume that the tires are always kept in contact with the road, which means that the vehicle-frame-fixed coordinates moves according to the road shape.
Motion sensors are installed in the vehicle-body-fixed coordinate, but the road shape is defined in the inertial coordinate. Furthermore, the sensors can be governed by the roll motion of the vehicle body, which is defined with the vehicle-body-fixed coordinate system. As a result, the relationship between the sensors and road shape or roll motion can be derived with coordinate transformation transformations.

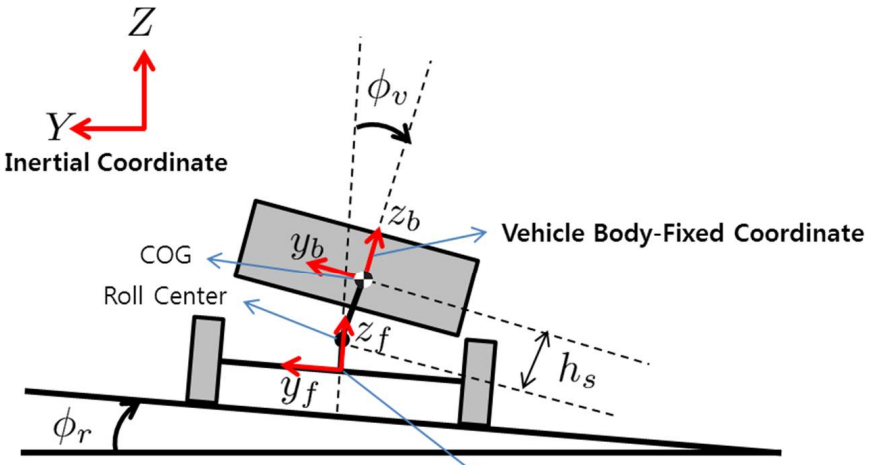

Figure 2.4: Kinematics - Vehicle Rear View

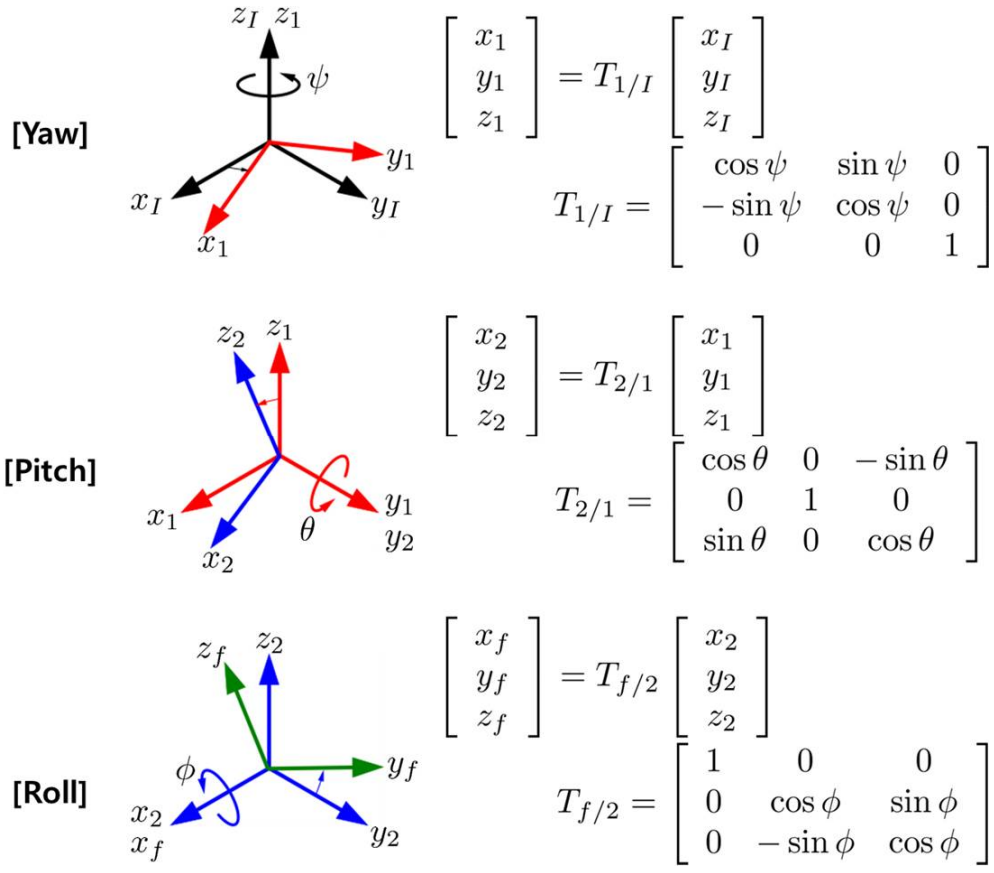

Figure 2.5: Kinematics - Euler Angle Definition

2.3.1 Step 1 : Motion in *Vehicle-Frame-Fixed Coordinate* with respect to *Inertial Coordinate*

The inertial coordinate is a coordinate that is applicable to the surface of the Earth. Then, the angular motion in the vehicle-frame-fixed coordinate can be defined with the Euler angles(ψ, θ,ϕ). Then, the angular motions in the vehicle frame fixed coordinate are defined as following:

$$\begin{bmatrix}\dot{\phi}_f\\ \dot{\theta}_f\\ \dot{\psi}_f\end{bmatrix} = \begin{bmatrix}\dot{\phi}\\ 0\\ 0\end{bmatrix} + T_{f/2}T_{2/1}\begin{bmatrix}0\\ \dot{\theta}\\ 0\end{bmatrix} + T_{f/2}T_{2/1}T_{1/I}\begin{bmatrix}0\\ 0\\ \dot{\psi}\end{bmatrix} \tag{2.2}$$

$$= T_{f/e}\begin{bmatrix}\dot{\phi}\\ \dot{\theta}\\ \dot{\psi}\end{bmatrix} \tag{2.3}$$

Now, considering reverse dynamics, angular velocity in the intermediate coordinate with Euler angles can be defined with Vehicle-Frame-Fixed Coordinate as follows

$$\begin{bmatrix}\dot{\phi}\\ \dot{\theta}\\ \dot{\psi}\end{bmatrix} = T_{f/e}^{-1}\begin{bmatrix}\dot{\phi}_f\\ \dot{\theta}_f\\ \dot{\psi}_f\end{bmatrix} \tag{2.4}$$

$$= \begin{bmatrix}1 & \sin\phi\tan\theta & \cos\phi\tan\theta\\ 0 & \cos\phi & -\sin\phi\\ 0 & -\sin\phi/\cos\theta & \cos\phi/\cos\theta\end{bmatrix}\begin{bmatrix}\dot{\phi}_f\\ \dot{\theta}_f\\ \dot{\psi}_f\end{bmatrix} \tag{2.5}$$

These Euler angles are connections to find a relationship between road shape and the vehicle's motion.

2.3.2 Step 2 : Motion in *Vehicle-Frame-Fixed Coordinate* with respect to *Intermediate Coordinate1*

Next, we consider the relationship between Euler angles and the road shape. Since the Euler angle θ is not zero, the road bank angle(ϕ_r) is not same as ϕ. This is because the road bank angle is defined between the vehicle frame fixed coordinate and the intermediate coordinate 1. Also, ϕ_r is not the same as ϕ, if θ is not zero. Therefore, in this step, angular motion of the vehicle-frame-fixed coordinate with respect to the inertial coordinate can be determined in the intermediate coordinate1 as follows.

$$\begin{bmatrix}\dot{\phi}_r\\ \dot{\theta}_r\\ \dot{\psi}_r\end{bmatrix} = T_{1/2}\begin{bmatrix}\dot{\phi}\\ 0\\ 0\end{bmatrix} + \begin{bmatrix}0\\ \dot{\theta}\\ 0\end{bmatrix} = \begin{bmatrix}\cos\theta\dot{\phi}\\ \dot{\theta}\\ -\sin\theta\dot{\phi}\end{bmatrix} \tag{2.6}$$

Using equations (2.5) and (2.6), the change rate of road shape, $\dot{\phi}_r$ and $\dot{\theta}_r$, can be defined as the following:

$$\dot{\phi}_r = \dot{\phi}_f \cos\theta + \dot{\theta}_f \sin\phi \sin\theta + \dot{\psi}_r \cos\phi \sin\theta \quad (2.7)$$

$$\dot{\theta}_r = 0 + \dot{\theta}_f \cos\phi - \dot{\psi}_f \sin\phi \quad (2.8)$$

As we do not know the exact values of Euler Angles θ and ϕ, the change rate of road shape can be assumed as such:

$$\dot{\phi}_r \approx \dot{\phi}_f + \epsilon \quad (2.9)$$

$$\dot{\theta}_r \approx \dot{\theta}_f + \epsilon \quad (2.10)$$

2.3.3 Step 3 : Motion in *Vehicle-Body-Fixed Coordinate* with respect to *Vehicle-Frame-Fixed Coordinate*

Now, we consider roll motion of the vehicle body. As before, conventional vehicle inertia sensors(yaw rate, longitudinal/lateral acceleration) are installed at the vehicle-body-fixed coordinate. We can define roll motion of body(ϕ_v) with respect to the vehicle-frame-fixed coordinate using transformation matrix $T_{v/f}$.

$$\begin{bmatrix} x_v \\ y_v \\ z_v \end{bmatrix} = T_{v/f} \begin{bmatrix} x_f \\ y_f \\ z_f \end{bmatrix}$$

$$T_{v/f} = \begin{bmatrix} 1 & 0 & 0 \\ 0 & \cos\phi_v & \sin\phi_v \\ 0 & -\sin\phi_v & \cos\phi_v \end{bmatrix} \quad (2.11)$$

Therefore, angular velocity at the measurement point(sensors) can be defined with vehicle-frame-fixed coordinate as follows:

$$\begin{aligned} \begin{bmatrix} \dot{\phi}_m \\ \dot{\theta}_m \\ \dot{\psi}_m \end{bmatrix} &= \begin{bmatrix} \dot{\phi}_v \\ 0 \\ 0 \end{bmatrix} + T_{v/f} \begin{bmatrix} \dot{\phi}_f \\ \dot{\theta}_f \\ \dot{\psi}_f \end{bmatrix} \\ &= \begin{bmatrix} \dot{\phi}_v + \dot{\phi}_f \\ \dot{\theta}_f \cos\phi_v + \dot{\psi}_f \sin\phi_v \\ -\dot{\theta}_f \sin\phi_v + \dot{\psi}_f \cos\phi_v \end{bmatrix} \end{aligned} \quad (2.12)$$

However, for the angular velocity measurements, only a yaw rate sensor is installed at the real vehicle. Yaw rate, $\dot{\psi}_m$ can be obtained using the following equation:

$$\dot{\psi}_m = -\dot{\theta}_f \sin\phi_v + \dot{\psi}_f \cos\phi_v \quad (2.13)$$

Finally, equations (2.9), (2.10) and (2.13) are used for the estimator to define a relationship between road shape and measurement motion.

2.4 Vehicle Dynamics

In this section, simple longitudinal and lateral vehicle dynamics are introduced. The vehicle dynamics define the vehicle's motion by comparing the vehicle's expected motion, determined from dynamics, to the measured motion from the sensors, allowing for the estimation of road shape.

2.4.1 Longitudinal Vehicle Dynamics

Longitudinal vehicle dynamics is affected by the road gradient. To obtain simple dynamics equations, torque converter dynamics and wheel dynamics, considering the tire slip, were neglected. First, the torque converter is assumed to be locked up. This means that the engine torque can be transmitted to the wheel directly through the gear ratio of a transmission and final gear reduction of a differential gear set. Also, since the wheel dynamics are neglected as well, mechanical efficiency, η, is added to the dynamics. Therefore, longitudinal vehicle dynamics can be defined as follows:

$$a_x = \frac{F_x}{m} = \frac{F_{engine} - F_{brake} - F_{aero} - F_{rolling} + F_{road,x}}{m} \tag{2.14}$$

$$F_{engine} = T_{eng} \times R_g \times R_f \times R_w \times \eta \tag{2.15}$$

$$F_{brake} = K_b \times P_{brake} \tag{2.16}$$

$$F_{aero} = \frac{1}{2}\rho \times C_a \times A_{front} \times {v_{x,f}}^2 \tag{2.17}$$

$$F_{road,x} = m \times g \times \sin\theta_r \times \cos\phi_r, \tag{2.18}$$

where, a_x is an acceleration term of the vehicle-frame-fixed coordinate. F_x, F_{engine}, F_{brake}, F_{aero}, $F_{rolling}$ and $F_{road,x}$ are total longitudinal tractive force of the vehicle, traction forces from engine, brake force, aerodynamic resistance force, rolling resistance force and driving load due to the road gradient, respectively. The term m is the vehicle's total mass. Engine tractive force can be calculated with net engine torque(T_{eng}), gear ratio(R_g), final gear reduction(R_f) and wheel radius(R_w). Brake force is proportional to the brake pressure with brake gain(K_b). Air drag force(F_{aero}) can be calculated with air density(ρ), air drag force coefficient(C_a), frontal area of vehicle(A_{front}) and longitudinal velocity. In the dynamics equations, input signals are engine torque, T_{eng}, and brake pressure, P_{brake}. As shown in the above equations, road gradient, θ_r, is included in the longitudinal force term.

2.4.2 Lateral Vehicle Dynamics

For lateral vehicle dynamics, a simple bicycle model with a linear tire model is used, as shown in Figure 2.6. Lateral acceleration can be defined in terms of tire forces and additional force

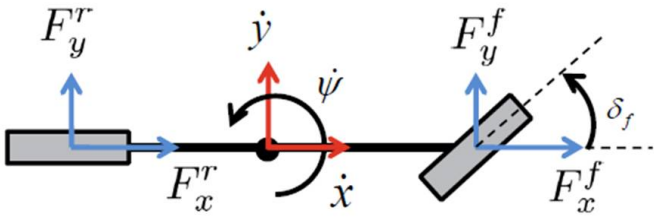

Figure 2.6: Lateral Vehicle Dynamics - Bicycle Model

induced by road bank:

$$a_y = \frac{F_y}{m} = \frac{F_y^f + F_y^r - F_{road,y}}{m}, \tag{2.19}$$

where, tire force is proportional to the tire coefficients of the front and rear tire, C_f and C_r, and tire side slip angles, α_f and α_r. l_f and l_r are the distances to the front and rear tires from the center of vehicle mass, respectively.

$$F_y^f = 2C_f \cdot \alpha_f = 2C_f \cdot (\delta - \frac{v_y + l_f\dot{\psi}}{v_x}) \tag{2.20}$$

$$F_y^r = 2C_r \cdot \alpha_r = 2C_r \cdot (-\frac{v_y - l_r\dot{\psi}}{v_x}) \tag{2.21}$$

$$F_{road,y} = m \times g \times \sin\phi_r \times \cos\theta_r, \tag{2.22}$$

Also, vehicle body roll dynamics, as shown in Figure 2.7, should be considered for accurate estimation of the road bank angle. This is because the measurement sensor at the vehicle body includes vehicle body's roll motion as well as vehicle frame's motion due to road geometry change. The roll dynamics can be defined as follows:

$$\begin{aligned}(I_{xx} + m_s h_R)^2(\ddot{\phi}_v + \ddot{\phi}_r) = &- k_\phi\phi_v - c_\phi\dot{\phi}_v \\ &+ m_s h_R\{\ g \times \cos\theta_r \times \sin(\phi_v + \phi_r) + a_y \times \cos\phi_v\}\end{aligned} \tag{2.23}$$

where I_{xx} is the moment of inertia along the x-axis of the vehicle. m_s and h_R are the sprung mass and the distance between roll center and center of vehicle mass, respectively. ϕ_v and ϕ_r are vehicle body's roll motion and road's roll motion(bank angle).

2.4.3 State Definition and Measurement

For the estimator setup, the system dynamics and measurement should be defined by states. Vehicle's motion consists of not only the translational but also the rotational motion.

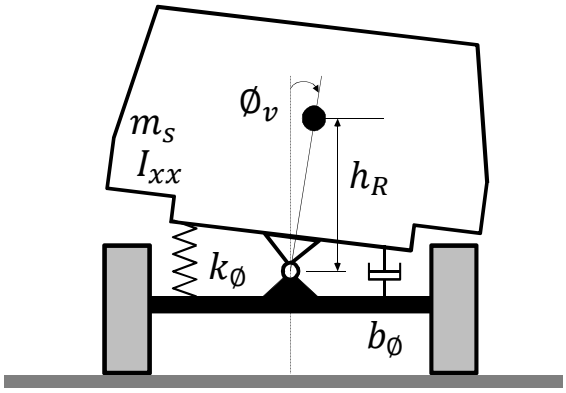

Figure 2.7: Lateral Vehicle Roll Dynamics

- Longitudinal dynamics
  Longitudinal dynamics of the vehicle can be defined as follows:

$$\begin{aligned} \dot{x}_1 =& \dot{v}_{x,f} \quad = a_{x,f} + \dot{\psi}_f \times v_{y,f} \\ \dot{x}_2 =& \ddot{v}_{x,f} \\ \dot{x}_3 =& \dot{\theta}_r \\ \dot{x}_4 =& \ddot{\theta}_r \end{aligned} \tag{2.24}$$

  In the equations, $\dot{x}_2$ and $\dot{x}_4$ are assumed to be equal to zero. This implies that the states have only the process noise. Also, $\dot{x}_3$ is a constant value, which is only affected by x_4 and the process noise.
  From the vehicle kinematics and state definition, sensor measurements can be defined as such:

$$\begin{aligned} a_{x,m} &= \dot{v}_{x,v} + \dot{\theta}_v \cdot v_{z,v} - \dot{\psi}_v \cdot v_{y,v} \\ &\approx \dot{v}_{x,f} - \{-\dot{\theta}_f \times \sin\phi_v + \dot{\psi}_f \times \cos\phi_v\} \times v_{y,v} \\ &\approx \dot{v}_{x,f} - \{-\dot{\theta}_r \times \sin\phi_v + \dot{\psi}_f \times \cos\phi_v\} \times v_{y,v} \\ &= x_2 - \{-x_4 \times \sin\phi_v + \dot{\psi}_f \times \cos\phi_v\} \times v_{y,v} + e_1 \end{aligned} \tag{2.25}$$

$$\begin{aligned} v_{x,m} &\approx v_{x,f} \\ &= x_1 + e_2, \end{aligned} \tag{2.26}$$

  For the longitudinal motion, an accelerometer and wheel speed sensor are used. Finally, the relationship between the measurements and the states are clearly found in equations (2.25) and (2.26).

- Lateral dynamics
  Lateral dynamics for the vehicle including the bicycle model and roll dynamics can be defined as follows. Translational and angular motion are also considered.

$$
\begin{aligned}
\dot{x}_1 = \quad \dot{v}_{y,f} \quad &= a_{y,f} - \dot{\psi}_f \times v_{x,f} \\
\dot{x}_2 = \quad \ddot{v}_{y,f} \quad & \\
\dot{x}_3 = \quad \ddot{\psi}_f \quad &= \frac{1}{I_{zz}}\{l_f \times (F_y^f - m_f \times g \times \sin\phi_r \times \cos\theta_r) \\
& \qquad -l_r \times (F_y^r - m_r \times g \times \sin\phi_r \times \cos\theta_r)\} \\
\dot{x}_4 = \quad \dot{\phi}_r \quad & \\
\dot{x}_5 = \quad \dot{\phi}_v \quad & \\
\dot{x}_6 = \quad \ddot{\phi}_v \quad &= \frac{1}{(I_{xx} + m_s h_R)^2}\{-k_\phi \phi_v - c_\phi \dot{\phi}_v \\
& \quad +m_s h_R(\ g \times \cos\theta_r \times \sin(\phi_v + \phi_r) + a_y \times \cos\phi_v)\} - \ddot{\phi}_r \\
& \approx \frac{1}{(I_{xx} + m_s h_R)^2}\{-k_\phi \phi_v - c_\phi \dot{\phi}_v \\
& \quad +m_s h_R(\ g \times \cos\theta_r \times \sin(\phi_v + \phi_r) + a_y \times \cos\phi_v)\}
\end{aligned}
\tag{2.27}
$$

  Similar to the longitudinal motion, $\dot{x}_2$ and $\dot{x}_4$ are considered equal to zero. Also, $\dot{x}_5$ is a constant value, that is only affected by x_6 and the process noise.
  Relevant measurements are lateral acceleration and yaw rate. These values can be defined with lateral dynamics states as follows:

$$
\begin{aligned}
a_{y,m} &= \dot{v}_{y,v} + \dot{\psi}_v \cdot v_{x,v} - \dot{\phi}_v \cdot v_{z,v} \\
&\approx (\dot{v}_{y,f} + h_R \dot{\phi}_v) - \{-\dot{\theta}_f \times \sin\phi_v + \dot{\psi}_f \times \cos\phi_v\} \times v_{x,f} \\
&\approx (\dot{v}_{y,f} + h_R \dot{\phi}_v) - \{-\dot{\theta}_r \times \sin\phi_v + \dot{\psi}_f \times \cos\phi_v\} \times v_{x,f} \\
&= (x_2 + h_R x_6) - \{-\dot{\theta}_r \times \sin x_5 + x_3 \times \cos x_5\} \times v_{x,f} + e_1
\end{aligned}
\tag{2.28}
$$

$$
\begin{aligned}
\dot{\psi_m} &= -\dot{\theta}_f \sin\phi_v + \dot{\psi}_f \cos\phi_v \\
&\approx -\dot{\theta}_r \sin\phi_v + \dot{\psi}_f \cos\phi_v \\
&= -\dot{\theta}_r \sin x_5 + x_3 \cos x_5 + e_2
\end{aligned}
\tag{2.29}
$$

  Finally, the relationship between the measurements and the states is clearly found in equations (2.29) and (2.30).

2.5 Estimator Design

In this section, the UKF approach for the estimator and its observability is described. Longitudinal and lateral vehicle dynamics equations are compactly written as the continuous state space model :

$$\begin{aligned} \dot{x}_{long}(t) &= F_{long}(x_{long}(t), u_{long}(t), w_{long}(t)) \\ \dot{w}_{long}(t) &= 0 \\ y_{long}(t) &= G_{long}(x_{long}(t), \dot{x}_{long}(t), u_{long}(t)) \end{aligned} \tag{2.30}$$

$$\begin{aligned} \dot{x}_{lat}(t) &= F_{lat}(x_{lat}(t), u_{lat}(t), w_{lat}(t)) \\ \dot{w}_{lat}(t) &= 0 \\ y_{lat}(t) &= G_{lat}(x_{lat}(t), \dot{x}_{lat}(t), u_{lat}(t)) \end{aligned} \tag{2.31}$$

As shown in the previous section, some states that need to be estimated have been defined with constant values such as:

$$\begin{aligned} w_{long}(t) &= [\theta_r, \dot{\theta}_r]^T \\ w_{lat}(t) &= [\phi_v, \dot{\phi}_v, \phi_r]^T \end{aligned}$$

Note that the time derivative of w is zero.
Using Euler forward discretization, the discretized state space representation of the continuous model is :

$$\begin{aligned} x_{long}(k+1) &= x_{long}(k) + \tau_s \times F_{long}(x_{long}(k), u_{long}(k), w_{long}(k)) + v_{long}(k) \\ w_{long}(k+1) &= w_{long}(k) + r_{long}(k) \\ y_{long}(k) &= G_{long}(x_{long}(k), \dot{x}_{long}(k), u_{long}(k)) + e_{long}(k) \end{aligned} \tag{2.32}$$

$$\begin{aligned} x_{lat}(k+1) &= x_{lat}(k) + \tau_s \times F_{lat}(x_{lat}(k), u_{lat}(k), w_{lat}(k)) + v_{lat}(k) \\ w_{lat}(k+1) &= w_{lat}(k) + r_{lat}(k) \\ y_{lat}(k) &= G_{lat}(x_{lat}(k), \dot{x}_{lat}(k), u_{lat}(k)) + e_{lat}(k) \end{aligned} \tag{2.33}$$

These state space equations can be summarized to be the representative equations for a dual-UKF:

$$\begin{aligned} s &= [x_{long}, w_{long}, x_{lat}, w_{lat}]^T \\ s(k+1) &= s(k) + \tau_s \times F(s(k), u(k), w(k)) + v(k) \\ &= T(s(k), u(k), w(k)) + v(k) \end{aligned} \tag{2.34}$$

$$w(k+1) = w(k) + r(k) \tag{2.35}$$

$$d(k) = G(s(k), \dot{s}(k), u(k)) + e(k), \tag{2.36}$$

where τ_s is the sampling time, v and r are the process noises, and e is the measurement noise. The noises v, r and e are assumed to be white, stationary, and normally distributed

with zero mean. The state space equations are used for the estimation of the states s, and the disturbance term, w.

2.5.1 Dual Unscented Kalman Filter Approach

As implied from the previous section, the relationship between the vehicle states and the measurements can be clearly defined with the noise terms. Also, the UKF algorithms for the longitudinal and the lateral state estimations can be executed. Although some variables may be coupled with each other in the dual-UKF framework, by using the previous step's state estimation result for the coupled states, the dual-UKF framework can be decoupled.
The basic concept of this framework is similar to the research of Sanghyun Hong and Chan Kyu Lee [58]. Also, the following explanation of the UKF approach has been referenced from Hong [58], Julier [57] and Wan [67]. The main advantages of the UKF approach are that it has a second-order accuracy for the nonlinear dynamics system, and its implementation is simplified using the Unscented Transformation (UT), as shown in Table 2.1. The UT conserves nonlinearity of the system and measurement dynamics through the statistics of a random vector.

Table 2.1: Scaling Factors and Weights

$\lambda = \alpha^2(L+\kappa) - L$
$W_0^{(m)} = \frac{\lambda}{L+\lambda}$
$W_0^{(c)} = \frac{\lambda}{L+\lambda} + 1 - \alpha^2 + \beta$
$W_i^{(m)} = W_i^{(c)} = \frac{1}{2(L+\lambda)}, \quad i = 1, ..., 2L$

The procedure of the UKF approach consists of two stages: prediction before the measurements and update after the measurements. It's procedure is the same as that of the traditional Kalman Filter approach, except that the UT is used to calculate the covariance of the state. The detailed algorithm has been skipped in this section.

2.5.2 Observability Analysis

This section demonstrates that the disturbance w can be uniquely determined with the measurement d. Since the state space model is a nonlinear function in terms of w and d, it will be presented that w is locally observable with the measurement $d = G(s, \dot{s}, u)$.
By investigating the rank of an observability codistribution matrix, the local observability can be proven as described in [30][48]. If the observability codistribution matrix has full rank, w is said to be locally observable.

Define a vector $\mathcal{O}$ consisting of the measurement vector d and its time derivative $\dot{d}$,

$$\mathcal{O} := \begin{bmatrix} G \\ \dot{G} \end{bmatrix}.$$

The observability codistribution matrix is defined as the Jacobian of $\mathcal{O}$ with respect to the parameter vector w,

$$\nabla\mathcal{O} = \left[\tfrac{\partial\mathcal{O}}{\partial w_1}, \cdots, \tfrac{\partial\mathcal{O}}{\partial w_n}\right].$$

For the longitudinal UKF algorithm, the observability codistribution matrix can be determined as the following:

$$\begin{aligned} \nabla\mathcal{O}_{long} &= \left[\tfrac{\partial\mathcal{O}_{long}}{\partial\theta_r}, \tfrac{\partial\mathcal{O}_{long}}{\partial\dot{\theta}_r}\right] \\ &= \begin{bmatrix} g\cos\phi_r\cos\theta_r & \sin\phi_v \times v_{y,f} \\ 0 & 0 \\ \frac{\partial\dot{a}_x}{\partial\theta_r} & \frac{\partial\dot{a}_x}{\partial\dot{\theta}_r} \\ g\cos\phi_r\cos\theta_r & 0 \end{bmatrix}. \end{aligned}$$

The $\frac{\partial\dot{a}_x}{\partial\theta_r}$ and $\frac{\partial\dot{a}_x}{\partial\dot{\theta}_r}$ terms have the input information term, u. If the input u is not zero, the codistribution matrix has full column rank. This proves the local observability of w based on d. For the lateral local observability, the same theory can be applied using the following vector. As before, the Jacobian is full column rank and the lateral disturbance can be locally estimated.

$$\begin{aligned} \nabla\mathcal{O}_{lat} &= \left[\tfrac{\partial\mathcal{O}_{lat}}{\partial\phi_v}, \tfrac{\partial\mathcal{O}_{lat}}{\partial\dot{\phi}_v}, \tfrac{\partial\mathcal{O}_{lat}}{\partial\phi_r}\right] \\ &= \begin{bmatrix} 0 & h_R & -g\cos\theta_r\cos\phi_r \\ -\dot{\theta}_r\cos\phi_v - \dot{\psi}_f\sin\phi_v & 0 & 0 \\ \frac{\partial\dot{a}_y}{\partial\phi_v} & \frac{\partial\dot{a}_y}{\partial\dot{\phi}_v} & \frac{\partial\dot{a}_y}{\partial\phi_r} \\ 0 & 0 & 0 \end{bmatrix} \end{aligned}$$



Figure 2.8: Test Vehicle(Hyundai AZERA)

2.6 Vehicle Model Validation

In order to achieve good disturbance estimation results, all vehicle states and parameters should have accurate values. In this section, vehicle parameters related to longitudinal and lateral vehicle dynamics are verified using real vehicle test results. Then, vehicle state estimation results, except for road disturbance, are validated on a flat road.
The test vehicle, Hyundai AZERA, is pictured in Figure 2.8. Also, for the measurement of reference values, OTS (Oxford Technical Solutions) RT2002 with a GPS base-station is used, as shown in Figure 2.9. The OTS RT2002 system is comprised of a differential GPS, an IMU (Inertial Measurement Unit) and a DSP (Digital Signal Processor).

2.6.1 Longitudinal Vehicle Model Validation

In equations (2.14) to (2.18), there are some fixed parameters and variant parameters under different conditions. Using the test vehicle, essential parameters for the longitudinal vehicle dynamics have been verified.

- Mechanical Efficiency
  Mechanical efficiency can be shown in equation(2.15). As shown in the upper figure of Figure 2.10, The car was driven with constant gas pedal manipulation. Also, engine torque and gear ratio information is transmitted to the vehicle information network (CAN - Controller Area Network). From the information, the mechanical efficiency could be estimated by comparing the measured values and the calculated values of the vehicle acceleration and velocity. The results are shown in the bottom graph of Figure 2.10. The estimated value of mechanical efficiency is 0.9 at 6th gear stage and 0.85 at



Figure 2.9: Reference Measurement Unit - GPS/IMU

4th and 5th gear stages.

- Air Drag Force and Rolling Resistance
  As shown in equations (2.14) and (2.17), there exist an air drag force and rolling resistance. Parameters for the air drag force are fixed values and known for the test vehicle. So, only the rolling resistance force was needed to be verified. The vehicle was driven in the neutral gear stage to avoid the engine torque's effect on the vehicle's acceleration. Also, the brake pedal was not pressed, so the vehicle exhibited a "coast down" condition under the air drag resistance and the rolling resistance. As shown in Figure 2.11, the rolling resistance force was calculated at 191N. Although the value depends on the vehicle speed, a fixed value was used.

- Brake Gain
  As shown in equation (2.16), brake gain, K_b should be estimated. The vehicle was driven in neutral gear stage to avoid engine braking when the brake pedal was pressed. When the brake pedal was pressed, the master cylinder brake pressure reached 40bar, as shown in the Figure 2.12. Then, the measured values and the calculated values, determined using equations (2.14)and (2.16) of the acceleration and the velocity, were compared. As a result, the brake gain was found to be 210N/bar. On the bottom graph of Figure 2.12, the red line shows simulation results using the validated brake gain.

- Combined Driving
  Under the combined driving condition consisting of acceleration and braking, the model

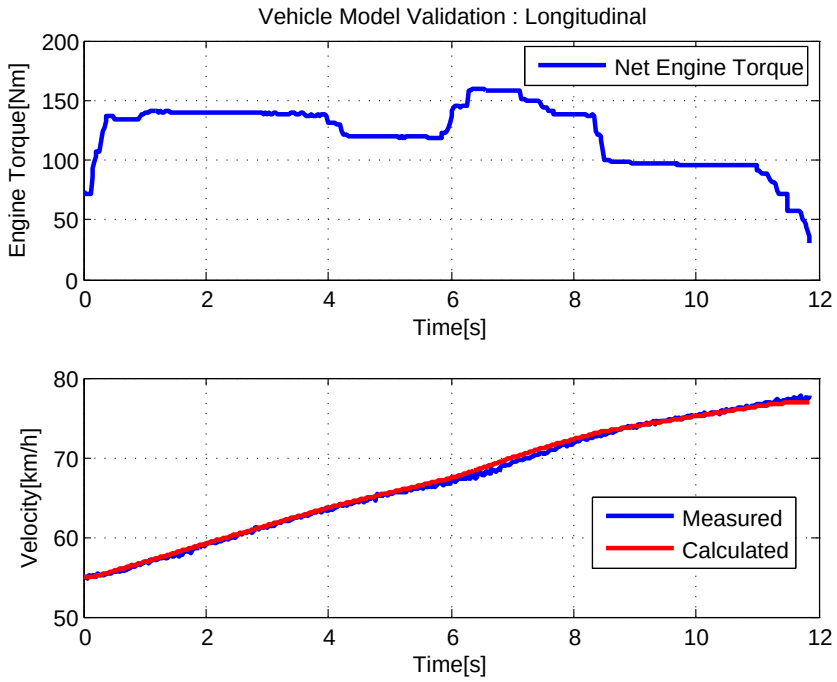

Figure 2.10: Vehicle Model Validation - Mechanical Efficiency

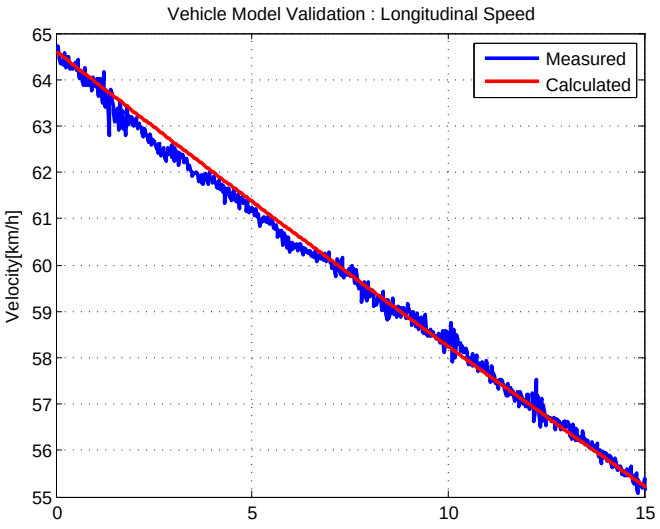

Figure 2.11: Vehicle Model Validation - Air Drag Force and Rolling Resistance

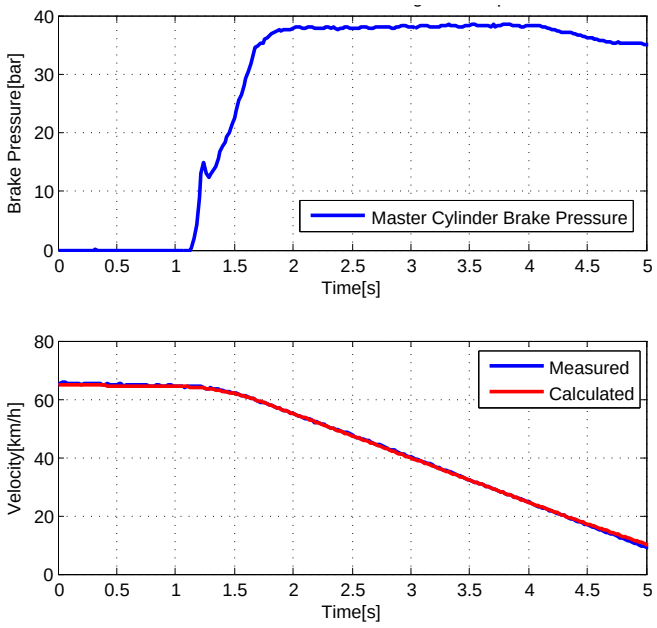

Figure 2.12: Vehicle Model Validation - Brake Gain

validation results using the estimated vehicle parameters are shown in Figure 2.13. The calculated vehicle motion using the validated vehicle parameters is nearly the same as the measured values. Consequently, the validated parameters are reasonable to be used for the vehicle dynamics estimator.

2.6.2 Lateral Vehicle Model Validation

For lateral vehicle dynamics, equations (2.19) to (2.22) were used. For lateral vehicle model validation, only the lateral tire side-slip coefficients, C_f and C_r needed to be determined, since the other values were fixed kinematic values. The tire coefficient of the linear lateral tire model depends on the vehicle's suspension, tire, and road characteristics. In order to get the value, the vehicle was driven at a constant speed and made a double lane change. Comparing the measured values and the calculated values (using equation(2.19) to (2.21)) for the lateral acceleration and yaw rate, C_f and C_r were found to be 63000N/rad and 70000N/rad, respectively. As shown in Figure 2.14, when the validated parameters were used, the simulation results of the lateral vehicle dynamics matched the measurement values.

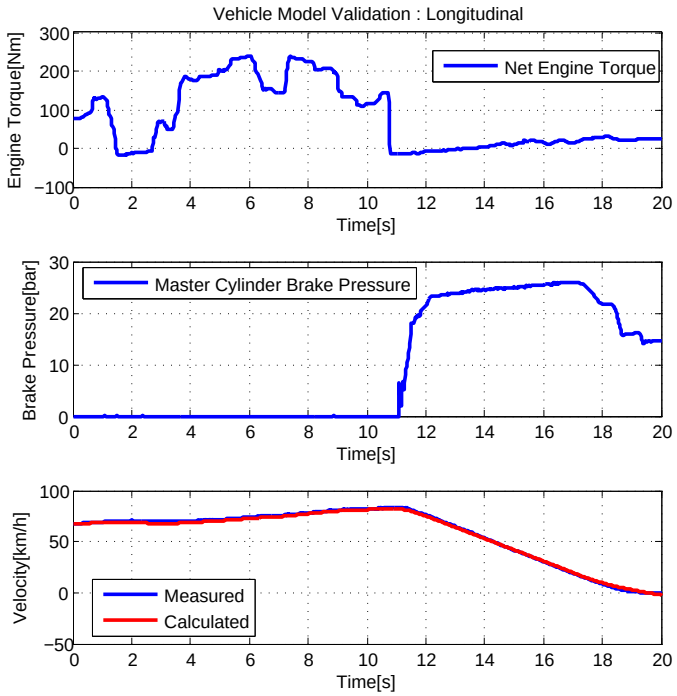

Figure 2.13: Vehicle Model Validation - Combined Longitudinal Dynamics

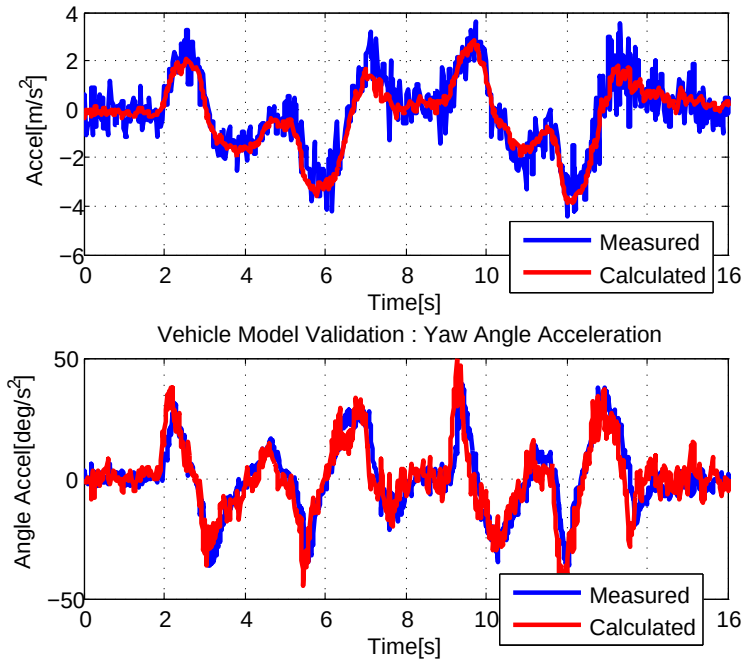

Figure 2.14: Vehicle Model Validation - Lateral Dynamics



Figure 2.15: Vehicle Test Facility - Hyundai California Proving Ground

2.7 Vehicle Test Results

For vehicle testing, the Hyundai AZERA is used with conventional vehicle sensors for estimation and measurement. The OXT RT2002 GPS/IMU is used for reference values only. In this section, the results of validation testing on a special testing ground for the basic state estimation logic is presented. Then, results from tests on public roads are presented.

2.7.1 Essential Vehicle State Estimation Validation

In the longitudinal and lateral UKF estimation logics, the longitudinal road gradient and the lateral road bank angle are the states to be estimated. These two states are considered as part of the disturbance term of the vehicle dynamics. The dual-UKF algorithms' main purpose is to estimate these two values as states in real-time. Before verifying the logic, the other states, except the road disturbances, are validated. This validation process was performed on a special test track where the road is nearly flat. A straight test track of the Hyundai California Proving Ground (CPG) as shown in Figure 2.15, was used. Figure 2.16 shows the state estimation results using the dual-UKF algorithm. The test vehicle was driven on the flat ground and maneuvered several double lane changes with brake manipulation at the end. For the reference measurement, RT2002 was used. The very top graphs shows the steering input of the test scenario. The second and third graphs show very good estimation results for longitudinal and lateral velocity, respectively. These two velocity terms can also be used for calculation of vehicle side-slip, which is one of the main dynamic behaviors of the vehicle. The side-slip angle can be defined as follows,

$$\beta := \tan^{-1} \frac{v_y}{v_x} \tag{2.37}$$

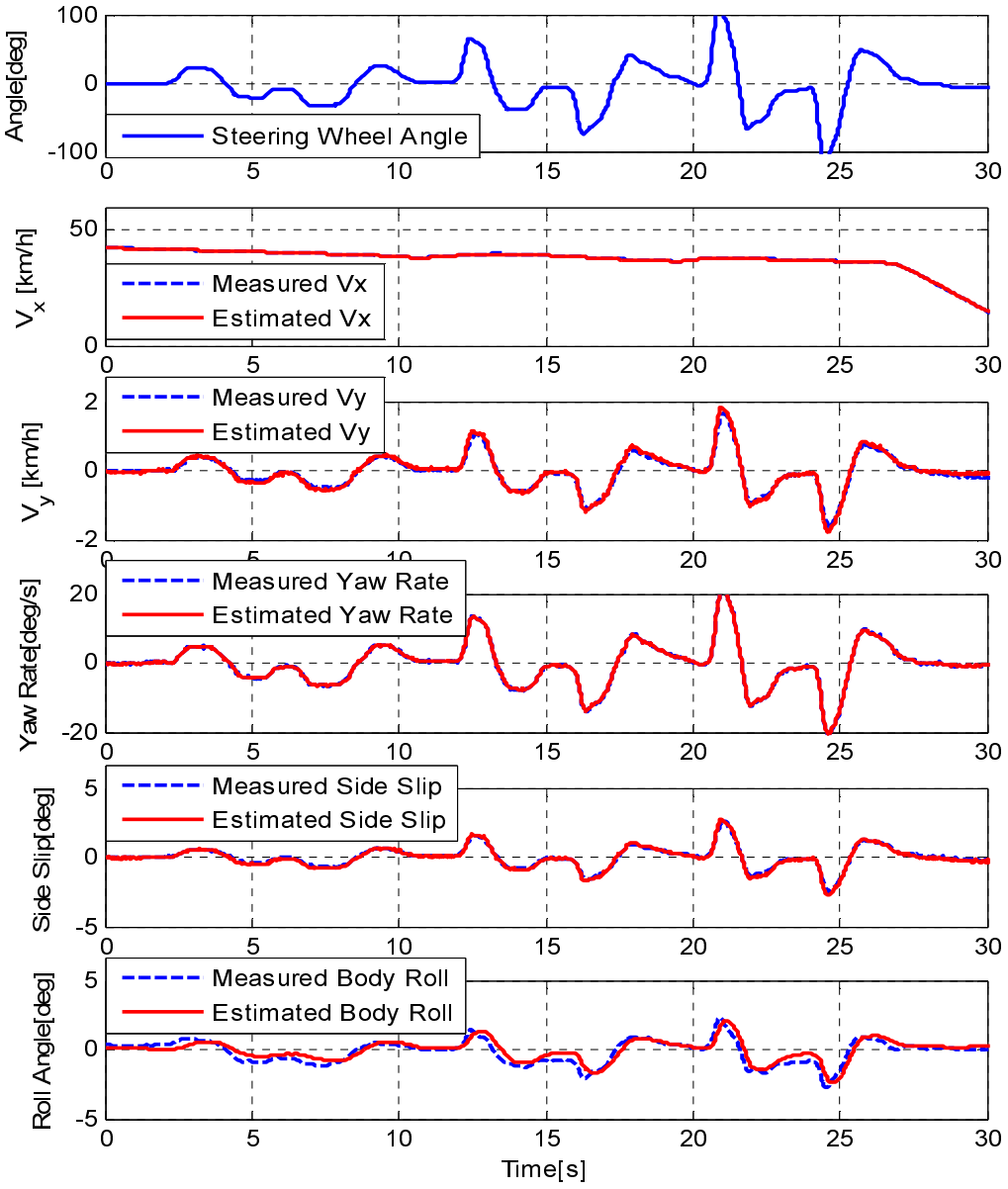

Figure 2.16: Vehicle State Estimation Results

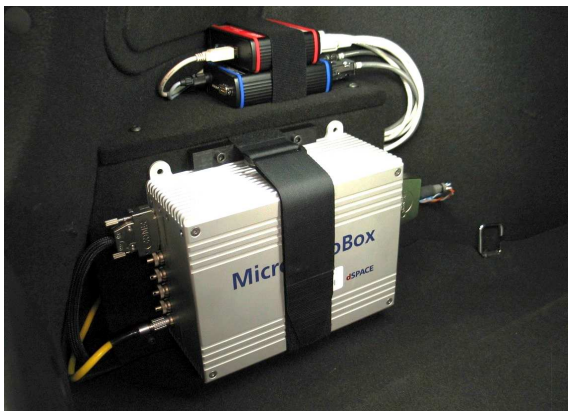

Figure 2.17: dSpace Microautobox

In the fourth graph, the estimated side-slip angle is very similar to the measurement values. Also, the fourth graph shows the estimation results of yaw rate. The estimated results show the vehicle's lateral motion accurately. The bottom graph shows the estimated body roll angle. The roll dynamics of the vehicle as shown in the equation (2.23) is also included. In the estimation graph, the estimated value has a slight delay compared to the measurement value, while the magnitudes of both estimated and measured values are nearly the same. However, since the roll angle is very small under normal driving conditions, the estimation delay does not significantly affect the estimation of road bank angle. Therefore, we can conclude that the estimator, without the longitudinal road gradient and the road bank angle, exhibits very good performance.

2.7.2 Vehicle Test on a Public Road

After the validation tests of the essential state estimators at the special proving ground, CPG, the logic is tested on public roads to estimate the road longitudinal gradient and bank angle. For logic implementation in real-time, a dSpace Microautobox was used. It was installed in the trunk as shown in Figure 2.17, and the logic was run every 0.02 seconds.

Figure 2.18 shows a public road where the estimator was validated in real-time. The road is a part of highway I-580 near Berkeley in California, USA. There are some curvy roads and changes in altitude as shown in Figure 2.19. Due to the curvy roads, road bank angle can be found using road information from the policy of Highway Design Manual[1]. Also, due to the altitude change, the longitudinal road gradient can be detected.

Figure 2.20 and 2.14 show vehicle test results for each of the longitudinal and lateral estimators. The test was performed for about 400 seconds. As shown in the top graph of Figure 2.20, the vehicle was driven at about 100km/h and the brake pedal was pressed twice, followed by acceleration to recover speed. The second and third graphs show engine torque, which were gathered from the Engine Management System and brake pressure, which was obtained from the Electrical Brake System. Under this driving condition, the longitudinal

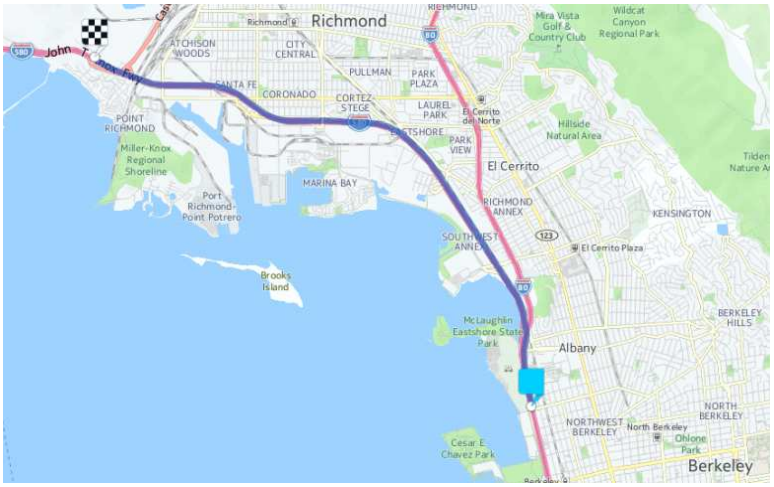

Figure 2.18: Vehicle Test Route

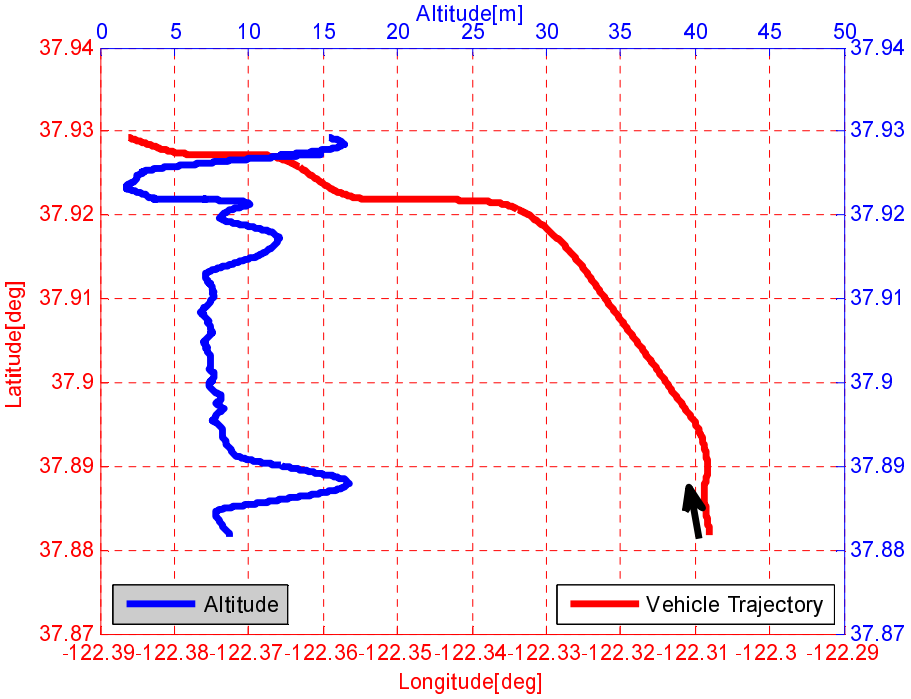

Figure 2.19: Vehicle Test Route - Road Shape

road gradient is estimated as shown in the fourth graph. The value perfectly estimates the measured value from the RT2002. The very bottom graph shows the estimator's performance. The mean value of the estimation error is 0.09 degree, and the standard deviation is 0.39 degree. It can be concluded from the results that the longitudinal road gradient estimator has good performance under real road conditions.

The top graph of 2.14 shows the steering wheel angle, and the second graph shows the estimated body roll angle and road bank angle. As shown in the graph, body roll angle is very small under normal driving conditions, as expected. The third graph shows the comparison between the measured values and the estimated values of the summation of the road bank angle and the body roll angle. Since the reference measurement equipment RT2002 is installed at the vehicle body, the equipment can only measure the combined body roll and road bank angle. As a result, only the combined values can be analyzed. The estimator very accurately estimates road bank angle changes. The bottom graph shows estimation error whose mean is 0.08 degrees and the standard deviation is 0.6 degrees. Therefore, we conclude that the lateral road bank angle estimator can extract accurate road bank angle in real-time on general public roads. Finally, the longitudinal and lateral estimators are executed simultaneously in real-time.

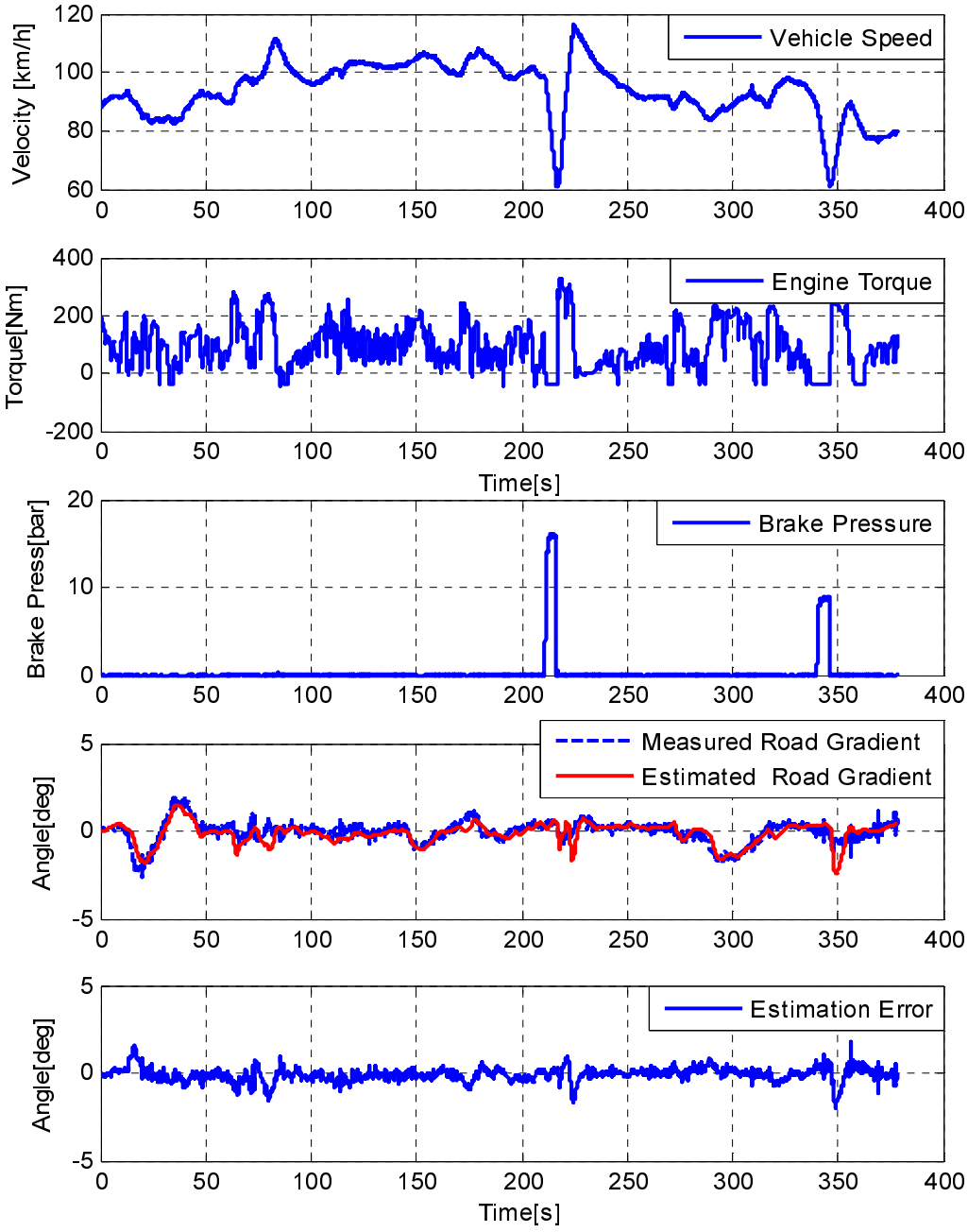

Figure 2.20: Vehicle Test Results - Road Gradient

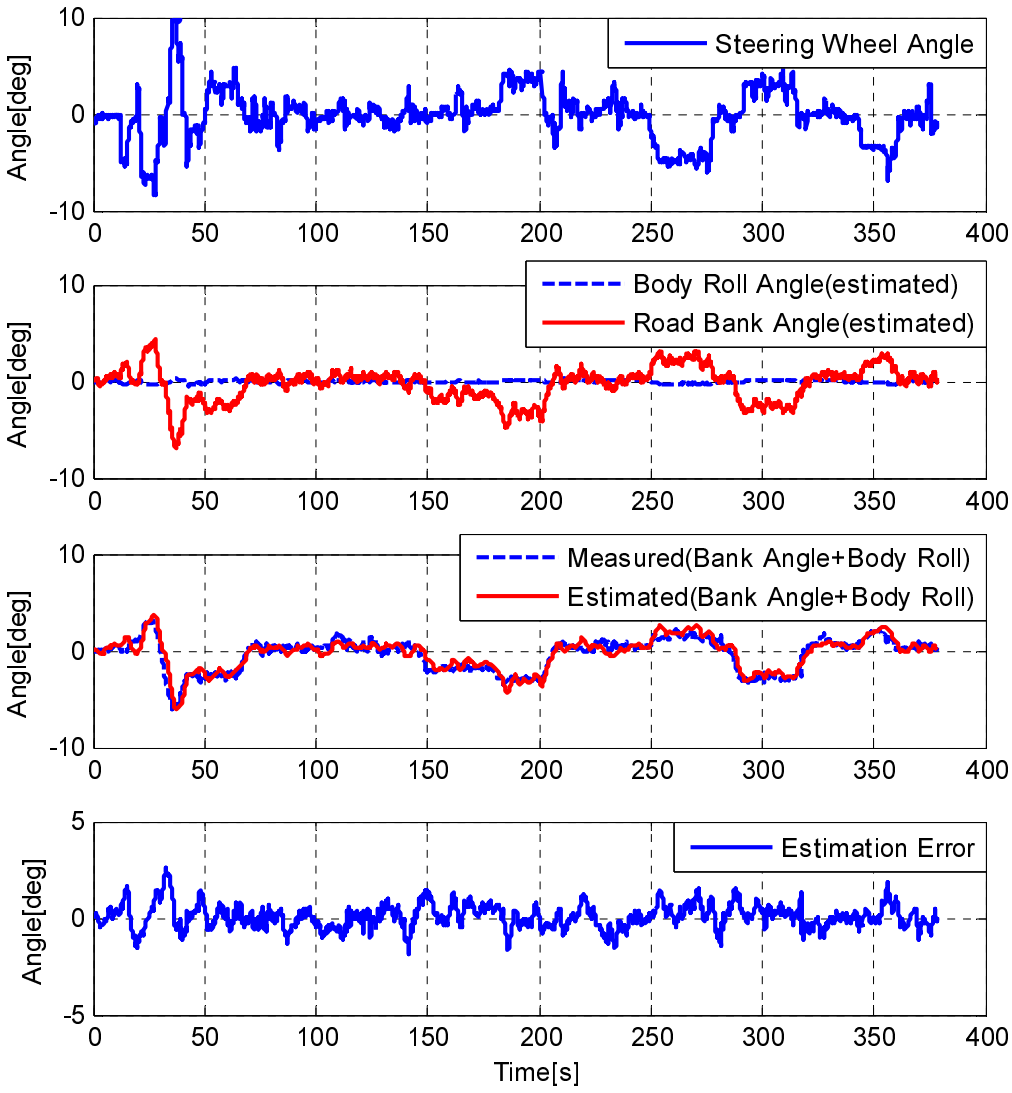

Figure 2.21: Vehicle Test Results - Bank Angle

2.8 Conclusion

This chapter proposed a kinematic relationship between the road shape and sensor measurements using several coordinate systems. All measurements were gathered at the vehicle body using only conventional vehicle sensors. Utilizing the vehicle longitudinal and the lateral dynamics, the longitudinal road gradient and the lateral road bank angle were estimated simultaneously. In order to preserve nonlinearity of the kinematics and dynamics, the dual-UKF approach was suggested. After verifying the proposed estimation approach on a special proving ground, the estimators were tested on public roads. The results indicate that the estimator accurately extracts the longitudinal road gradient and the bank angle simultaneously on public roads in real-time.

Chapter 3

Lateral Motion Controller : Lane Keeping Controller associated with Road Disturbance Estimator

3.1 Introduction

In this chapter, a lateral vehicular motion control logic is presented. A lane keeping control system is a very basic function of an autonomous vehicle or a driver assistance system. In order to improve the control performance of the system, disturbance terms such as road gradient should be considered. For this purpose, a model-based controller can easily take account of these disturbances. This means that a vehicle dynamics model including the disturbance term should be considered in the controller design. The control logic in this chapter is associated with the disturbance estimator, which was presented in the previous chapter. In this chapter, the motivation for a new vehicle dynamics model is introduced and then a new control law is presented. Then, the new model and the control law is presented in detail. Finally, the simulation and vehicle test results are described.

3.1.1 Motivation for a New Vehicle Dynamics Model

A dynamic vehicle model has been used for the lateral control of an autonomous vehicle such as a lane keeping system or other driver assistance systems [55][65]. The dynamics equation for the lateral motion of the vehicle uses Newton's laws. In the dynamics equation, the tire side-slip angle, which is defined as an angle difference between the orientation of the tire and the direction of the velocity vector of the wheel, is used for lateral tire force calculation. This is defined as a linear tire model. The tire side-slip angle is generated by the driver's steering manipulation or by the yaw rate generated under certain driving conditions. Therefore, many lateral control systems are designed to operate even if there exists high speed, large steering angles or sudden yaw rate variations. This is the reason why the dynamic model

has been widely used for lateral control logics. Dynamic models use a nonlinear tire model such as Pacejka or Fiala tire model, but including these linear or nonlinear tire models in the vehicle dynamics equations has its disadvantages. It is computationally expensive, and any tire model becomes singular at low vehicle speeds. The latter happens because, in the vehicle dynamics, vehicle side slip, which is defined as a ratio of lateral vehicle velocity over longitudinal vehicle velocity, is included. This disadvantage prohibits the use of the lateral controller at low speeds such as urban driving or in stop-and-go situations.
The kinematic vehicle model is not derived from Newton's laws of motion but from the Ackermann steering geometry. Because the kinematic model is derived under the assumption that there is no tire slip angle, it is reliable when the velocity vector of each wheel is in the direction of the wheel. This is the reason why the kinematic model has been used for low speed situations such as smart parking assist system with limited tire side-slip. But, at higher speeds, vehicle side-slip can easily be generated, and this phenomenon violates the assumption of no side-slip of tire. Therefore, the kinematic model cannot represent the exact vehicle motion at high speeds.
Due to these reasons, prior research has conventionally used a kinematic vehicle model at low speeds and a dynamic vehicle model at high speeds. For an autonomous vehicle, two separate controllers for low and high speeds should be used and tuned. A comparison between these two models is rarely found [6][37]. In the following section, the representative vehicle model for both low and high speeds will be suggested.

3.1.2 Motivation for a New Control Law

To make more efficient and precise control logic, certain issues should be considered:

- Nonlinear System Dynamics
  The simplest control law for the lane keeping system is a PID control approach. By using a linearized model for nonlinear system dynamics, a simple state feedback control law can be adopted. Even when using the Model Predictive Control (MPC) approach, an iterative linearization model is used for the control law.[10][21] However, in order to keep the nonlinearity of the system dynamics, Sliding Model Control (SMC) can be one of the simplest control laws to choose. Furthermore, MPC logic can easily be set up as a nonlinear control logic.

- Cheap Computational Cost
  MPC approach is very easy to construct while considering constraints and nonlinear system dynamics. However, it requires very expensive computational cost. As a result, various computationally efficient methods such as Explicit MPC are suggested [7][56]. Compared with MPC approach, the SMC approach has a distinctly low computational cost.

- Disturbance Consideration
  In order to include the disturbance term in the controller, the methods based on SMC

and MPC are suggested. In the Sliding Mode Controller, a Disturbance Observer can be included to reject not only the mismatched disturbance but also the other disturbances [39]. In the MPC formulation, the disturbance can be considered as a stochastic term [11] or a band [22] in order to guarantee robustness of the control performance to the disturbance.

- Constraint Setting
  In designing an effective controller, constraints are crucial elements to consider in order to guarantee the stability and performance for the real system. Using a SMC approach, a state constraint algorithm was suggested [34], but it does not consider the control input constraint. Using the MPC approach, state and input constraints can be easily included in the optimal cost problem.

Therefore, in order to make a more efficient and robust controller, nonlinear system dynamics, cheap computational cost and robustness to disturbances should be considered in the control law.

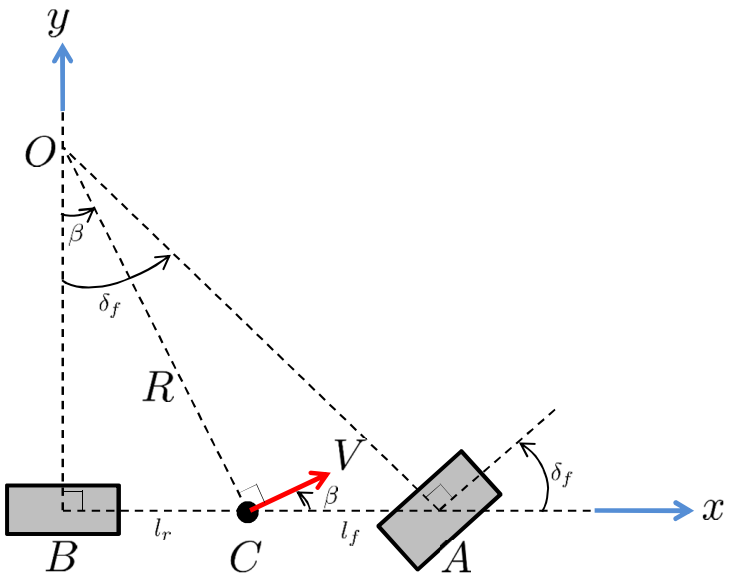

Figure 3.1: Kinematic Model of Lateral Vehicle Motion

3.2 New Lateral Vehicle Dynamics Model

In the beginning of this chapter, some limitations using kinematic and dynamic vehicle models for lateral motion were introduced. In this chapter, simulation results will show such limitations when the models are used to describe lateral vehicle motion. Then, in order to overcome the limitation, a steady state dynamic vehicle model will be derived. The new vehicle model will be used for the derivation of error dynamics for tracking of the desired lane path.

3.2.1 Current Vehicle Model of Lateral Vehicle Motion and Its Limitation

There are two types of vehicle models to describe the vehicle's lateral motion.

- Kinematic Model
  This model, as shown in Figure 3.1, describes a mathematical description of the vehicle motion without the tire force effects and tire slip. The model only presents the

geometric movement of the vehicle. The representative equations are,

$$\begin{aligned}\dot{x} =& V\cos(\psi+\beta)\\ \dot{y} =& V\sin(\psi+\beta)\\ \dot{\psi} =& \frac{V}{l_r}\sin(\beta)\\ \beta =& \tan^{-1}(\frac{l_r}{l_f+l_r}\tan(\delta_f)),\end{aligned} \tag{3.1}$$

where δ_f is front tire's steering angle. $\dot{x}$, $\dot{y}$, $\dot{\psi}$ and β are longitudinal velocity, lateral velocity, yaw rate and vehicle side slip angle, respectively. This motion is generated by front steering, and we assume that the front tire moves perfectly along the steering angle without tire side-slip. Therefore, this model has two main problems. At higher speeds over 40 km/h, the tire slip increases and the model does not represent the vehicle's lateral motion accurately. Also, under the road bank angle, there exists a lateral gravitational force on the vehicle. Since the model does not consider lateral forces, the bank angle effect cannot be included in the model.

- Dynamic Model
  The dynamic model, as shown in Figure 2.6, describes the tire forces resulting from tire side-slip due to difference between the vehicular direction and the tire direction. The lateral tire force can be described with the equations (2.20) and (2.21) in the previous chapter. This linear tire model is widely used although there are many other nonlinear or empirical tire models, such as Magic Formula and Dugoff model. The lateral vehicle motion can be derived for vehicle side-slip angle and yaw rate.

$$\begin{aligned}\dot{\beta} =& -\dot{\psi}+\frac{2C_\alpha^f}{mV_x}\left\{\delta_f-\beta-\frac{l_f\dot{\psi}}{V_x}\right\}+\frac{2C_\alpha^r}{mV_x}\left\{-\beta-\frac{l_r\dot{\psi}}{V_x}\right\}\\ I_z\cdot\ddot{\psi} =& l_f\times 2C_\alpha^f\left\{\delta_f-\beta-\frac{l_f\dot{\psi}}{V_x}\right\}-l_r\times 2C_\alpha^r\left\{-\beta-\frac{l_r\dot{\psi}}{V_x}\right\},\end{aligned} \tag{3.2}$$

  where β, $\dot{\psi}$ and I_z are vehicle side-slip, yaw rate and moment of inertia along the z-axis, respectively. This model has good accuracy at high vehicle speeds, but due to the denominator term, V_x, in the equations, the model exhibits a singularity at low speeds.

- Validation Results for the kinematic and dynamic models
  In order to validate the vehicle models, Carsim, a vehicle dynamics software, is used for simulation. Figures 3.2 to 3.4 show simulation results under fast and slow steering maneuvers using both kinematic and dynamics vehicle models. The left and right graphs show the results for kinematic and dynamic vehicle models, respectively. As shown

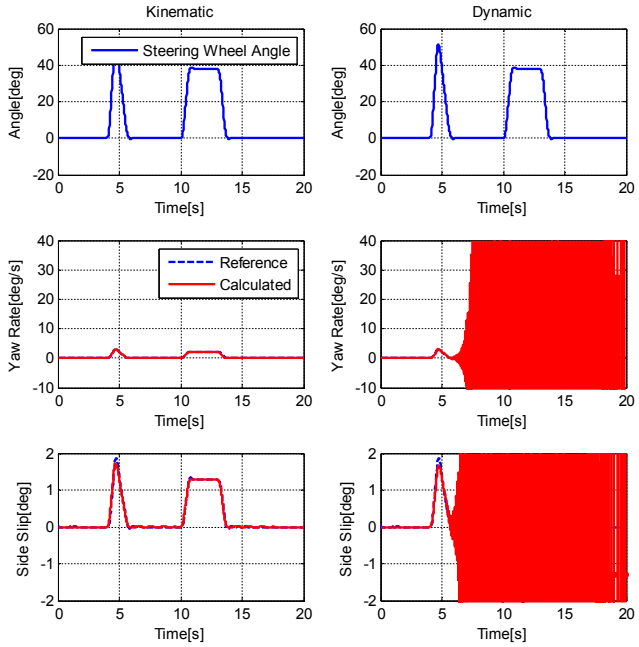

Figure 3.2: Vehicle Model Limitation - 20km/h

in Figure 3.2, at low speeds, the kinematic model shows good simulation performance compared to the Carsim results. On the other hand, using the dynamic model, there arises a chattering problem as described at the beginning of this chapter. As velocity increases, the dynamics vehicle model displays better performance than the kinematic model, as shown in the Figure 3.3. In Figure 3.4, the kinematic model's yaw rate and vehicle side-slip have very different values than those of the Carsim results. From these results, we can conclude that we cannot use any one of these vehicle model alone to cover the entire velocity range of a vehicle.

3.2.2 Steady State Dynamic Model

As mentioned in the previous section, we need to overcome two problems. First, the model should be applicable over all ranges of speed. Secondly, bank angle effect should be included in the dynamics. Starting from the dynamic vehicle model, bank angle effect is included in the last term, $-\frac{g\sin\phi_r}{V_x}$, in equation(3.3). However, the bank angle does not have an effect on yaw rate equation as shown in equation (3.4).

$$\dot{\beta} = -\dot{\psi} + \frac{2C_\alpha^f}{mV_x}\left\{\delta_f - \beta - \frac{l_f\dot{\psi}}{V_x}\right\} + \frac{2C_\alpha^r}{mV_x}\left\{-\beta - \frac{l_r\dot{\psi}}{V_x}\right\} - \frac{g\sin\phi_r}{V_x} \tag{3.3}$$

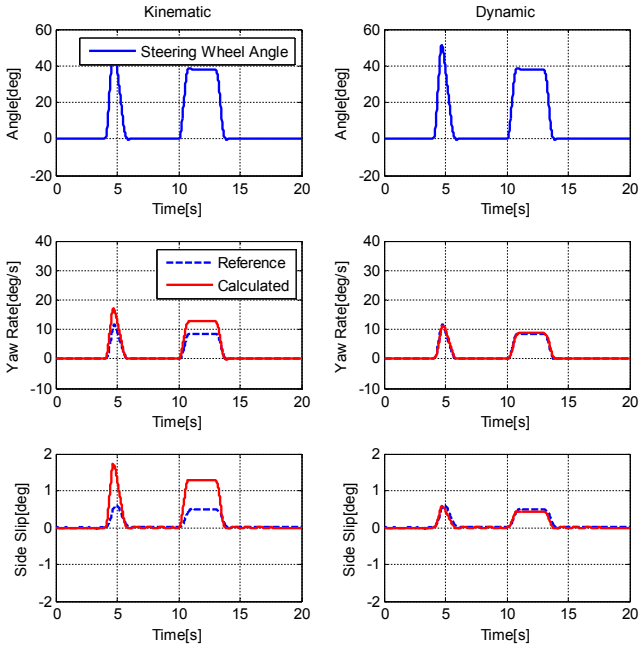

Figure 3.3: Vehicle Model Limitation - 60km/h

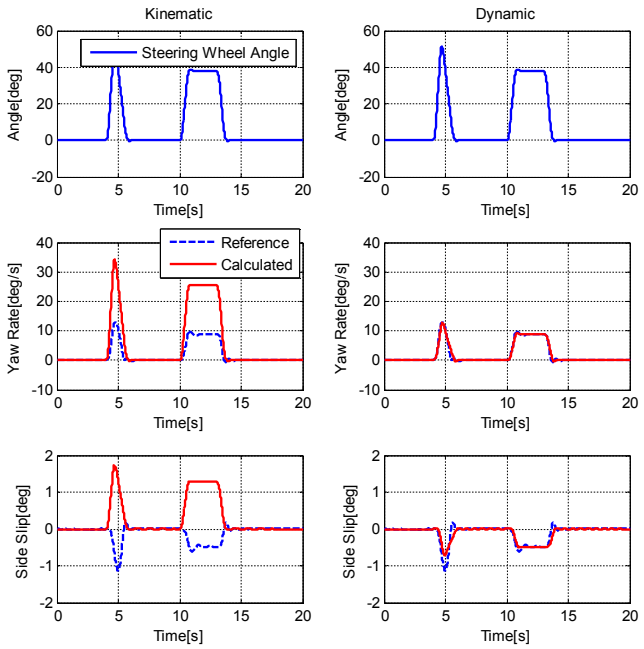

Figure 3.4: Vehicle Model Limitation - 120km/h

$$\begin{aligned} I_z \cdot \ddot{\psi} &= l_f \times F_y^f - l_r \times F_y^r \\ &= l_f \times 2C_\alpha^f \left\{ \delta_f - \beta - \frac{l_f \dot{\psi}}{V_x} \right\} - l_r \times 2C_\alpha^r \left\{ -\beta - \frac{l_r \dot{\psi}}{V_x} \right\} \end{aligned} \tag{3.4}$$

With the following steady-state assumptions:

$$\begin{aligned} \dot{\beta} &= 0 \\ \ddot{\psi} &= 0, \end{aligned}$$

equations (3.5) and (3.6) can be set up.

$$\left\{ mVx + \frac{2C_\alpha^f l_f - 2C_\alpha^r l_r}{V_x} \right\} \dot{\psi}_{ss} \quad +2(C_\alpha^f + C_\alpha^r)\beta_{ss} \quad = 2C_\alpha^f \times \delta_f - mg \sin \phi_r \tag{3.5}$$

$$\left\{ \frac{C_\alpha^f l_f^2 + C_\alpha^r l_r^2}{V_x} \right\} \dot{\psi}_{ss} \quad +(l_f C_\alpha^f - l_r C_\alpha^r)\beta_{ss} \quad = l_f C_\alpha^f \times \delta_f \tag{3.6}$$

From the equations, we derive the following solutions which can be called steady state dynamic motion.

$$\begin{aligned} \dot{\psi}_{ss} &= \frac{2C_\alpha^f l_f (C_\alpha^f + C_\alpha^r) \times V_x \times \delta_f}{mV_x^2 (l_r C_\alpha^r - l_f C_\alpha^f) + 2C_\alpha^f C_\alpha^r (l_f + l_r)^2} \\ &\quad - \frac{2C_\alpha^f (l_f C_\alpha^f - l_r C_\alpha^r) \times V_x \times \delta_f}{mV_x^2 (l_r C_\alpha^r - l_f C_\alpha^f) + 2C_\alpha^f C_\alpha^r (l_f + l_r)^2} \\ &\quad + \frac{V_x \times (lf C_\alpha^f - l_r C_\alpha^r) mg \sin \phi_r}{mV_x^2 (l_r C_\alpha^r - l_f C_\alpha^f) + 2C_\alpha^f C_\alpha^r (l_f + l_r)^2} \end{aligned} \tag{3.7}$$

$$\begin{aligned} \beta_{ss} &= \frac{2C_\alpha^f (l_f^2 C_\alpha^f + l_r^2 C_\alpha^r) \times \delta_f}{mV_x^2 (l_r C_\alpha^r - l_f C_\alpha^f) + 2C_\alpha^f C_\alpha^r (l_f + l_r)^2} \\ &\quad - \frac{C_\alpha^f l_f (mV_x^2 + 2l_f C_\alpha^f - 2l_r C_\alpha^r) \times \delta_f}{mV_x^2 (l_r C_\alpha^r - l_f C_\alpha^f) + 2C_\alpha^f C_\alpha^r (l_f + l_r)^2} \\ &\quad - \frac{(lf^2 C_\alpha^f + l_r^2 C_\alpha^r) mg \sin \phi_r}{mV_x^2 (l_r C_\alpha^r - l_f C_\alpha^f) + 2C_\alpha^f C_\alpha^r (l_f + l_r)^2} \end{aligned} \tag{3.8}$$

In the dynamic vehicle model, geometric differences between front and rear suspension systems can be shown as tire coefficients, C_α^f and C_α^r. These parameters have an effect on understeer or oversteer characteristics. Therefore, if we neglect these characteristics, neutral steer can be assumed with the following equation,

$$l_f C_\alpha^f = l_r C_\alpha^r. \tag{3.9}$$

Under this assumption, the steady-state dynamic equation can show the kinematic model's equations. First, using the assumption, the first term of the yaw rate equation, (3.7) can be

written as:

$$\dot{\psi}_{ss} \cong \frac{V_x}{L} \times \delta_f \tag{3.10}$$

The equation (3.9) perfectly matches the term of the kinematic model as shown in equation(3.10).

$$\dot{\psi}_{kinematic} = \frac{V_x}{L} \times \delta_f \tag{3.11}$$

Next, if we look at the side-slip equation, (3.8), the first term becomes

$$\beta_{ss} \cong \frac{l_r}{L} \times \delta_f \tag{3.12}$$

Thus, the equation (3.11) is shown to be the same as the kinematic model's side-slip in equation (3.12),

$$\beta_{kinematic} \quad = \quad \frac{l_r}{L} \times \delta_f. \tag{3.13}$$

Therefore, we can conclude that the steady-state dynamics equations show the kinematic model's motion under the assumption of neutral steer. Even though the assumption cannot be held at low speeds, the tire side-slip is small at low speeds. The small tire side-slip makes the neutral steer assumption feasible. As a result, the steady state dynamic model acts as a kinematic model at low speeds.
However, there are still two additional terms in the right side of the slip angle equation, (3.8). The second term shows the body side-slip due to tire slip:

$$\frac{m}{2(C_\alpha^f + C_\alpha^r)} \frac{V_x^2}{L} \times \delta_f. \tag{3.14}$$

The steady-state model can be treated as a dynamic model in the presence of tire side-slip. In other words, the model can be treated as a dynamic model at high speeds.
Also, the last term in equation (3.7) and (3.8) result from bank angle. Therefore, the steady-state dynamics model includes bank angle effect on the motion.
Consequently, the suggested steady-state model can be used over all vehicle speed ranges considering the bank angle effect. However, in the real system, vehicle response such as yaw rate and vehicle side-slip cannot be generated directly from steering manipulation. We need to consider a delay term from tire response to vehicle inertial response. So, in the lateral dynamics, a first order lag has been normally considered as follows.[14][32]

$$\dot{\psi} \quad = \quad \dot{\psi}_{ss} - \tau_v \times \ddot{\psi} \tag{3.15}$$

$$\beta \quad = \quad \beta_{ss} - \tau_v \times \dot{\beta} \tag{3.16}$$

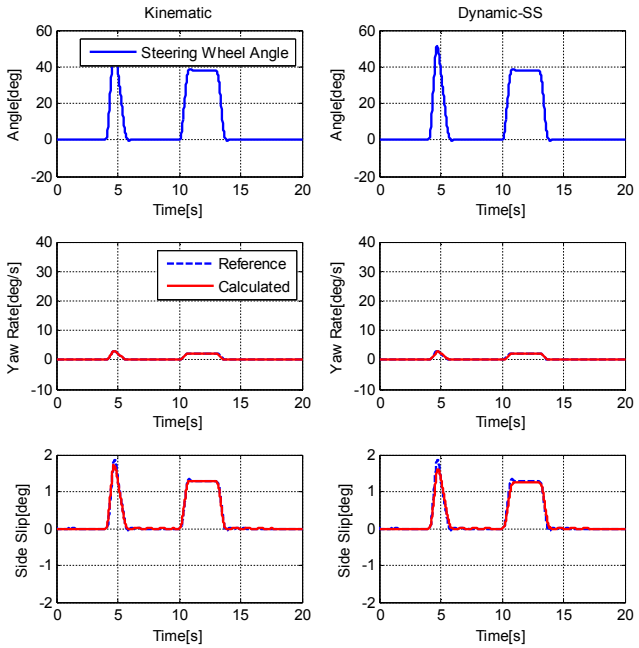

Figure 3.5: New Vehicle Model Validation - 20km/h

3.2.3 Simulation and Vehicle Test for Steady State Dynamic Model Validation

From Figures 3.2 to 3.4, issues with using kinematic and dynamic models were found. As shown in Figure 3.5, at low speeds, the steady state dynamics model (right graph) perfectly matches the kinematic model (left graph). Also, the results are the same with the Carsim results(highlighted in blue dotted line as a reference). Even at higher speeds (60km/h, 120km/h), as shown in Figure 3.6 and 3.7, the results are similar to the dynamics model's results. Lateral motions such as yaw rate and vehicle side-slip are very similar with Carsim simulation results.

For real vehicle validation tests, the Hyundai AZERA is used on the Hyundai California Proving Ground (CPG). Figure 3.8 shows the results. The vehicle is driven at 60km/h and then the driver made several double lane changes with the steering input as shown on the top graph. Real motion was measured by a GPS/INS equipment (RT2002) as a reference. The calculated graph represents the steady-state dynamic vehicle model including first order lag. As shown in the graph, the lateral motion using the proposed model perfectly matches the real vehicle motion. Based on the results, we conclude that the proposed steady-state dynamic vehicle model can be used for all ranges of speed.

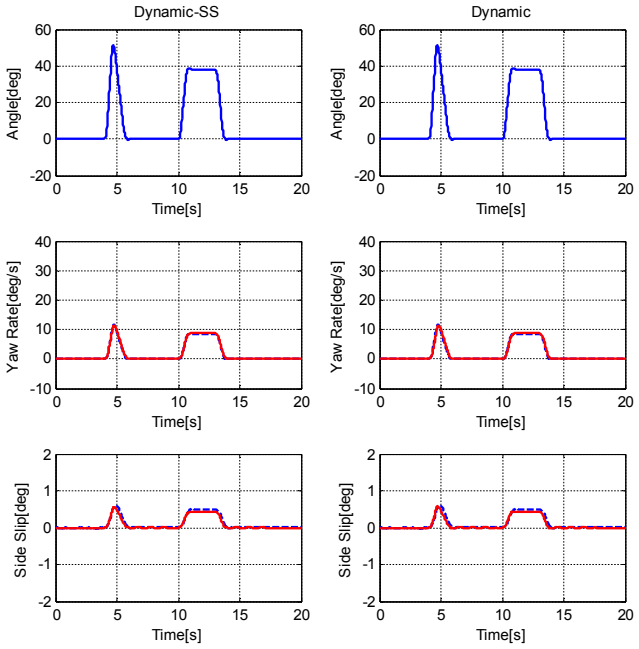

Figure 3.6: New Vehicle Model Validation - 60km/h

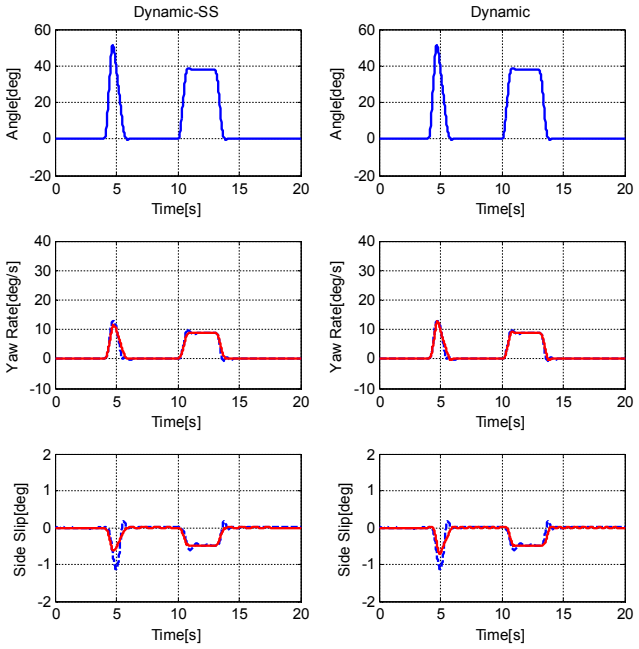

Figure 3.7: New Vehicle Model Validation - 120km/h

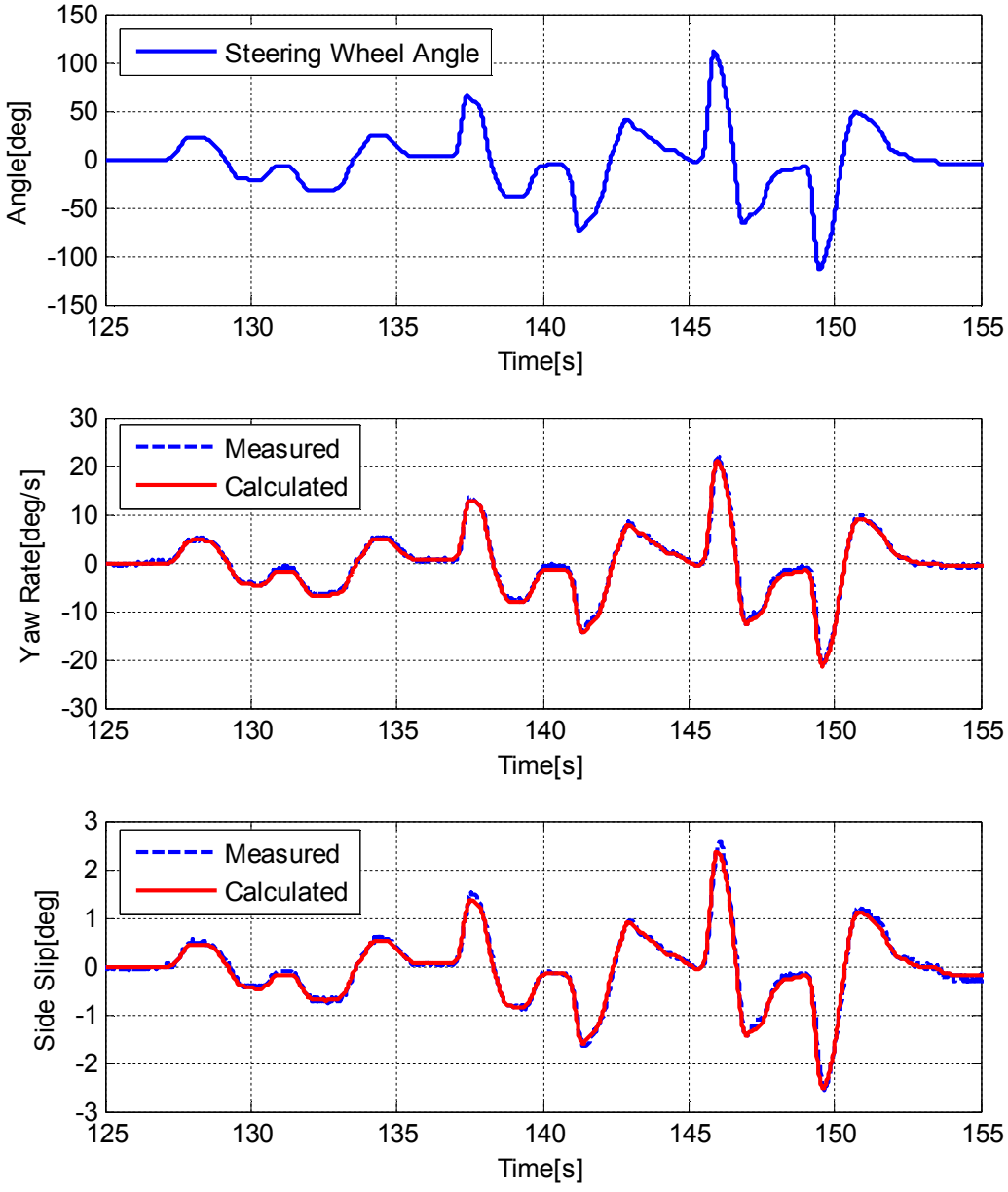

Figure 3.8: New Vehicle Model Validation Test - 60km/h

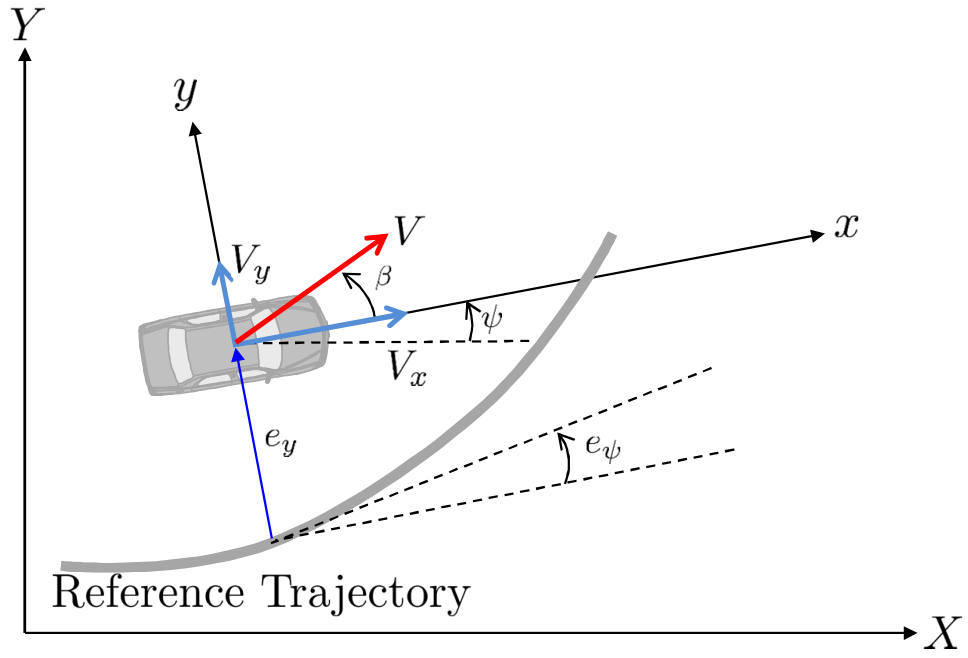

Figure 3.9: Error Dynamics of Path Following or Lane Keeping

3.2.4 Error Dynamics

To construct system dynamics for lane keeping or path following purposes, error dynamics with respect to the desired (reference) trajectory should be considered, as shown in Figure 3.9. From the geometric relationship between the trajectory and vehicle motion, the following equations can be derived for the lateral offset error, e_y, and heading error, e_ψ:

$$\begin{aligned} \dot{e_y} &= V_y + V_x \tan e_\psi \\ &= V_x \tan\beta + V_x \tan e_\psi \\ &\approx V_x(\beta + e_\psi) \end{aligned} \tag{3.17}$$

$$\dot{e_\psi} = \dot{\psi} - \frac{V_x}{R} \tag{3.18}$$

Using the steady-state vehicle dynamics equation, yaw rate($\dot{\psi}$), and side-slip angle(β), we define error dynamics. Also, the path radius, R, directly affects the heading angle error as shown in equation (3.14). Thereafter, the heading error affects offset error in equation (3.13).

3.3 Lane Keeping Controller

In this section, a new control law is presented. Then, using a steady-state lateral dynamics equation and error dynamics, which are suggested in the previous section, a discretized system dynamics model is derived. Using a Receding Horizon Sliding Control approach, a detailed control logic for a lane keeping controller is introduced.

3.3.1 Control Law Design

As mentioned in section 3.1.2, sliding control and model predictive control have advantages and disadvantages. In order to satisfy criteria such as low computational cost, consideration of nonlinear dynamics, robustness to disturbances, and consideration of constraints, a combination logic between the sliding control and model predictive control was suggested [36]. Also, A. Hansen and K. Hedrick [27] used a discrete difference operator to adopt the Receding Horizon Sliding Control (RHSC) algorithm on a discrete time case. In this logic, the reaching phase and the sliding phase can be easily included to minimize a predefined cost when considering system states over a receding horizon. This research is mainly based on this approach [27].
First, we take a discrete-time nonlinear system, as shown in the following equations, with n states.

$$x(k+1) = f_d(x(k), u(k), k), \tag{3.19}$$

$$y(k) = h(x(k)), \tag{3.20}$$

where $x \in \mathbb{R}^n$ and $u, y \in \mathbb{R}$ are state vector, input and output of the system, respectively. Also, the discretized system dynamics, f_d, is derived from the continuous time system dynamics. h is defined as a measurement function of the system.

If $\mathcal{D}(\,\cdot\,)$ is a kind of stable difference operator, $\mathcal{D}(\,\cdot\,) \equiv 0$ should be a stable difference equation. Therefore, a discrete-time case sliding variable can be defined as following:

$$s_k = \mathcal{D}(\epsilon_k), \tag{3.21}$$

where $\epsilon_k = y_k - y_k^{des}$ is defined as the tracking error between the current output and the desired output. In order to illustrate the role of $\mathcal{D}$, it can be defined as $\mathcal{D}(\epsilon_k) = \rho\epsilon_k - \epsilon_{k+1}, \rho \in [0, 1]$. Therefore, $\mathcal{D}(\epsilon_k) \equiv 0$ is a stable difference equation of order $d = 1$, and the definition guarantees convergence of ϵ_k to zero.
Also, in the error dynamics with the difference operator, s_{k+1} should be defined with u_k through the system dynamics. A necessary and sufficient condition for a discrete time sliding variable to converge to zero is

$$|s_{k+1}| < |s_k|\,. \tag{3.22}$$

In order to construct the error dynamics over N-step prediction horizon, the variable S can be defined as follows.

$$S_{k+1} = \begin{bmatrix} s_{k+1} & s_{k+2} & \dots & s_{k+N} \end{bmatrix}^T \tag{3.23}$$

Similarly, the system dynamics including the state and input over the receding horizon are formulated as follows.

$$X_k = \begin{bmatrix} x_k & x_{k+1} & \dots & x_{k+\bar{N}+1} \end{bmatrix}^T, \tag{3.24}$$

$$U_k = \begin{bmatrix} u_k & u_{k+1} & \dots & u_{k+\bar{N}} \end{bmatrix}^T, \tag{3.25}$$

where $\bar{N} = N + d - 1$. The control input sequence, U_k, is derived from an optimization problem as shown in the equation (3.22),

$$\begin{aligned} &\min_{U_k} J_k(S_{k+1}) \\ &\text{s. t.} \quad s_{i+1} = \rho\epsilon_{i+1} - \epsilon_{i+2},\ i = k, \dots, k+N-1 \\ &\qquad \epsilon_{i+1} = h(x_{i+1}) - y_{i+1}^{des},\ i = k, \dots, k+\bar{N} \\ &\qquad x_{i+1} = f_d(x_i, u_i, i),\ i = k, \dots, k+\bar{N} \\ &\qquad x_{i+1} \in \mathcal{X}, u_i \in \mathcal{U},\ i = k, \dots, k+\bar{N} \\ &\qquad x_k = x(k) \end{aligned} \tag{3.26}$$

where $\mathcal{X}$ is a feasible or a constrained state set, and $\mathcal{U}$ is a constrained control input set. At each time step, current state is measured and is used to initialize the optimization problem as $x_0 = x(k)$. Then, the optimization problem (3.26) is solved at every time step, and the first control input is applied to the plant. This process can be shifted at the next time step. Therefore, it is treated as receding horizon sliding control.

3.3.2 Lane Keeping Controller

3.3.2.1 Controller Setup

For the lane keeping controller, the states can be defined as follows.

$$[x_1, x_2, x_3, x_4, x_5]^T = [e_y, e_\psi, \beta, \dot{\psi}, \delta_f]^T \tag{3.27}$$

From equations (3.7),(3.8),(3.17) and (3.18), the discretized system dynamics can be derived as shown in equations (3.28) through (3.32). As shown in states x_3 and x_4, the first order lag term, τ_v, from actual steering input to the vehicle motion was considered. Also, in order to control the steering angle, the steering torque interface between the controller and the steering system was used. Once the desired steering angle is calculated from RHSC logic, a desired steering torque is generated and transmitted to the steering system over CAN (controller area network) in order to track the value. This interface and actuator control, however, also have delayed, as shown in Figure 3.10. Therefore, the steering actuator delay term, τ_s, can be described as first order lag, and it is included in the state x_5 of system dynamics. τ_v and τ_s are 0.06 and 0.85, respectively.

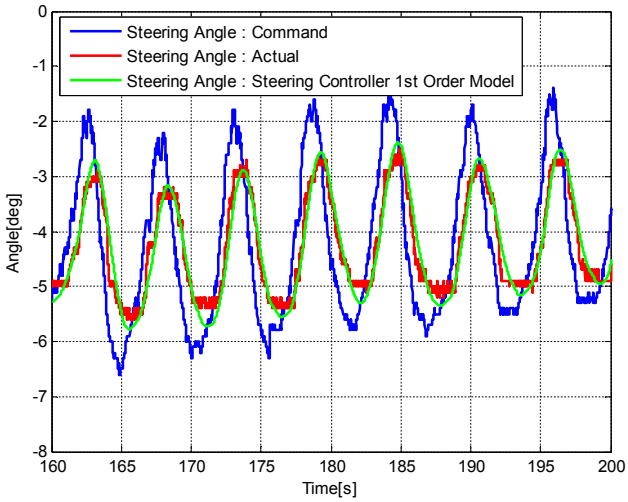

Figure 3.10: Steering Actuator Delay

$$x_1(k+1) = x_1(k) + T_s \times V_x \times \{x_2(k) + x_3(k)\} \tag{3.28}$$

$$x_2(k+1) = x_2(k) + T_s \times \left\{ x_4(k) - \frac{V_x}{R} \right\} \tag{3.29}$$

$$x_3(k+1) = x_3(k) + \frac{T_s}{\tau_v} \times \{\beta_{ss}(k) - x_3(k)\} \tag{3.30}$$

$$x_4(k+1) = x_4(k) + \frac{T_s}{\tau_v} \times \{\dot{\psi}_{ss}(k) - x_4(k)\} \tag{3.31}$$

$$x_5(k+1) = x_5(k) + \frac{T_s}{\tau_s} \times \{u(k) - x_5(k)\} \tag{3.32}$$

A control error, $e(k)$, can be constructed with lateral offset, e_y, heading error, e_ψ, and offset error integral, $\sum e_y$. This control error term has weighting factors, η_1 and η_2, for each control error(offset error and heading error). The next time step's error, $e(k+1)$, is defined in terms of $e_y(k+1)$ and $e_\psi(k+1)$ from system dynamics. Finally, the sliding manifold, $s(k)$ is formulated with current control error, $e(k)$, and the next control error, $e(k+1)$, with weighting factor $\rho \in [0, 1]$. Note that the error summation term, $\sum e_y$, is added to the total tracking error calculation. Without this term, a small steady-state offset error was found during vehicle tests. As a results, the integral offset error is added to the control error

calculation term with a constrained value.

$$e(k) = e_y(k) + \eta_1 \times e_\psi(k) + \eta_2 \times \sum e_y(k) \tag{3.33}$$

$$e(k+1) = e_y(k+1) + \eta_1 \times e_\psi(k+1) + \eta_2 \times \sum e_y(k+1) \tag{3.34}$$

$$s(k) = \rho \times e(k) - e(k+1) \tag{3.35}$$

Then, the optimization problem can be formulated as follows:

$$\min_{U_k} J_k(S_{k+1}) = \min_{U_k} \sum_{k=0}^{N} \{s_k^2 + w_1 \times (\dot{\psi}_k - \dot{\psi}_{des,k})^2 + w_2 \times \dot{\psi}_k^2\} \tag{3.36}$$

$$\text{s.t.} \quad x_{i+1} = f_d(x_i, u_i, i), i = k, \cdots, k+N \tag{3.37}$$

$$x_{i+1} \in \mathcal{X}, i = k, \cdots, k+N \tag{3.38}$$

$$x_k = x(k) \tag{3.39}$$

$$u_i \in \mathcal{U}, i = k, \cdots, k+N \tag{3.40}$$

$$U_k = [u_k, u_{k+1}, \cdots, , u_{k+N}]^T \tag{3.41}$$

$$S_{k+1} = [s_{k+1}, s_{k+2}, \cdots, , s_{k+N+1}]^T \tag{3.42}$$

In the cost function(equation (3.31)), the tracking error is an essential term. In order to follow a desired path, the yaw rate difference between the current yaw rate and the desired yaw rate, which is calculated by $\dot{\psi}_{des} = V_x/R$, is considered. This term acts like a feed-forward term to track the desired path, and the s_k term acts as a feed-back term to compensate for the path tracking error. Also, in order to guarantee a smooth steering action, minimum steering manipulation should be considered, including minimum yaw rate generation, as shown in the last term.

This optimization problem is governed by system dynamics $f_d(x_i, u_i, i)$, and state constraints are considered. For example, the vehicle must stay in the lane, and that means e_y needs to be constrained. For the input constraint($\mathcal{U}$), the maximum steering input and its rate were constrained for smooth driving condition.

From the point of tuning parameters, compared to a normal MPC formulation, RHSC approach may have less tuning parameters, since only one sliding surface needs to be formulated in the optimization problem instead of considering all states.

In the receding horizon formulation, at every time step, future states should be defined with system dynamics over the prediction horizon. In equation (3.29), future road radius, which is measured by a front looking camera, is considered. Also, in equations (3.30) and (3.31), future yaw rate and side-slip angle can be calculated from the steering angle input as shown in equations (3.7) and (3.8). However, in equations (3.7) and (3.8), we need information about the road bank angle over a prediction horizon. Although we are estimating the current road curvature, we still need to consider the future road bank angle. Fortunately, there exists a bank angle design guide (Highway Design Manual, Table 202.2, page. 200-10) that defines the proper road curvature and road type, from the California Department of Transportation

[1]. With this guide, the future road bank angle can be calculated from a weighted(ξ_i) combination of the estimated current road bank angle and the road bank angle, suggested by the Highway Design Manual, as shown in the following equation:

$$\phi_{r,i} = \xi_i \times \phi_{est,i} + (1 - \xi_i) \times \phi_{manual,i}, i = k, \cdots, k + N \tag{3.43}$$

3.3.2.2 Stability of the Controller

As a robust lane keeping controller, the RHSC approach should guarantee stability. The procedure of proving the stability of the controller follows a similar procedure used for MPC as analyzed by Francesco Borrelli.[24] First, it requires certain assumptions as follows.

- Assumption 1: The initial state is feasible.
- Assumption 2: There is no model mismatch.
- Assumption 3: The sliding manifold, s, is control invariant. At a certain time step k, the controlled system goes to the sliding manifold, $s = 0$, with control input, u_k^*, that makes the system stay on the manifold. In addition to that, the next step's system can be feasible.

With these assumptions, if we add a terminal constraint, $s_{k+N} = 0$, then the RHSC approach is persistently feasible and asymptotically stable. To prove the feasibility and stability, first, persistent feasibility should be guaranteed. From Assumption 2, the initial state x_0 is feasible, and then the feasible control sequence, U_0, can be determined. This optimal solution was calculated from the optimization problem with the terminal constraint, $s_N = 0$. At the next time step, the feasible optimal control sequence is updated with U_1. This solution is also feasible, and makes $s_{N+1} = 0$. So, with Assumption 3, all control sequences can be found over the time steps and they make the system feasible. Therefore, we conclude that the feedback system is persistently feasible.
In order to prove the stability of the RHSC approach, the Lyapunov stability theorem is used. For penalizing the cost, $\mathcal{W}_{k+1} = diag(w_{k+1}, \ldots, w_{k+N})$ can be used. For a more simple case, $\mathcal{W}_{k+1} = \mathcal{I}$ is easy to prove the stability. The Lyapunov function is:

$$V_k = \mathcal{S}_k^T \mathcal{S}_k. \tag{3.44}$$

One step later,

$$\begin{aligned} V_{k+1} = \mathcal{S}_{k+1}^T \mathcal{S}_{k+1} &\leq \mathcal{S}_k^T \mathcal{S}_k - s_k^2 + s_{k+N}^2 \\ &= \mathcal{S}_k^T \mathcal{S}_k - s_k^2 \leq V_k. \end{aligned} \tag{3.45}$$

Since V_k is a decreasing function or it is equal to zero over the feedback control sequence, we conclude that the feedback system with the controller is asymptotically stable.

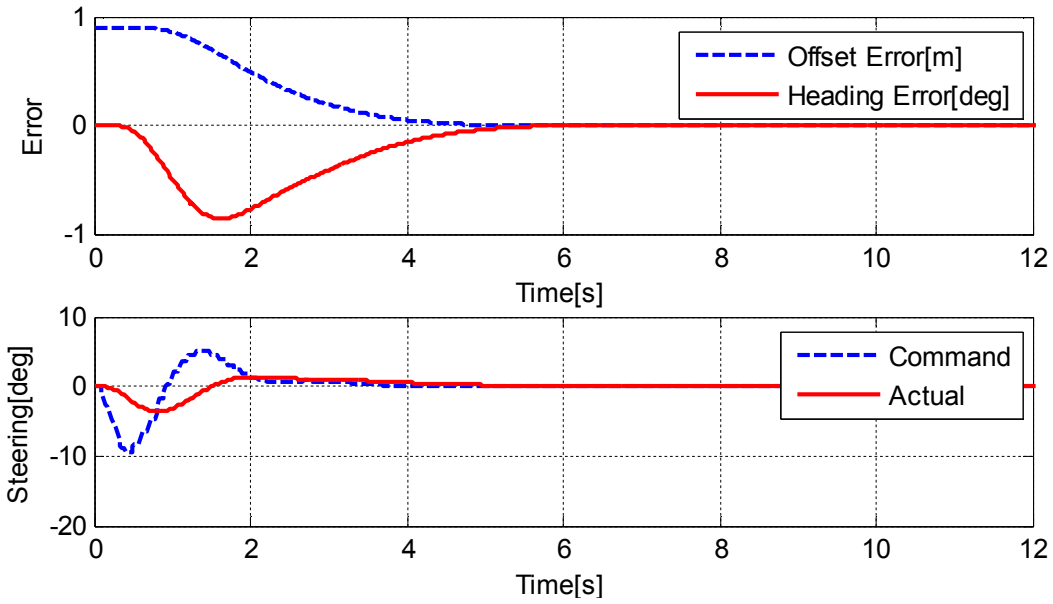

Figure 3.11: Simulation Results - Lane Keeping Control with Initial Offset Error

3.4 Simulation Results

Basic simulation tests have been conducted to verify the control logic before implementation on a real vehicle. Carsim and Matlab were used for this purpose. The sampling time is 0.1s, but in the prediction horizon, a different sampling time of 0.2s is used to predict longer future motion. The prediction horizon is 12 steps (2.4s). For the MPC solver, NPSOL [51] , a widely used tool for general nonlinear optimization problems, is used.

3.4.1 Basic Control Performance

For the first simple test scenario, there is an initial lateral offset error with no heading error at the beginning. Also, desired path is a straight line. As shown in Figure 3.11, within 5 seconds, the vehicle goes to the center line (no offset error) with steering angle input. On the bottom graph, we can see steering angle delay, and see that the delay was included in the system dynamics over the prediction horizon. In Figure 3.12, the controlled vehicle's trajectory smoothly goes to the center of the desired path. The open loop trajectory with 12 steps is also plotted (highlighted with black dots).
On the curved road, Figure 3.13 shows a good path tracking performance under varying road curvature, which is plotted in the top graph. The vehicle travels on a straight road, enters a curved road with R=500m, then exits the curved road to the straight lane again. In the second graph, we can find that the controller perfectly controls the vehicle to track the lane with very small offset and heading error even on the transient curvy conditions. Also, as

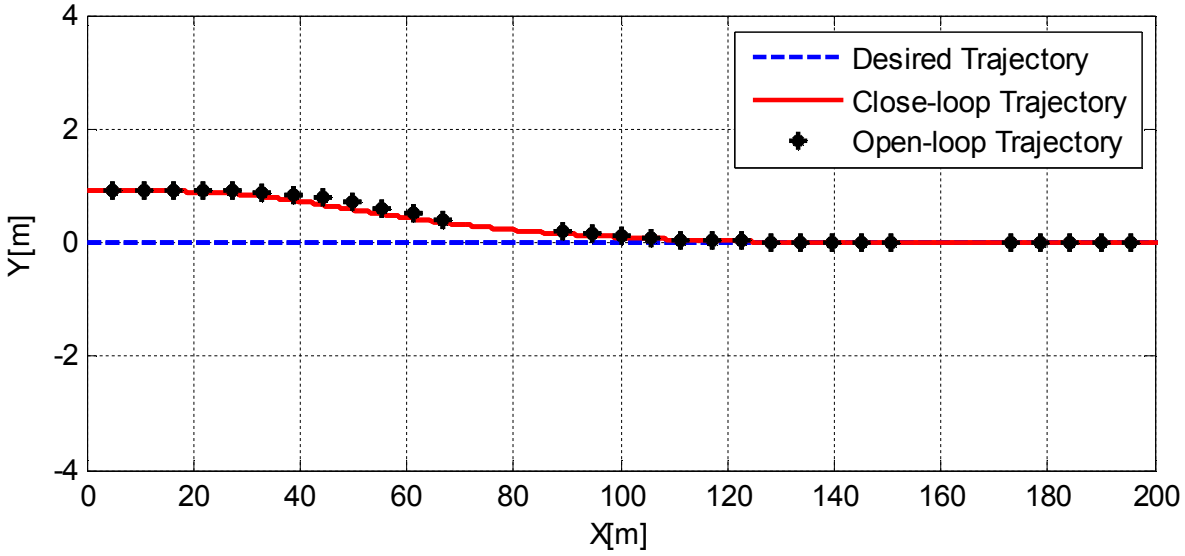

Figure 3.12: Simulation Results - Closed-loop vs. Open-loop

depicted on the bottom graph, the steering delay is fully considered to generate a moderate steering control input. In the cost function of equation (3.36), a yaw rate term was included to minimize yaw motion. Due to this term, in Figure 3.14, we found that the controlled trajectory (in red) goes to the shortest path to minimize yaw rate generation.

3.4.2 Bank Angle Effect Simulation

Now, we observe th effect of a lack of bank angle information on the controlled system. Figure 3.15 shows the comparison results between the controlled system with and without bank angle information. When a vehicle enters a curved road, there exists bank angle, as shown in the second graph. The other graphs show offset error, heading error and steering control input, respectively. Although there is no significant difference in heading error, if we do not consider bank angle, we clearly observe that there exists a steady-state error on the offset error graph. However, this characteristic can be shown differently with different gain scheduling. We will see these different aspects in the following section.

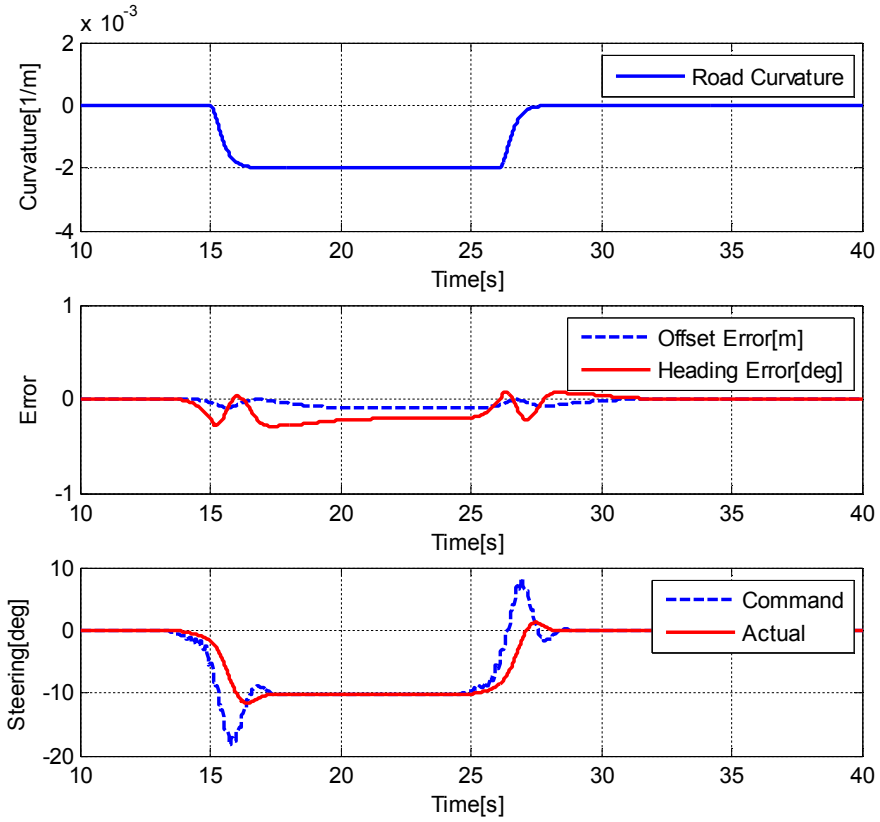

Figure 3.13: Simulation Results - On the curved road

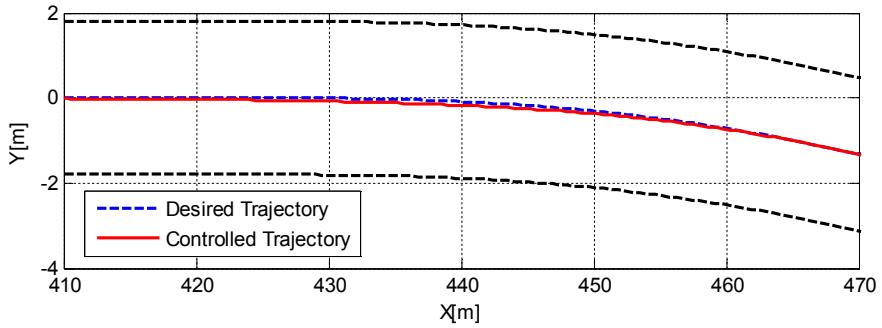

Figure 3.14: Simulation Results - Shortest path On the curved road

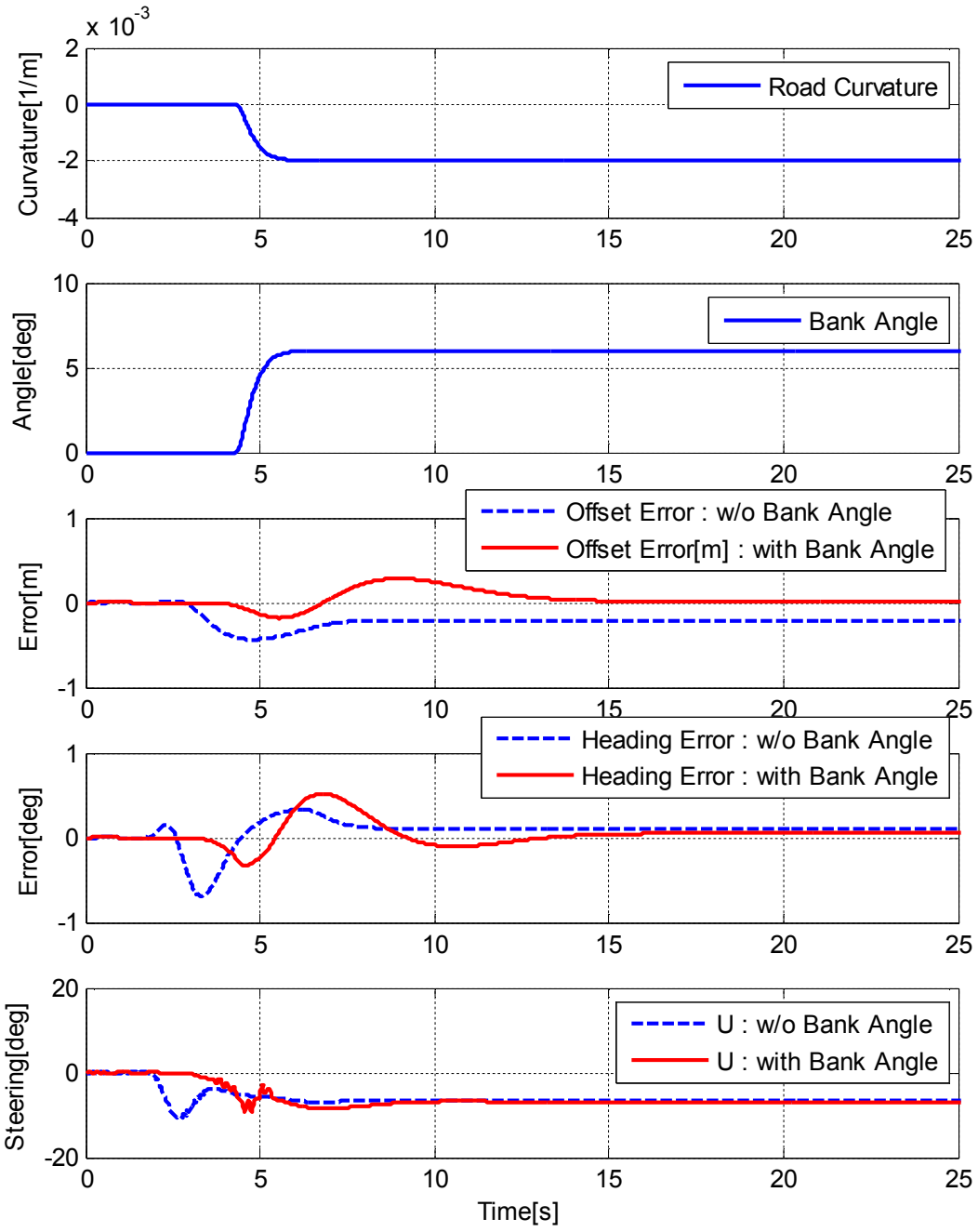

Figure 3.15: Simulation Results - Bank Angle Effect



Figure 3.16: Test Vehicle equipped with a Forward Looking Camera

3.5 Vehicle Test Results

For implementation on a real vehicle, the Hyundai AZERA, equipped with steering angle controller, was used. To detect front lane markers, a Mobileye-Mando camera is installed in the center of the front windshield, as shown in Figure 3.16. Control logic is implemented on the dSpace Microautobox for real-time implementation. Before testing on public roads, basic validation tests were performed at the Hyundai California Proving Ground. Sampling time was 0.1s, and in receding horizon, a different sampling time of 0.2s and 12 steps prediction horizon were used. For optimization solver, NPSOL was used.

3.5.1 Vehicle Test on the Public Roads

Afterwards, the control logic was tested on the public roads, I-580 in California (from Bay View Exit to Richmond Bridge Exit) as shown in Figure 2.18. Figure 3.17 shows road gradient estimation results, which were introduced in the previous chapter. The measured values(in blue) is from the RT2002 as a reference and we see that the estimation has good accuracy under real-time vehicle control. The road disturbance information can be fed to the lane keeping controller and Figure 3.18 shows these results. The offset error has $\mu = 0.079m$ (mean) and $\sigma = 0.237m$ (standard deviation). If the offset error is less than $\pm 1m$, the vehicle is considered to be in the lane. Therefore, as shown in the second graph, we found that the vehicle is controlled to stay in the lane. Also, the heading error has $\mu = -0.032deg$ and $\sigma = 0.281deg$. The controlled steering wheel angle is within $\pm 8deg$, and was observed to be controlled very smoothly by the control logic.

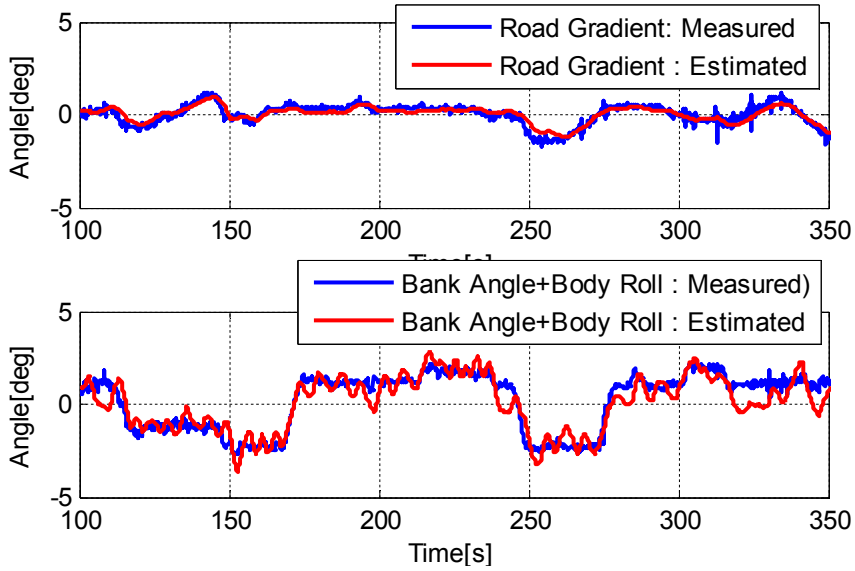

Figure 3.17: Road Gradient Estimation in Real Time

3.5.2 Bank angle Effect

As we have seen in the previous simulation section, there exists a steady-state offset error without bank angle information. On the Hyundai CPG, vehicle tests were performed to verify this characteristic. The tests were performed on the curvy track with R=1000m where the bank angle is about 6 degrees.

Figure 3.19 shows exactly the same results as the simulation results in Figure 3.15. Without bank angle estimator, there exists an offset error of about 0.5m. Using a bank angle estimator, there is very small offset error less than 0.1m. An effort was attempted to decrease the offset error without bank angle information by increasing the relative offset gain by assigning a lower value to the heading error gain, η_1, in equation (3.33). As a result, as depicted in the top graphs in Figure 3.20, although steady-state offset error has been removed, we found large oscillations in control input. In the bottom graph, a controller with a bank angle estimator was able to decrease the amplitude of the offset error due to additional lateral force of road bank angle compared to the controller without bank angle estimator by 29%. So, we conclude that if we include bank angle information as a disturbance from the road, control performance can be easily improved.

As can be seen in Figure 3.21 and 3.22, this characteristic can be easily found even on public roads. As shown in 3.21, with the bank angle estimator, the vehicle stays in the lane with limited offset error ($\mu = 0.142m$). On the other hand, without bank angle information, as shown in Figure 3.22, the controlled vehicle stays at the edge of the lane ($\mu = 0.507m$). In conclusion, between the two controllers with or without bank angle information, the heading errors are almost the same, but we can see large offset errors without bank angle information.

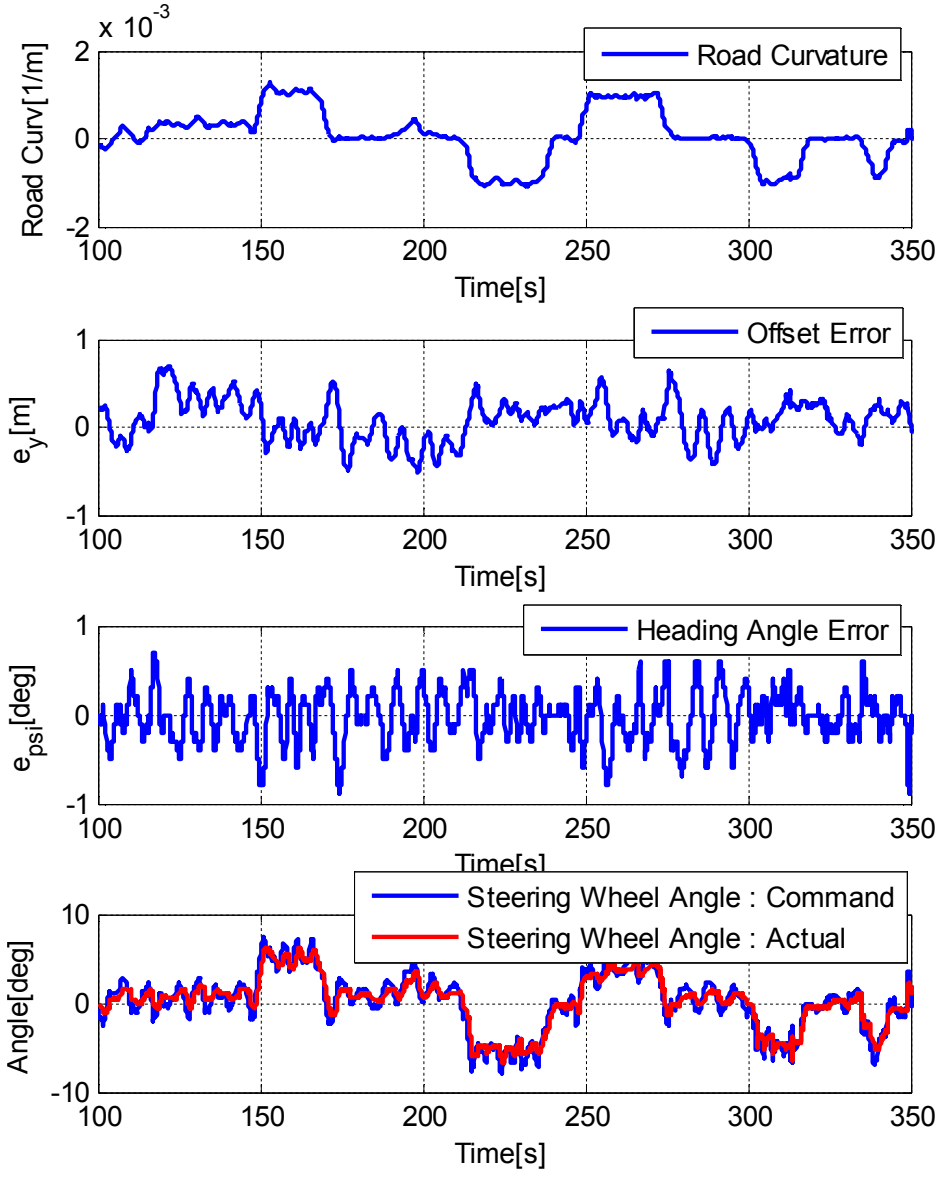

Figure 3.18: Lane Keeping Control Results on a Public Road

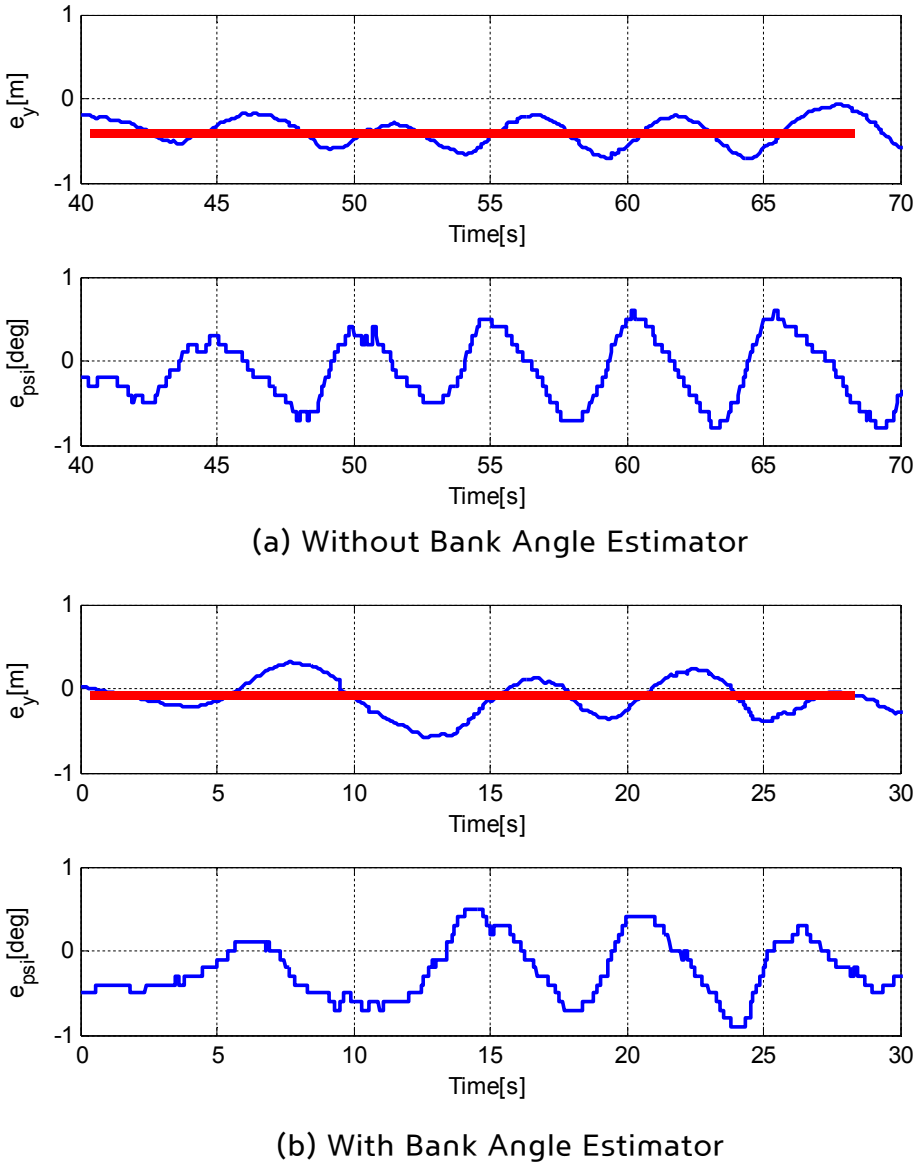

Figure 3.19: Bank Angle Effect - Low Offset Error Gain

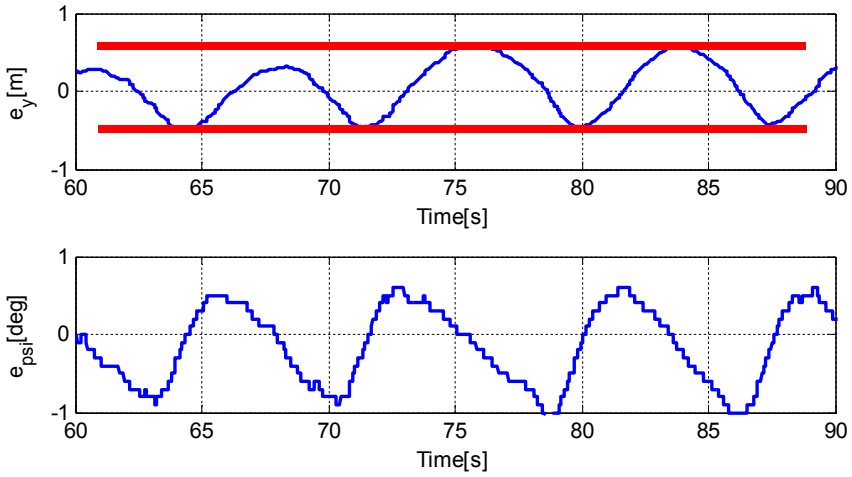

(a) Without Bank Angle Estimator

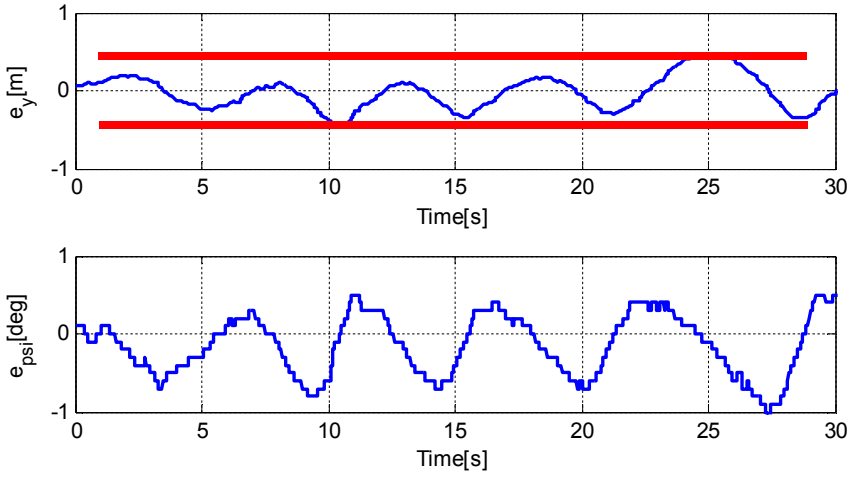

(b) With Bank Angle Estimator

Figure 3.20: Bank Angle Effect - High Offset Error Gain

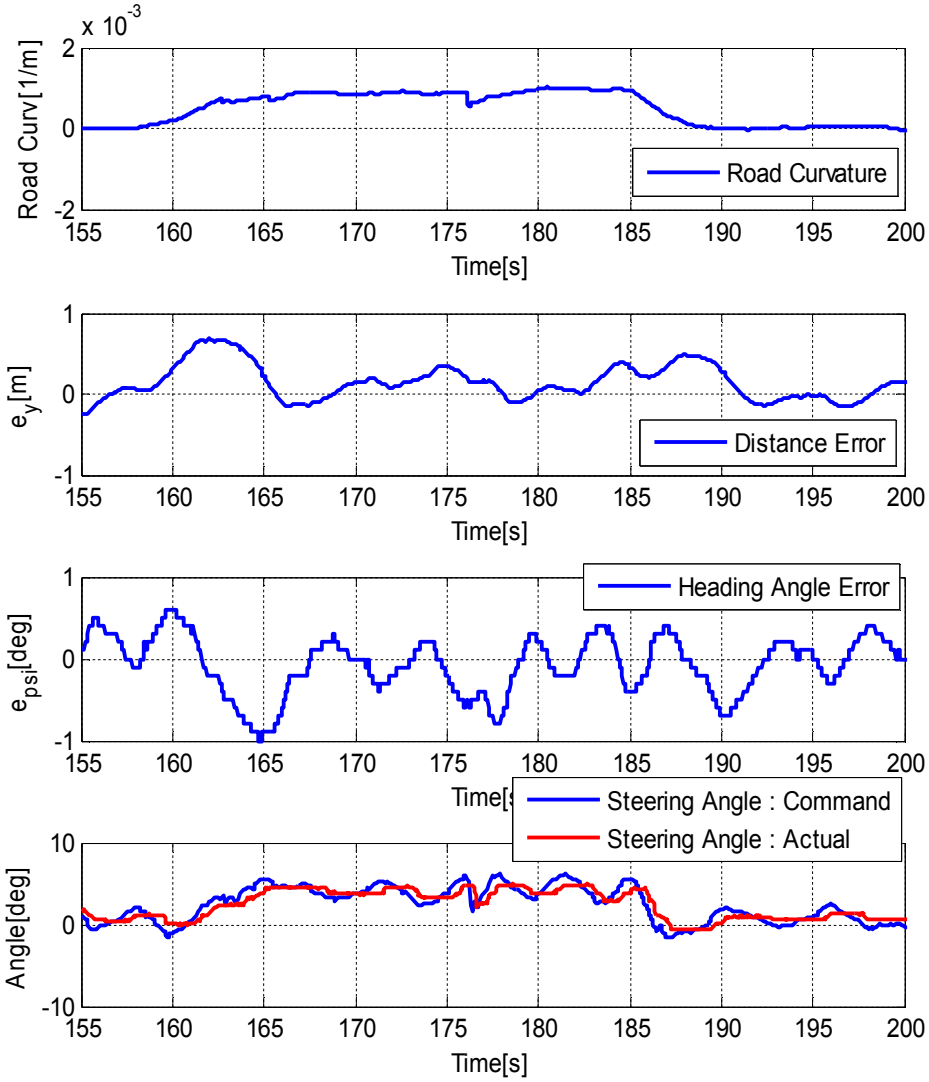

Figure 3.21: Controller with Bank Angle Estimator

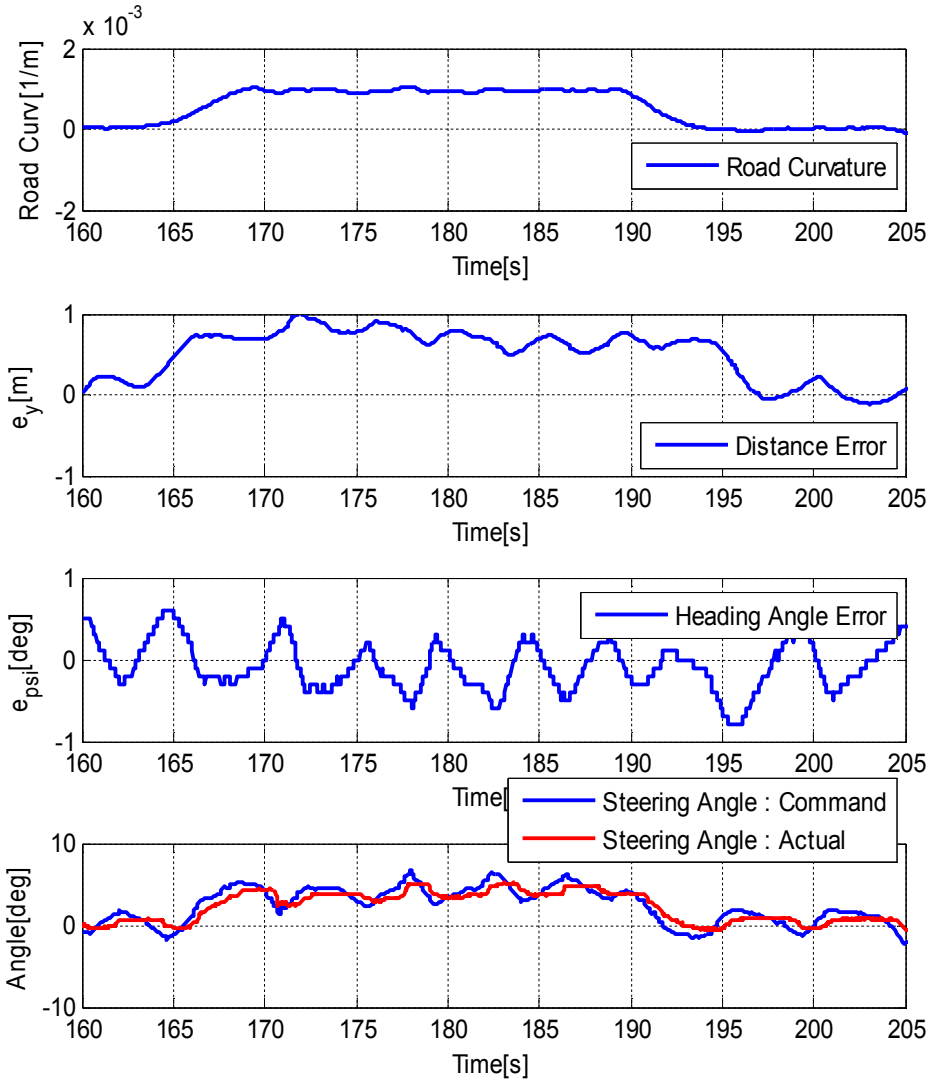

Figure 3.22: Controller without Bank Angle Estimator

3.6 Conclusion

This chapter proposed a steady-state dynamic model to describe lateral vehicle dynamics over all speed ranges. It was also useful to consider bank angle effect. Through simulation and real vehicle tests, we found that the model was very reasonable and has good accuracy. The model was also used to derive error dynamics of offset error and heading error for lane keeping or path following purposes. From the steady-state dynamic model and error dynamics, a lane keeping controller using RHSC approach was designed. The control approach was simple to formulate and easy to add constraints to with the receding horizon technique. From simulation, the controller and dynamic models were verified. Subsequently, real vehicle tests were performed on public roads. Simultaneously, road angle estimation results were fed to the lane keeping controller to compensate for the lateral force disturbance effect. In conclusion, the proposed logic was very good at controlling the vehicle to follow the lane.

Chapter 4

Longitudinal Disturbance Estimation : Front Vehicle's Future Motion

4.1 Introduction

Another example of a driver assistance system is an Adaptive Cruise Control (ACC) system. It tries to maintain the speed set by the driver. If there exists a front vehicle, the system maintains a safe distance with the front vehicle automatically. To detect the front vehicle, the system usually uses a forward pointing radar that measures the current relative distance and velocity between the controlled ego vehicle and the front vehicle. Therefore, depending on the current state of the vehicles, the ACC algorithm controls the ego vehicle with the desired acceleration control input. Therefore, the front vehicle's future motion is one of the key disturbance terms in the controller. In this chapter, a new approach of predicting future motion of the front vehicle is presented. The approach consists of three steps: base car following model, driver aggressivity factor estimation, and future motion calculation. Finally, the advantages of future motion prediction will be mentioned.

4.1.1 Motivation

If we can predict the front vehicle's future motion, we may have two potential advantages. The first advantage is the improvement of the vehicle's collision avoidance capability. Before the front vehicle starts to decelerate, if the front vehicle's deceleration is predicted, the ego vehicle can decelerate in advance with smaller braking effort. This situation is shown in Figure 4.1. The results are obtained from basic control simulation. With the prediction of the front vehicle's braking, the ego vehicle starts to apply braking at 3.2 seconds (in red line) with smooth braking, even though the front vehicle actually starts to decelerate at 4 seconds (in blue line).
Energy or fuel saving is another potential advantage. As shown in Figure 4.2, when the front vehicle decelerates and then accelerates, if the ego vehicle predicts the movement, the ego vehicle does not have to maintain the same movement to follow the front vehicle.

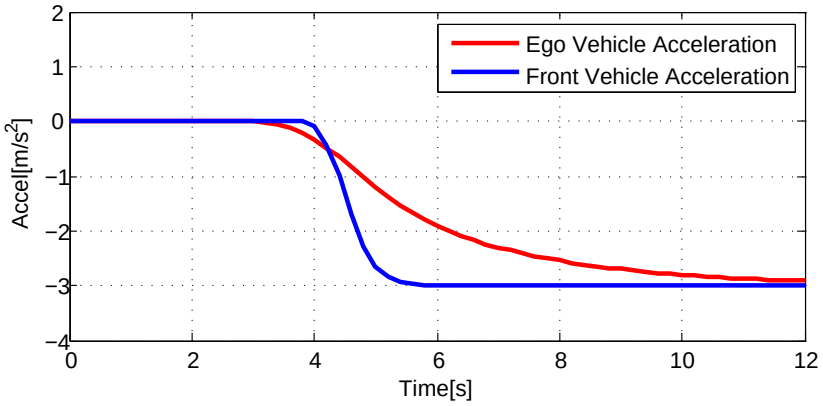

Figure 4.1: Advantage of the Front Vehicle's Future Motion Prediction - Early Braking

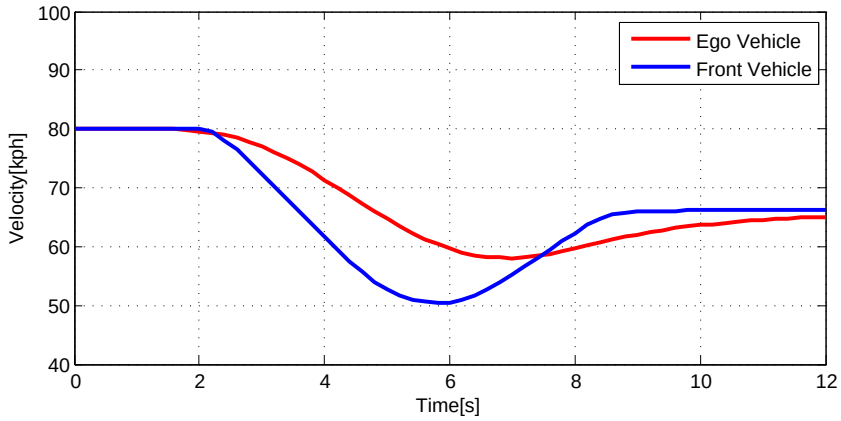

Figure 4.2: Advantage of the Front Vehicle's Future Motion Prediction - Smooth Velocity Profile

Consequently, the ego vehicle can achieve a smooth velocity profile as shown in Figure 4.2, resulting in a fuel savings improvement.

4.1.2 Method for Prediction of the Front Vehicle's Motion

Since driving is a complex human-machine interaction, predicting the front vehicle's future velocity or acceleration proves to be a challenging research topic. The decisions made by a

human driver are not only affected by traffic conditions but also the driver's unique driving style as well. To simplify the problem, this research focuses on the ego lane vehicle's longitudinal control motion without consideration of the adjacent lane's traffic. Under this limited case, the front driver will react only depending on the movement of the leading vehicle (the front of the front vehicle). This reaction can be described by a car-following model with a representative equation. Therefore, a new method for predicting the front vehicle's motion is suggested as follows.

- Step 1 : Car-Following Model
  This model describes a certain driver's distance control and velocity control reaction depending on the current relative distance and velocity to the front moving vehicle. It can be defined with a deterministic equation or a stochastic expression. So, first, we need to select a good car-following model to describe the front vehicle's reaction. But, every driver has a different driving style. To predict the motion accurately, we also need to estimate the current front vehicle driver's driving style in real-time.

- Step 2 : Driver Aggressivity Estimation
  Driving style can be described with several features. Desired relative distance to the front vehicle is one of the features. Furthermore, reaction to distance error, which is defined as the difference between actual distance and desired distance, and reaction to relative velocity are key features of driving style. This reaction can be defined as a driver aggressivity factor. Therefore, we need to extract the aggressivity factor from the car-following model in real-time. Once a car-following model is fixed, some parameters for the car-following model can be determined in real-time.

- Step 3 : Front Vehicle's Future Motion Estimation
  We have a base car-following model and a driver aggressivity estimator extracting current front driver's driving style in real-time. If we then assume the leading vehicle moves with constant acceleration, we can propagate the front vehicle's future velocity as we assume that the front driver tries to keep desired distance and zero relative velocity.

These procedures are presented with detail in this chapter.

4.2 Step 1 : Base Car-Following Model

In this section, various approaches and ideas for car-following models are introduced.

4.2.1 Literature Review

Over the past several years, many simplified car-following models have been proposed as deterministic approaches. The goal of the models is to keep safe distance and to converge the relative velocity to zero. Sometimes, these methods are treated as a kind of controller or adaptive filter [46] to follow the goal. In this approach, all parameters for each model have been extracted from real car-following data sets, and a representative equation was chosen. Recently, non-parametric approaches have been suggested for the car-following model. The method does not have any fixed equation at the beginning. However, using several sets of real data, called training data sets, probability parameters can be defined. In addition to the non-parametric model, combining probability models under various situations using a hybrid dynamical model was also suggested [19]. This is meaningful because the driver's behavior is affected by various traffic situations.
First, some parametric approaches are introduced as follows (Original notations used in the references were preserved):

- Constant Acceleration Assumption Model
  This is a very simple equation to describe the vehicle following behavior. It assumes that the following vehicle will keep the same acceleration. Due to its simplicity, this equation is widely used.

$$a(t + T_s) = a(t) \tag{4.1}$$

  where T_s is a sampling time.

- Constant Speed Assumption Model
  The other simple model assumes that the following vehicle will keep constant speed.

$$v(t + T_s) = v(t) \tag{4.2}$$

- Helly Model [28]
  A liner traffic flow model is suggested by Helly in 1950's. It was used for watching a macroscopic traffic flow. The model's equations are as follows.

$$a(t + T_s) = C_1\Delta v(t) + C2(\Delta x_n(t) - D_n(t + T_s)) \tag{4.3}$$
$$D_n(t + T_s) = \alpha + \beta v_n(t) + \gamma a_n(t) \tag{4.4}$$

  where $x(t), v(t)$ and $a(t)$ are the position, speed and acceleration of the vehicle, respectively. Also, Δx and Δv are relative distance and relative speed between the two cars at time t. D_n is desired distance of the driver.

- GM-type Model [8]
  In addition to the Helly Model, a nonlinear equation model was suggested by General Motors in the 1950's.

$$a(t+T_s) = \alpha \frac{v_n(t+T_s)^l}{\Delta x_n(t)^m} \Delta v_n(t) \tag{4.5}$$

  where all variable definitions are the same as that of the Helly Model. Additionally, this model considered a delay term depending on the relative distance.

- Sultan Model [5]
  Other research has modified the GM-type model to add reality [3]. For example, Sultan extends the GM-type model using an acceleration term for the front and the following vehicles.

$$a(t+T_s) = \alpha \frac{v_n(t+T_s)^l}{\Delta x_n(t)^m} \Delta v_n(t) + \beta_1 a_{n-1}(t) + \beta_2 a_n(t) \tag{4.6}$$

- Intelligent Driver Model [45]
  Treiber suggested a more intelligent model starting from the desired distance calculation. From the desired distance, desired acceleration of the following vehicle can be calculated in the model.

$$d_{des} = \quad d_m + \tau_h \cdot v(t) + \frac{v(t) \cdot v_{rel}(t)}{2\sqrt{a_{mx} \cdot b_{cmf}}} \tag{4.7}$$

$$a(t+T_s) = \quad a_{mx} \left[1 - (\frac{v(t)}{v_{mx}})^4 - (\frac{d_{des}}{d(t)})^2 \right] \tag{4.8}$$

  In equation(4.7), d_m is the minimum relative distance that a driver wants to keep under any condition even including stop, and τ_h is the desired time headway. Also, a_{mx} and b_{cmf} are maximum acceleration and comfortably allowed deceleration of the driver, respectively. Using this equation, a desired acceleration of the vehicle can be calculated with the equation (4.8).

For the non-parametric method, an Artificial Neural Network approach was suggested [54]. Also, the combination of the Gaussian Mixture Regression and the Hidden Markov Model is an alternative method for stochastic representation of motion.
A number of research results show a comparison of the performances of the car-following models. Some research focus on parametric benchmarking [26][52][53]. The results normally state that it is important to determine not only a basic equation but to also conduct parameter tuning. For the non-parametric model comparison, Angkititrakul compared the Gaussian mixture model (GMM) and the piecewise auto regressive exogenous (PWARX) algorithms [50]. However, both approaches are very dependent on the situation, and show inaccurate prediction under heavy traffic conditions.
Recently, Stéphanie compared the performance of using both parametric and non-parametric

approaches to predict the following vehicle's future movement [63]. The results showed that parametric models' performances are better than those of non-parametric models for short-term prediction within 3 seconds. However, for long-term prediction, non-parametric models and advanced parametric models are quite better than simple parametric approaches.

4.2.2 New Car Following Model

Long term prediction (more than 3 seconds) has uncertainty and if the predicted information is included in a vehicle distance controller, the driver can encounter a dangerous situation under poor prediction. Therefore, we focus on short term prediction to avoid an increase of uncertainty. Secondly, a car-following model needs to be applied to various scenarios. But, non-parametric approaches, which is based on a certain scenario, have more uncertainty than parametric approaches. From these view points, short term prediction and consideration of various scenarios, a parametric approach is more reasonable than a non-parametric approach in predicting the following vehicle's short term movement with more robustness to driving conditions. Although there are many advanced parametric models, Stéphanie [63] concluded that the *Constant Acceleration Model* has the best prediction performance for the next 3 seconds.

Parametric models proposed in the previous section are missing certain behaviors of a driver. First, the driver has faster reaction if the real distance is smaller than the desired distance. Second, the driver reacts differently depending on the sign of relative velocity. Third, the driver adopts the front vehicle's acceleration and deceleration to get faster response on controls. Therefore, we need a more accurate parametric model under various driving conditions to consider these characteristics.

In addition to the car-following model, we need to extract the current front driver's driving tendency in order to predict the front vehicle's motion more accurately, since all vehicle drivers have different driving styles. For this purpose, a base car-following model should be a suitable equation to include driving style. Furthermore, it should include some parameters to represent the drivers' driving style.

Consequently, a simple deterministic car-following model including the driver's driving style can be defined. The new car-following model represents both the steady state and the transient car following motions to apply to any driving conditions. A general procedure to derive a car following model is as follows. We acquire the overall driver's real car-following data and then, make one representative equation describing the car-following motion. An Adaptive Cruise Control (ACC) is a very popular driver assistance system. It is very well-tuned to provide a safe and smoothing distance control performance. Therefore, a base car-following model can be derived by extracting representative equation from a well-tuned ACC controller. Although this is not a nominal equation, it is verified that the equation is one candidate for a car-following model, and it can be adopted to predict the front vehicle's future motion through this thesis.

To explain a car-following model, two vehicle's motions were considered, as shown in Figure

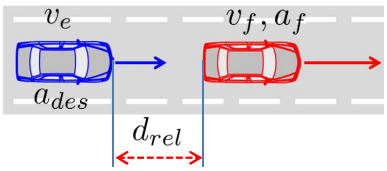

Figure 4.3: Definition of Control Variable for the Ego Vehicle

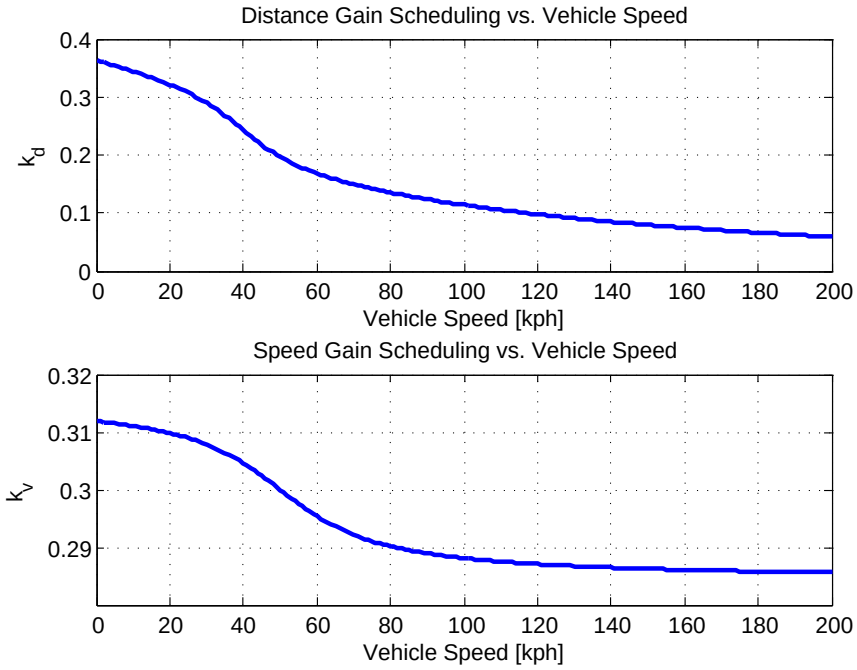

Figure 4.4: Gain Scheduling of an ACC controller depending on Vehicle Speed

4.3. Equations (4.9) to (4.14) are main equations describing the ego vehicle's motion to follow the front vehicle.

$$a_{des} = k_d \cdot d_e + k_v \cdot v_{rel} + k_a \cdot a_f \tag{4.9}$$
$$d_e = d_{rel} - d_{des} \tag{4.10}$$
$$v_{rel} = v_f - v_e \tag{4.11}$$
$$d_{des} = d_0 + \tau_h \cdot v_e \tag{4.12}$$

The car-following model calculates the desired acceleration, a_{des} of the following vehicle, where k_d, k_v, k_a are distance gain, velocity gain and acceleration gain, respectively. Also,

d_{rel} is a current clearance distance between two vehicles, and d_{des} is a desired distance with a time headway, τ_h set by the driver. v and a are velocity and acceleration. Subscript e and f symbolize the following ego vehicle and the leading front vehicle.
All gains(distance, velocity, acceleration) consist of sub-gains and have tuning tables depending on the ego vehicle and the front vehicle's conditions in the ACC algorithm of the commercial vehicle. However, in this thesis, simple gain scheduling graphs can be written in mathematical equations such as arc tangent functions that were derived, as defined in equations (4.13) and (4.14). Figure 4.4 shows the gain scheduling feature which depends on the ego vehicle's current speed. However, the acceleration gain can be assumed to be a constant value because it is not a dominant parameter for the controller. Also, each gain has negative weighting factors ($k_{d,negativewtng}, k_{v,negativewtng}$) to include urgent deceleration when distance error or relative velocity is of negative value. Due to this gain scheduling, the car-following model has nonlinearity characteristics as follows:

$$\begin{aligned} k_d &= f(v_e, d_e, v_{rel}) \qquad (4.13) \\ &= k_{d,negativewtng} \cdot (\alpha_{d1} \cdot \arctan(\beta_{d1} \cdot (v_e - \beta_{d2})) + \alpha_{d2} \cdot \arctan(\beta_{d3} \cdot v_e + k_{d0})) \\ k_v &= f(v_e, d_e, v_{rel}) \qquad (4.14) \\ &= k_{v,negativewtng} \cdot (\alpha_{v1} \cdot \arctan(\beta_{v1} \cdot (v_e - \beta_{v2})) + k_{v0})) \end{aligned}$$

where, v_e, d_e and v_{rel} are ego vehicle's velocity, relative distance to the front vehicle and relative velocity, respectively. All other parameters such as $\alpha, \beta, k_{d0}, k_{v0}$ are fixed parameters for gain scheduling of k_d and k_v

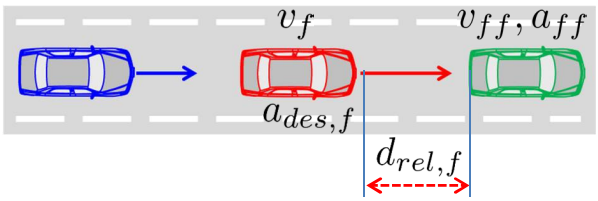

Figure 4.5: Definition of Control Variable for the Front Vehicle

4.3 Step 2 : Aggressivity Factor Estimation

In the previous section, a new car-following model was derived. In this section, the model is applied on the front vehicle, as shown in the Figure 4.5. A logic to predict the front vehicle's motion is derived. All equations for the car-following model, from equations (4.9) to (4.14) should be changed for the front vehicle's motion as represented with equations (4.15) to (4.20) with new notations. (f and ff are representing the front vehicle and the front of the front vehicle, respectively) These equations show the fundamental car-following motion of the front vehicle depending on the motion of the vehicle in front of it.

$$
\begin{aligned}
a_{des,f} &= k_d \cdot d_e + k_v \cdot v_{rel} + k_a \cdot a_{ff} && (4.15)\\
d_e &= d_{rel,f} - d_{des,f} && (4.16)\\
v_{rel,f} &= v_{ff} - v_f && (4.17)\\
d_{des,f} &= d_0 + \tau_h \cdot v_f && (4.18)\\
k_d &= f(v_f, d_e, v_{rel,f}) && (4.19)\\
&= k_{d,negativewtng} \cdot (\alpha_{d1} \cdot \arctan(\beta_{d1} \cdot (v_f - \beta_{d2})) + \alpha_{d2} \cdot \arctan(\beta_{d3} \cdot v_f + k_{d0}))\\
k_v &= f(v, d_e, v_{rel}) && (4.20)\\
&= k_{v,negativewtng} \cdot (\alpha_{v1} \cdot \arctan(\beta_{v1} \cdot (v_f - \beta_{v2})) + k_{v0}))
\end{aligned}
$$

Whenever the ego vehicle encounters a new front vehicle, we have to predict the new vehicle's behavior because each driver has his own different driving style. In equations (4.15) to (4.20), all control gains should be estimated in real-time to exactly predict the front vehicle's future motion. However, with limited measurement, scenario, and time, we cannot extract all control gains in real-time with very exact values. Fortunately, dominant factors describing each car driver's driving style in the equation (4.15) are k_d and k_v. (Although time headway, τ_h in equation (4.18) is another driver-dependent factor, it is considered as a fixed value because the desired acceleration due to different time headway error is very small.) Since the two gains are nonlinear functions, as defined in equation (4.19) and (4.20), we cannot estimate the values directly. Therefore, the simplest way is to rescale the gains with AF_{dis} and AF_{vel} which are aggressivity factors for each car driver:

$$a_{des,f} = k_d \cdot AF_{dis} \cdot d_e + k_v \cdot AF_{vel} \cdot v_{rel} + k_a \cdot a_{ff} \quad (4.21)$$

Then, only the rescaling factors as shown in equation (4.21), should be estimated in real-time. In order to estimate the two aggressivity factors, AF_{dis} and AF_{vel}, optimal theory was used. The logic found aggressivity factors minimizing the difference between current acceleration and estimated acceleration of the front vehicle using the aggressivity factor. However, the logic proved to be too sensitive under different scenarios and steady state conditions. Another approach is derived to estimate the two parameters simultaneously using nonlinear system dynamics equations. We have system dynamics equations, including a car-following model which is defined with nonlinear equations. Also, we can measure some states with measurement noise. Therefore, the Unscented Kalman Filter (UKF) approach is one of the good options. Below is the procedure to estimate the aggressivity factors in real-time.

- State Definition and System Dynamics
  States can be defined as follow.

$$[x_1, x_2, x_3, x_4, x_5, x_6, x_7, x_8, x_9]^T = [v_f, a_f, d_{rel,f}, v_{rel,f}, a_{ff}, a_{des,f}, \dot{a_{ff}}, AF_{dis}, AF_{vel}] \quad (4.22)$$

  Also, the system dynamics can be written as follows

$$\dot{x}_1 = a_f \quad (4.23)$$
$$\dot{x}_2 = \dot{a}_{des,f} - \tau_x \cdot \ddot{a}_f \quad (4.24)$$
$$\dot{x}_3 = v_{rel,f} \quad (4.25)$$
$$\dot{x}_4 = a_{ff} - a_f \quad (4.26)$$
$$\dot{x}_5 = \dot{a}_{ff} \quad (4.27)$$
$$\dot{x}_6 = \dot{a_{des,f}} \quad (4.28)$$
$$\dot{x}_7 = \dot{j}_{ff} = 0 \quad (4.29)$$
$$\dot{x}_8 = \dot{AF}_{dis} = 0 \quad (4.30)$$
$$\dot{x}_9 = \dot{AF}_{vel} = 0 \quad (4.31)$$

  where τ_x is time delay of a longitudinal control actuator and j is jerk(the derivative of acceleration). From the equation (4.21), $\dot{a}_{des,f}$ is derived analytically. Also, $\dot{a}_{ff}$ is calculated from a_{ff}. However, x_7, x_8 and x_9 are assumed to be constant states and have only process noise since we do not know their exact values. Therefore, the values are updated with the process noise from the UKF approach.

- Measurement Definition
  Equations for measurement from vehicle sensors and radar are shown as follows. The forward pointing radar can detect the front vehicle's distance, velocity, and acceleration

as well as that of the vehicle in front of it.

$$y_1 = v_f + m_v \tag{4.32}$$
$$y_2 = a_f + m_a \tag{4.33}$$
$$y_3 = d_{rel,f} + m_{dis} \tag{4.34}$$
$$y_4 = v_{rel,f} + m_{vel,rel} \tag{4.35}$$
$$y_5 = a_{ff} + m_{a,ff} \tag{4.36}$$

where, m is measurement noise.

- Unscented Kalman Filter Approach
  Discretized models can be derived from continuous models using Euler's method. The system dynamics and measurement can be written as follows.

$$x_1(k+1) = x_1(k) + \tau_s x_2(k) + n_1(k) \tag{4.37}$$
$$x_2(k+1) = x_2(k) + \tau_s/\tau_v \times (x_6(k) - x_2(k)) + n_2(k) \tag{4.38}$$
$$x_3(k+1) = x_3(k) + \tau_s x_4(k) + n_3(k) \tag{4.39}$$
$$x_4(k+1) = x_4(k) + \tau_s(x_5(k) - x_2(k)) + n_4(k) \tag{4.40}$$
$$x_5(k+1) = x_5(k) + \tau_s x_8(k) + n_5(k) \tag{4.41}$$
$$x_6(k+1) = x_6(k) + \tau_s \dot{a}_{des}(k) + n_6(k) \tag{4.42}$$
$$x_7(k+1) = x_7(k) + n_7(k) \tag{4.43}$$
$$x_8(k+1) = x_8(k) + n_8(k) \tag{4.44}$$
$$x_9(k+1) = x_9(k) + n_9(k) \tag{4.45}$$

  where τ_s and τ_v are sampling time and a lag of vehicle response due to a lower level actuator, respectively. These equations can be compactly written as:

$$x(k+1) = x(k) + \tau_s \times F(x(k), u(k), w(k)) + n(k) \tag{4.46}$$
$$w(k+1) = w(k) + r(k) \tag{4.47}$$
$$y(k) = G(x(k), \dot{x}(k), u(k)) + m(k), \tag{4.48}$$

  where x consists of x_1 to x_6, and w is the state to be estimated without direct measurements. $n(k)$ and $r(k)$ are process noise terms, and $m(k)$ is the measurement noise term. A detailed UKF approach is already introduced in Section 2.5.1.

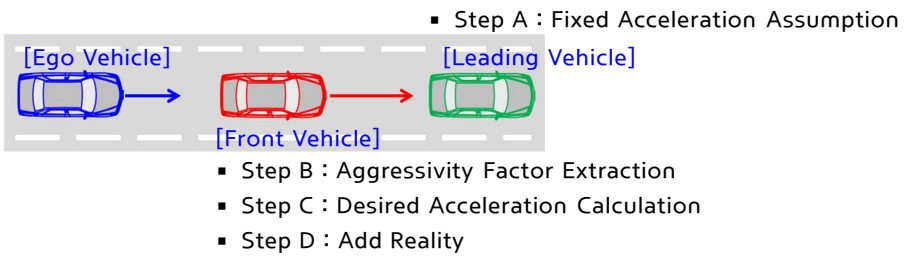

Figure 4.6: Concept of Front Vehicle's Future Motion Prediction

4.4 Step 3 : Front Vehicle's Future Motion Estimation

Here are the procedures for predicting the front vehicle's future motion as shown in Figure 4.6.

- Step A : Fixed Acceleration Assumption of the leading vehicle
  First, we assume that the leading vehicle keeps moving with a current constant acceleration during the prediction horizon. It is a reasonable assumption based on Stéphanie's results [63] for short prediction times.

- Step B : Aggressivity Factor Extraction
  The UKF approach is used to estimate the aggressivity factor of the current front vehicle driver in real-time using a car-following model. The estimation results should be initialized whenever the ego vehicle meets a new front vehicle.

- Step C : Desired Acceleration Calculation
  We know a base car-following model with aggressivity factors. Therefore, the front vehicle's desired acceleration is calculated from the equations.

- Step D : Adding Reality and Propagation of the Motion
  In order to add reality, this research considers driver's reaction delay, smooth driving which can be achieved from limited jerk, maximum acceleration, and maximum deceleration. Finally, from inter-vehicle dynamics between the front and the leading vehicles, the desired acceleration sequence at current time, t, is propagated over the prediction horizon, N, as follows. The leading vehicle is assumed to be moving with constant acceleration.

$$\mathcal{A}_t^f = [a_t^f(k), a_t^f(k+1), a_t^f(k+2), \cdots, a_t^f(k+N-1)] \tag{4.49}$$

  If the leading vehicle does not exist, the aggressivity factor estimation (Step B) cannot be executed and future accelerations of the front vehicle (Step D) are assumed to be constant values.

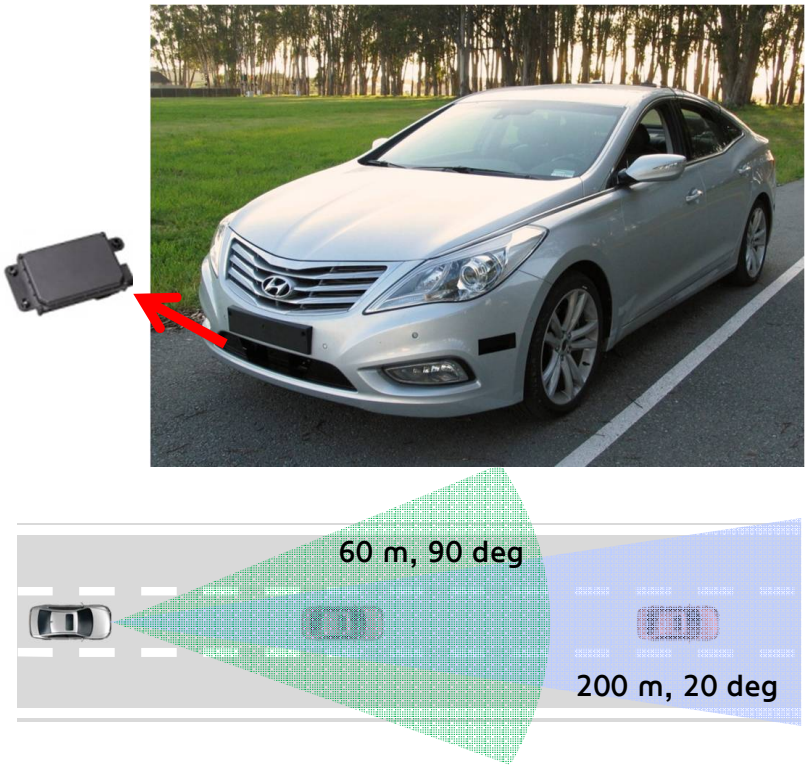

Figure 4.7: Radar and its detection Coverage

4.5 Vehicle Test Results

Figure 4.7 shows the test vehicle setup. The Hyundai AZERA was equipped with a Delphi 77GHz radar for frontal vehicle detection. The radar can detect 64 targets up to 200m in front of the vehicle. For real-time implementation, the dSpace Microautobox was used with a 0.2s sampling time. Vehicle tests were performed on Highway I-80 near Berkeley, CA as shown in Figure 4.8. In this paper, one example of tests is represented.
Before showing aggressivity estimation results, we need to verify the estimation performance of basic states (x_1 to x_5), which is measured by a radar. In Figure 4.9, estimation results and measurement results are shown in blue and red line, respectively. Vehicle velocity is less than 60km/h. As shown in the graph, all estimation states follow measured states very well. The other states (x_6 to x_9) are also estimated. For example, aggressivity factors, AF_{dis} (x_8) and AF_{vel} (x_9), are estimated in real-time, as shown in Figure 4.10. The distance gain aggressivity factor reaches a value of almost 1 during 4 minutes. This means that the front driver's reaction to the distance error is similar to the reaction of the base car following model. The velocity gain aggressivity factor is less than 1. This means that the front vehicle driver's reaction to the relative velocity is smoother than the reaction of the base car-following model.

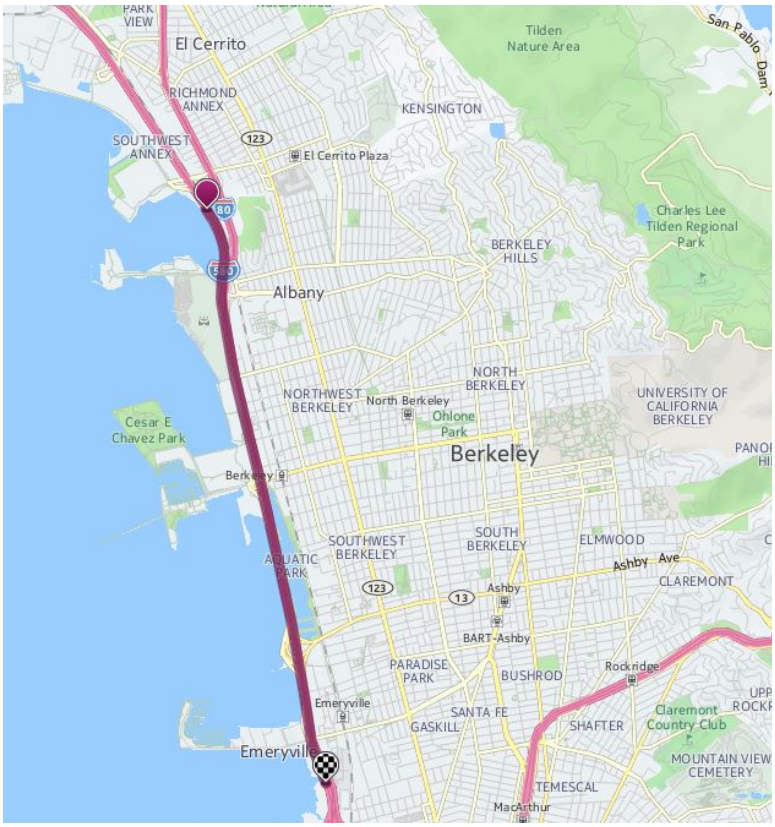

Figure 4.8: Vehicle Test Route

In this thesis, the base car-following model is assumed to show an average driver's driving style. Therefore, depending on the aggressivity factor's value, the driver's driving style can be defined. In order to observe the consistency of the estimation of the driver aggressivity factor, the test vehicle was driven to follow only one target vehicle for 4 minutes.
Using the base car-following model and real-time estimated aggressivity factors, the front vehicle's future motion was calculated for the next 2 seconds at every 0.2 second, as shown in Figure 4.11. The results were shown at every 2 seconds to compare real motion and predicted motion. In both graphs of velocity and acceleration, the predicted motion has very similar movement to the real motion.
A zoom-up graph is shown in Figure 4.12. The results of the proposed logic are compared to the results of the constant acceleration method, which is very widely used. The green line shows real velocity of the front vehicle. The blue line shows the velocity prediction of the front vehicle using the proposed car-following model with aggressivity factor. The red line shows the velocity prediction of the front vehicle using the constant acceleration method. Specifically, at velocity changing points, the suggested logic has much better prediction performance than the prediction of the constant acceleration method. This performance is important in the point of safety and fuel efficiency improvement under velocity changing con-

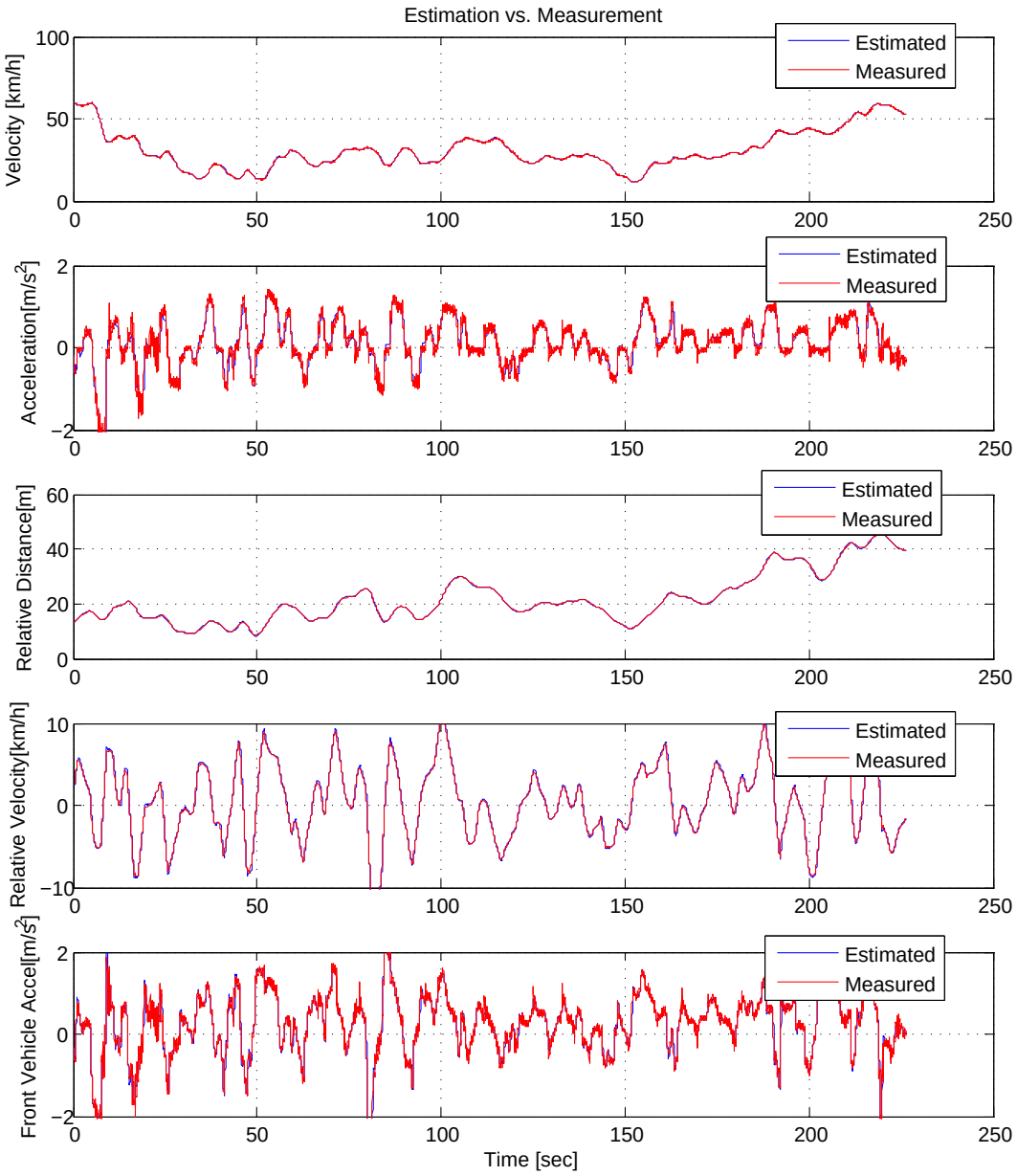

Figure 4.9: State Estimation Results

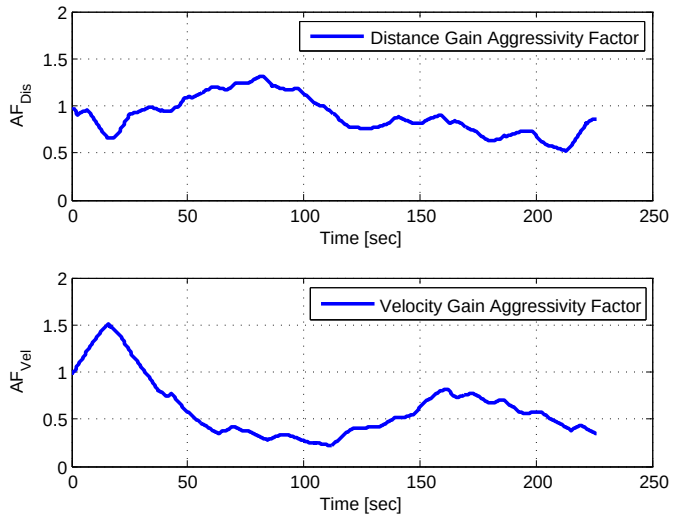

Figure 4.10: Aggressivity Factor Estimation Results

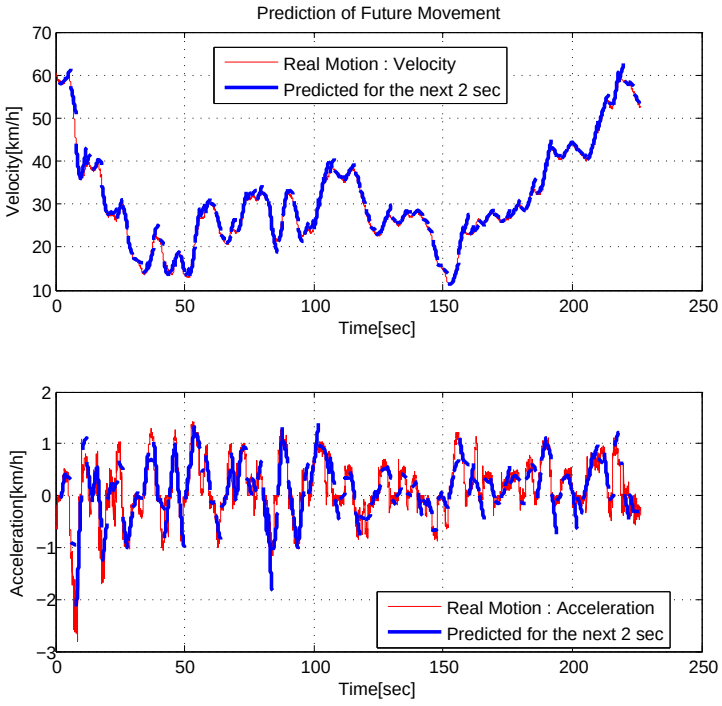

Figure 4.11: Future Motion Prediction(0-250 sec)

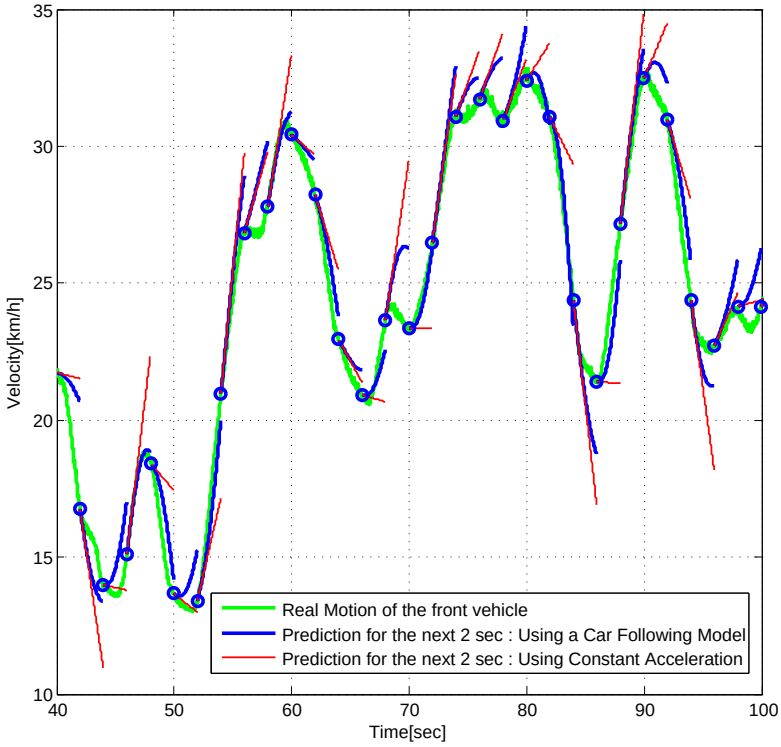

Figure 4.12: Future Motion Prediction(40-100 sec)

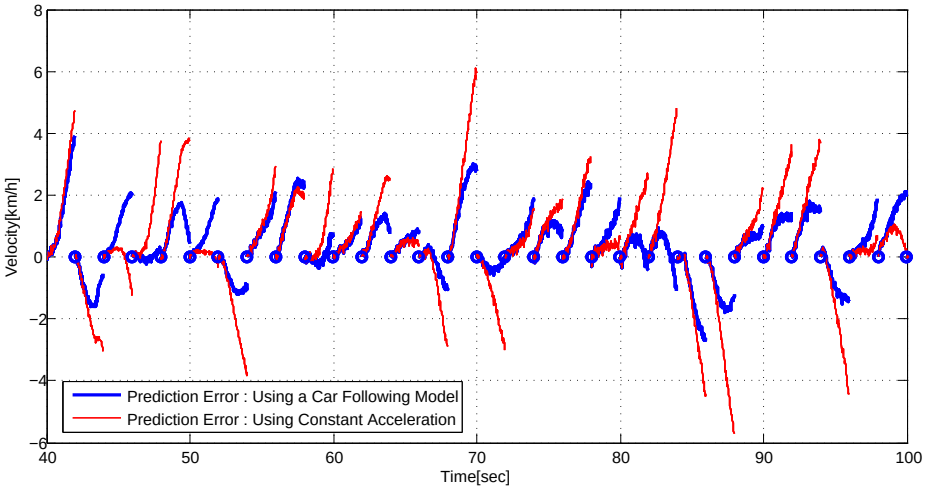

Figure 4.13: Future Motion Prediction Error

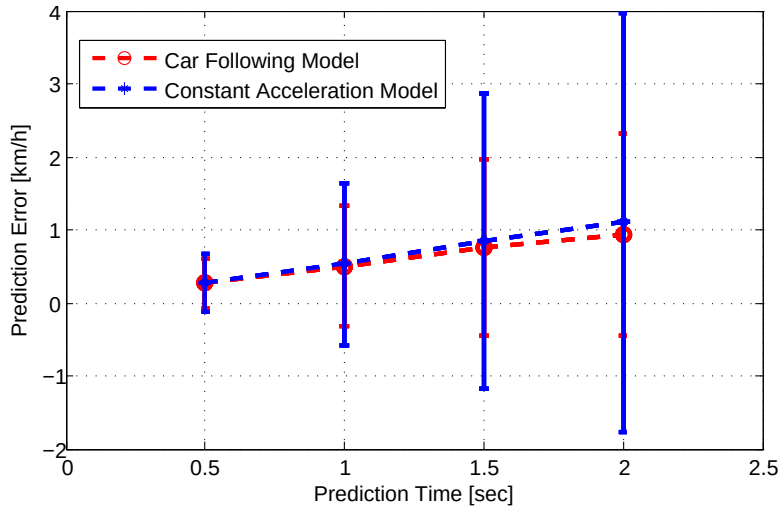

Figure 4.14: Future Motion Prediction Error Analysis

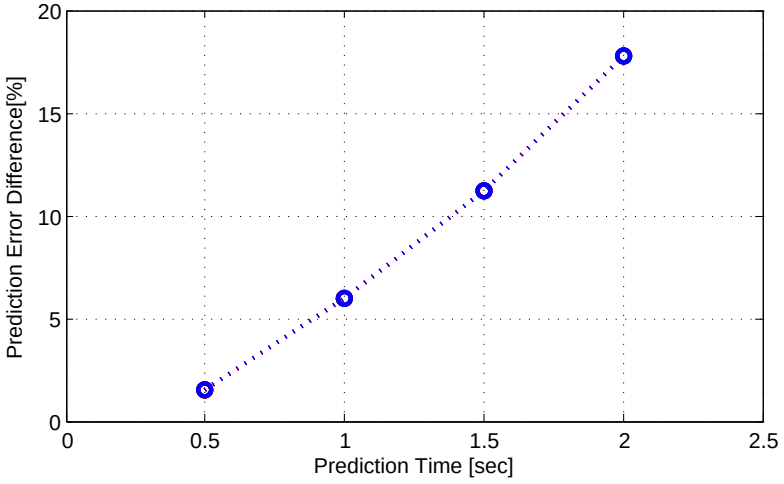

Figure 4.15: Future Motion Prediction Error Rate - Constant Acceleration Model vs. Car Following Model

ditions. The prediction error of both approaches is compared to the measured actual vehicle speed of the front vehicle is shown in Figure 4.13. The results are shown for every 2 seconds for simplicity. The graph clearly shows that the proposed approach using a car-following model has smaller estimation error than that of the constant acceleration assumption model. Also, the performances of prediction for short time horizons (0.5s, 1.0s, 1.5s) are compared in Figure 4.14. The graph shows the mean and the standard deviation of error between predicted velocity and measured velocity of the front vehicle at each prediction time. Prediction errors using a car-following model and a constant acceleration assumption model are shown in red and blue lines, respectively. As prediction time increases, the car-following model-based prediction has less errors. Figure 4.15 shows percent error of both models. As the prediction horizon increases, the prediction error using constant acceleration assumption is 18% larger than the error from the car-following model method.

Stéphanie [63] showed that a car following model with an assumption of constant velocity or acceleration has the best prediction performance within 3 seconds. However, as we have seen in this chapter, the car following model-based prediction has better performance than the acceleration models in this time horizon. Therefore, the proposed approach is reasonable, and additionally, if we improve the base car-following model, we may achieve better prediction results.

4.6 Conclusion

In this chapter, a new car-following model was proposed. It is a deterministic and parametric model extracted from a well tuned ACC system. In order to extract driver's driving style, a driver aggressivity factor was defined. Using the UKF approach, the aggressivity factor could be extracted in real-time by comparing measurements and updating system states. By adopting a base car-following model and am aggressivity factor estimator on the front vehicle, we could propagate the front vehicle's future motion sequence for the next 2 seconds. Furthermore, real vehicle tests on public roads verified that the performance of the proposed approach was better than that of the constant acceleration assumption method.

Chapter 5

Longitudinal Motion Controller : Fuel Efficiency ACC associated with Front Vehicle's Future Motion

5.1 Introduction

Recently, the Adaptive Cruise Control (ACC) System has become a well-adopted technology as an Advanced Driving Assistance System (ADAS). The system provides the occupants with convenient driving without manipulation of gas and brake pedals. However, it focuses only on control performance which tries to converge relative speed(preceding vehicle speed - ego vehicle speed) and relative distance error(relative distance - desired distance) to zero. In this chapter, another feature of ACC will be presented. The new algorithm is designed to improve fuel efficiency while maintaining good control performance.
First, the motivation for the research and framework of the controller are introduced. Secondly, some models for the controller are defined. Thereafter, the fuel efficiency distance controller is introduced. Finally, some simulation results, using real traffic data, are verified using the suggested control law.

5.1.1 Motivation

For the vehicle equipped with automatic speed and distance control function, there are several methods that improve the ego(controlled) vehicle's fuel consumption. First, if we know the traffic signal and traffic conditions in advance, an optimal velocity profile can be generated to minimize waiting time at stop lights and total fuel consumption [4][61]. The second method considered road slopes [13][25][44]. This is reasonable because longitudinal traction force and fuel consumption are related to the up-down slope of the road profile. This method is particularly useful for heavy truck. Third, Vehicle-to-Vehicle (V2V) communication was adopted for a platoon control system [23][41][68]. The platoon with communication increased

traffic efficiency and decreased vehicle-to-vehicle distance to reduce air drag force. Also, optimal gear shift selection considering fuel consumption is another approach for controlling vehicle speed [38].
This research focuses only on the distance control scenario with preceding vehicle information using a conventional sensor such as radar. Special information such as Look-ahead traffic signal and road shape was not considered in this research. To focus on a normal ACC system, platoon dynamics or V2V communication were excluded. Therefore, we only have current ego vehicle's information and current relative distance and velocity to the front vehicle. Since Jonathan [62] showed that fuel economy is very related to driver aggressivity, we need to develop very smooth car-following distance controller. In Lang's research [42], prediction of the preceding driver's behavior improved fuel efficiency for cooperative adaptive cruise control systems. If the front vehicle's future movement is predicted, an optimal distance and gear selection with smooth movement can be constructed. This research focuses on developing logic that can improve fuel efficiency of an ACC equipped vehicle under normal situations using conventional sensors. In the previous chapter, a front vehicle's future motion sequence was predicted. The sequence is utilized for this fuel efficiency ACC controller.

5.1.2 Framework of Fuel Efficiency ACC Controller

Figure 5.1 shows a framework of an ACC controller. The logic consists of four parts. The free cruise control [FCC] logic is a basic logic to track a driver's set speed. It calculates a desired acceleration depending on the current velocity error. The Following Control [FOC] part is for distance control, to minimize relative velocity and distance error. The Curve Speed Limit block controls the ACC vehicle on the curved road to avoid large lateral acceleration to prevent possible rollover. Then, three desired accelerations from each module are sent to the selection block [min[FCC,FOC,CSL]]. The block selects minimum acceleration to send out desired acceleration as a control input to an actuator of the vehicle. The block has saturation and rate limiter(jerk limit) modules to maintain smooth ride quality. This thesis focuses on the Following Control block as a distance controller. A Car-Following Module calculates the future motion of the front vehicle. Also, from the Following Control block, the Optimal Gear Selection block can derive a desired gear stage to minimize fuel consumption.

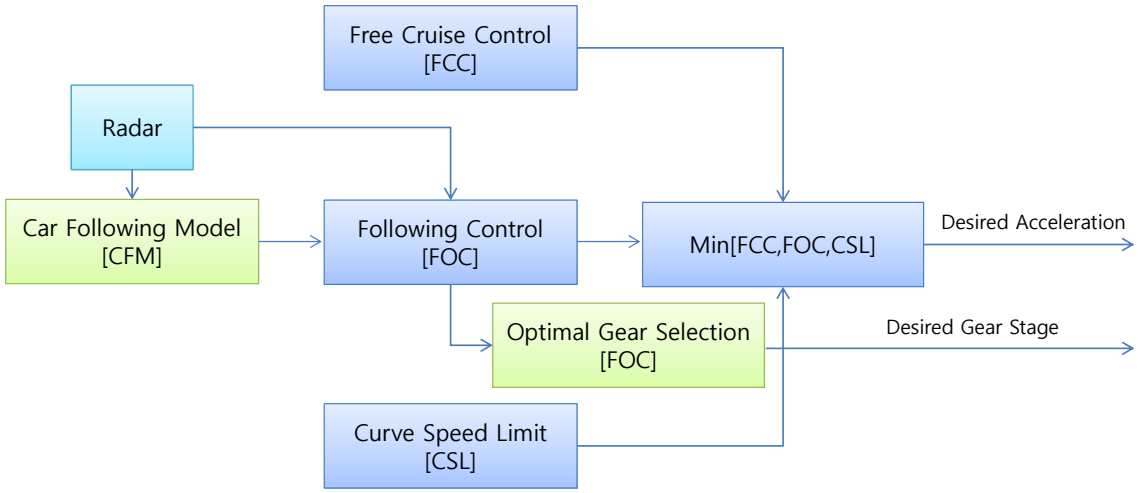

Figure 5.1: Framework of Fuel Efficiency ACC Controller

5.2 Modeling

To calculate optimal control input (acceleration) of the ego vehicle considering fuel consumption, some models need to be derived for a model-based controller.

5.2.1 Fuel Consumption and Vehicle Model

Since the goal of the logic is to minimize fuel consumption while controlling the vehicle with desired speed and distance, the fuel model, which is applicable for the optimization problem is an essential part. In order to be to be easily included in the optimization problem, an accurate yet simple model is needed. In this section, a new fuel consumption model is derived for this purpose. After that, a plant model is described.

- Fuel Consumption Model From Literature Review
  There are several fuel consumption models that need to be taken into account for this research. *Engine Torque Based Model* [40] is simple as shown in equation (5.1).

$$\dot{fuel} = c_1 + c_2 T \tag{5.1}$$

  where the fuel consumption rate, $\dot{fuel}$, is a function of engine torque, T. Also, c_1 and c_2 are parameters depending on the type of vehicle. However, this model does not consider engine speed for calculating fuel consumption, despite it being one of the key factors for fuel consumption.
  The second model is the *Engine Power Model* [29] as shown in equation (5.2).

$$\dot{fuel} = k_1 + k_2 T + k_3 \Delta N_S \tag{5.2}$$

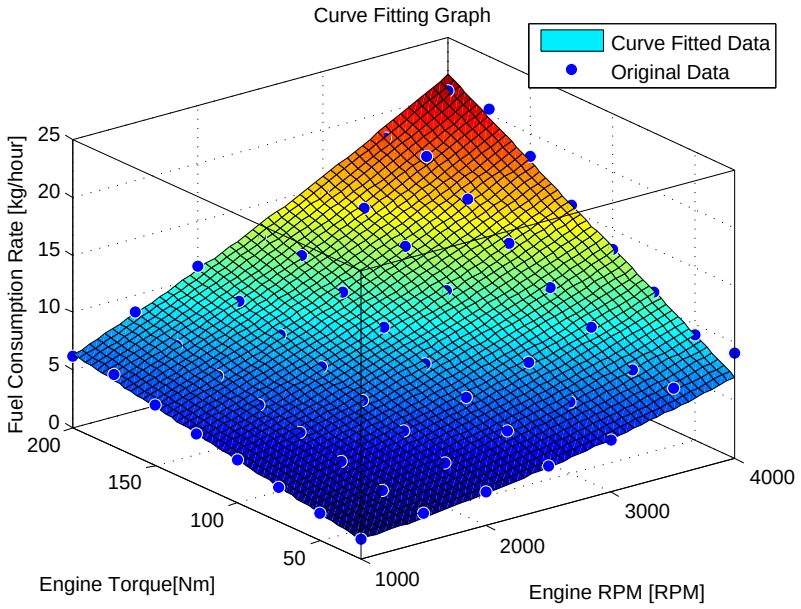

Figure 5.2: Engine Fuel Consumption Map

where T is trip time per unit distance, ΔN_S is a deviation from the average number of stops per unit distance. Also, k_1, k_2 and k_3 are parameters to be tuned. This model considers the vehicle's running time and stop counting. However, this model does not show the transient motion of the vehicle.
The third model is *Comprehensive Power-Based Fuel Model* [31].

$$\dot{fuel} = \alpha_0 + \alpha_1 P + \alpha_2 P^2 \tag{5.3}$$

where P is the engine power and, α_1, α_2 and α_3 are parameters to be tuned. This model shows quite accurate fuel consumption. However, the three parameters should be tuned under various conditions to accurately adopt the model to the controller.

- Fuel Consumption Model From Fuel Consumption Map
  As shown in the previous section, there are several fuel consumption models. Used widely in industry, a fuel consumption map is a function of engine speed and engine torque. For this research, an accurate fuel consumption map is defined with ego vehicle's states, such as velocity and acceleration. Therefore, a fuel consumption equation is derived using curve fitting from a fuel consumption map of the engine with a 1st-order engine torque term and a 2nd-order engine speed term. The curve fitting equations are shown in equation (5.4) and they match the fuel consumption map very closely, as shown in Figure 5.2. Only low-medium engine torque and speed range are used because an ACC system uses limited acceleration and deceleration. The curve-fitted

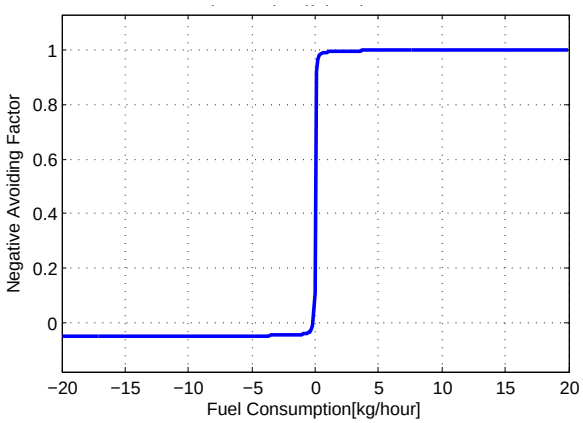

Figure 5.3: Negative Fuel Consumption Avoiding

fuel consumption model is derived as follows.

$$\dot{fuel}_{base} = c_0 + c_1 w_e + c_2 T_e + c_3 w_e^2 + c_4 w_e T_e \tag{5.4}$$

where w_e and T_e are engine speed and engine torque. Also, c_0 to c_4 are coefficients of the curve fitting results. If we assume that the torque converter is locked-up, the wheel is directly connected to the engine via final gear reduction and a transmission. Therefore, engine speed and engine torque can be written by using vehicle speed, v and acceleration, a as shown in equations (5.5) and (5.6). Therefore, these equations allow us to derive the fuel consumption rate using ego vehicle states (velocity and acceleration) as follows.

$$w_e = \frac{1}{R_w \cdot R_f \cdot R_g} \cdot v \tag{5.5}$$

$$T_e = R_w \cdot R_f \cdot R_g \times (M \cdot a + F_{air} + F_{rr}) \tag{5.6}$$

where, R_w, R_f, R_g and M are wheel radius, final gear reduction, gear ratio and vehicle mass. Also, F_{air} and F_{rr} are air drag force and rolling resistance. Also, air drag force can be calculated by the equation:

$$F_{air} = \frac{1}{2}\rho \cdot A \cdot C_{air} \cdot v^2 \tag{5.7}$$

where ρ is air density, A is front area and C_{air} is air drag coefficient.

- Linearization and Adjustment of the Fuel Consumption Model
  In order to keep all systems in a linear quadratic form to guarantee a global optimal solution and cheap calculation cost, linearized equations at each (v_0, a_0) point from the nonlinear curve fitted fuel consumption equation were calculated using the equation:

$$\dot{fuel}_l(v,a) = f(v,a) = \frac{\partial f}{\partial v} \cdot (v - v_0) + \frac{\partial f}{\partial a} \cdot (a - a_0) + f(v_0, a_0) \tag{5.8}$$

However, under braking conditions(deceleration, $a < 0$), using the fuel consumption equation lead to negative fuel consumption, although a real engine generates idle fuel consumption of $1.13kg/hour$. So, an *arctan* function in equation (5.9) is added at the end of the fuel model to avoid negative fuel consumption and to generate idle fuel consumption. The equation is as follows and the graph is shown in Figure 5.3.

$$\dot{fuel}_{adj} = 1.05 \cdot \frac{\arctan(50 \cdot \dot{fuel})}{\pi} + 0.475 \tag{5.9}$$

Due to the above equation, the whole fuel consumption equation becomes a nonlinear function. Finally, the fuel consumption model can be defined as follows.

$$\dot{fuel} = \dot{fuel}_l \times \dot{fuel}_{adj} \tag{5.10}$$

5.2.2 Plant and Distance Dynamics

- Plant Dynamics
  To guarantee cheap calculation time, a very simple plant model is suggested. A simple point mass model is utilized to consider vehicle inertial motion.

$$\dot{v} = a \tag{5.11}$$

$$\dot{a} = j \tag{5.12}$$

  where j is jerk of the ego vehicle.

- Actuator Dynamics and Delay Term
  From desired acceleration as a control input, the lower level actuators, such as brake and engine torque controller, follow the value. This motion is considered as a first-order lag as follows:

$$\tau_a \dot{a}(t) + a(t) \quad = \quad u(t) \tag{5.13}$$

  where τ_a is a time delay for longitudinal motion of the vehicle due to lower level controller (actuator) delay, a is acceleration and u is control input (desired acceleration).

- Discrete Model of Plant and Actuator
  Discretized models for the continuous dynamics can be written as follows.

$$a(k+1) \quad = \quad (1 - \frac{T_s}{\tau_a})a(k) + \frac{T_s}{\tau_a}u(k) \tag{5.14}$$

$$j(k) \quad = \quad \frac{a(k) - a(k-1)}{T_s} \tag{5.15}$$

  where T_s is sampling time.

- Distance Dynamics
  Also, in order to describe two vehicle's relationship, such as relative distance and velocity, the same definition as shown in Figure 4.3 is used.

5.3 Distance Controller

The essential goal of the distance controller is to converge the relative velocity and distance error to zero. For this purpose, a simple PID or LQ controller is very widely used in industry. However, to improve the ride comfort and fuel efficiency, a multi-purpose Model Predictive Control (MPC) is suggested [60][64][66]. In this research, we consider nonlinear dynamics, a multi-purpose optimization problem, and the front vehicle's future motion. Therefore, the Nonlinear Model Predictive Control (NMPC) approach is a good option for this purpose. In this section, basic concepts of NMPC are described and a detailed control logic for fuel efficiency is followed. Finally, a method to determine optimal gear stage is suggested.

5.3.1 Control Law Design : Nonlinear Model Predictive Control

From continuous-time nonlinear system dynamics, a discrete-time nonlinear system dynamics, f_d, and measurement update, h_d, can be derived with n states and a fixed sampling time, T_s,

$$\xi(k+1) = f_d(\xi(k), u(k), k) \tag{5.16}$$

$$\zeta(k) = h_d(\xi(k)) \tag{5.17}$$

where $\xi \in \mathbb{R}^n$ and $u, \zeta \in \mathbb{R}^m$ are state vector, input and output of the system, respectively. Also, the above system is subject to the following state constraints and input constraints,

$$\xi(k) \in \mathcal{X}, u(k) \in \mathcal{U}, \forall k \geq 0 \tag{5.18}$$

where $\mathcal{X} \subseteq \mathbb{R}^n$ and $\mathcal{U} \subseteq \mathbb{R}^m$ are usually defined with polyhedra. If the state is measured or estimated at each time step, a finite time optimal control problem is solved at each time step as follows.

$$\begin{aligned} \min_{U_k, \Xi_k} \ & J_N(\Xi_k, U_k) \\ \text{s.t.} \ & \xi_{i+1,k} = f_d(\xi_{i,k}, u_{i,k}, i), \ i = k, \ldots, k+N-1 \\ & \xi_{i,k} \in \mathcal{X}, \ i = k, \ldots, k+N \\ & u_{i,k} \in \mathcal{U}, \ i = k, \ldots, k+N-1 \\ & \xi_k = \xi(k) \\ & \xi_{i+N,k} \in \mathcal{X}_f \end{aligned} \tag{5.19}$$

The optimization problem is solved at time k and the predicted state, $\xi_{k,i}$, can be obtained by applying the optimal control sequence, U_k. The predicted state trajectory and optimal control input sequence are formulated as follows.

$$\Xi_k = \begin{bmatrix} \xi_k & \xi_{k+1} & \ldots & \xi_{k+N+1} \end{bmatrix}^T, \tag{5.20}$$

$$U_k = \begin{bmatrix} u_k & u_{k+1} & \ldots & u_{k+N} \end{bmatrix}^T, \tag{5.21}$$

At each time step, k, the initial state is updated with $\xi_k = \xi(k)$. The final propagated state should be constrained with a kind of polytope, $\mathcal{X}_f$.
Then, the cost function, $J_N(\Xi_k, U_k) : \mathbb{R}^n \times \mathbb{R}^{Nm} \to \mathbb{R}^+$ is generally defined as,

$$J_N(\Xi_k, U_k) = P_N(\xi(N)) + \sum_{i=0}^{N-1} P(\xi(i), u(i)) + R(u(i)) \tag{5.22}$$

where P_N, P and R are terminal cost, state cost and input cost, respectively. From the optimization problem, if the optimal input, $U_k^* = \{u_{k,k}^*, u_{k+1,k}^*, \ldots, u_{k+N,k}^*\}$, is found, the optimal trajectory, Ξ_k^*, can be generated. Then, we only apply the first optimal control input to the system:

$$u(k) = u_{k,k}^*(\xi(k)) \tag{5.23}$$

At the next time step, the optimization problem will be solved over the shifted time horizon using the newly updated state $\xi(k+1)$. This concept uses Nonlinear Model Predictive Control as a state feedback closed loop controller.

5.3.2 Controller without Optimal Gear Selection

A fuel efficiency ACC logic will be presented in this section without considering an optimal gear selection. Therefore, during the prediction horizon, we assume that the gear stage keeps the current gear stage.

5.3.2.1 Control Goal

The basic control objective of the distance controller is to make distance error and relative speed converge to zero. Distance error,d_e, and desired distance,d_{des}, can be calculated as follows:

$$d_e = d_{rel} - d_{des} \tag{5.24}$$

$$d_{des} = d_0 + \tau_h \times v \tag{5.25}$$

where τ_h is a time gap in seconds between two vehicles.

5.3.2.2 State Definition and System Dynamics

The states can be defined using models already defined in section 5.1. The states include an ego vehicle's longitudinal motion and relative motion between an ego vehicle and a front vehicle.

$$x_1 = \quad v \quad : \text{Ego Vehicle Velocity} \tag{5.26}$$

$$x_2 = \quad a \quad : \text{Ego Vehicle Acceleration} \tag{5.27}$$

$$x_3 = \quad j \quad : \text{Ego Vehicle Jerk} \tag{5.28}$$

$$x_4 = \quad d_{rel} \quad : \text{Clearance(Distance to the Front Vehicle)} \tag{5.29}$$

$$x_5 = \quad v_f - v \quad : \text{Relative Velocity} \tag{5.30}$$

Also, the discretized state equations are written in the following form.

$$x(k+1) = Ax(k) + Bu(k) + W(k) \tag{5.31}$$

where W(k) is a disturbance term which represents acceleration of the front vehicle. It is written as a_f in the state equations. The information can be utilized by a car-following model of the front vehicle. All discretized equations of motion can be written as follows:

$$\begin{aligned}
x_1(k+1) &= x_1(k) + T_s x_2(k) && (5.32)\\
x_2(k+1) &= (1 - \frac{T_s}{\tau_x})x_2(k) + \frac{T_s}{\tau_x}u_x(k) && (5.33)\\
x_3(k+1) &= -\frac{1}{\tau_x}x_2(k) + \frac{1}{\tau_x}u_x(k) && (5.34)\\
x_4(k+1) &= x_4(k) + T_s x_5(k) - \frac{1}{2}{T_s}^2 x_2(k) + \frac{1}{2}{T_s}^2 a_f(k) && (5.35)\\
x_5(k+1) &= x_5(k) - T_s x_2(k) + T_s a_f(k) && (5.36)
\end{aligned}$$

5.3.2.3 Nonlinear MPC

The control output of the ACC logic is desired acceleration. To minimize velocity error and distance error, optimal control theory is applied. However, model predictive control is better than a traditional optimal control since we can account for future motion of the front vehicle.

- Cost Function
  A simple quadratic cost function for the Finite Time Constrained Optimal Control is defined in this form. In order to minimize fuel consumption, the fuel consumption cost is included in the cost equation.

$$J = \sum_{k=0}^{N-1} \{ w_u \cdot {u_k}^2 + w_{dis} \cdot d_e^2 + w_{vel} \cdot v_{rel}^2 \ + w_{fuel} \cdot \dot{fuel}_k \} \tag{5.37}$$

  where w_u, w_{dis}, w_{vel} and w_{fuel} are weighting factors for the cost function. Three terms are 2-norm and the fuel term is treated as an infinite norm case. This is because the total fuel consumption cost should be minimized under the control. As shown in equations (5.4) through (5.10), the fuel consumption rate is defined as a nonlinear equation which is a function of velocity and acceleration.

- Constraints
  The first constraint is due to the limited control input as follows:

$$u_{min} \leqq \ \ u \ \ \leqq u_{max} \tag{5.38}$$

  Also, the input constraint matrix can be defined as follows:

$$H_u \times u \leqq \ \ K_u \tag{5.39}$$

The second constraint set can be considered to improve driving quality. Acceleration and its change rate (jerk) should be constrained.

$$a_{min} \leqq \quad a \quad \leqq a_{max} \tag{5.40}$$
$$j_{min} \leqq \quad j \quad \leqq j_{max} \tag{5.41}$$

To guarantee safety, the maximum velocity of ego vehicle must not exceed the driver's set speed.

$$v_1 \quad \leqq \quad v_{set} \tag{5.42}$$

Also, the minimum distance between an ego vehicle and a front vehicle should be bounded for safety.

$$d_{rel} \quad \geqq \quad d_{des} \times \eta_{min} \tag{5.43}$$

where d_{des} is the driver's desired distance and $\eta_{min} \in [0, 1]$ is the minimum distance ratio of the desired distance.
All of these state constraints can be written in the following matrix form:

$$H_x \times x \leqq \quad K_x \tag{5.44}$$

5.3.3 Controller with Optimal Gear Selection

In this section, optimal gear selection of a transmission gear box is included in the receding horizon optimization problem. As shown in equations (5.5) and (5.6), gear ratio, which is defined by gear stage, is directly connected to engine RPM, w_e, and engine torque, T_e. These two factors are used for calculating fuel consumption, as shown in equation (5.4). Since fuel consumption cost is included in the cost function of the optimization problem, optimal gear selection is meaningful for fuel efficiency ACC. However, if the optimal gear stage is included in the Nonlinear Optimization Problem, it can be considered as a Mixed Integer Nonlinear Optimization Problem, and finding the optimal solution is a very challenging process. For implementation of this research, the MPT toolbox with YALMIP as a formulation tool and IPOPT as an optimization problem solver for the Nonlinear MPC were used. However, for the mixed integer nonlinear problem, no solver could be adopted to the formulation tool.
As a second approach, three different gear stage cases (shift up case, shift down case and current shift case) were considered at each time step as shown in Figure 5.4. The ego vehicle is assumed to keep the gear stage during prediction horizon. Then, at each time step, the NMPC finds the optimal solution and optimal cost for each shift-up, shift-down, and keeping case, respectively. After that, the three stages' cost were compared, and the minimum cost for the optimal gear stage was selected. Through this simple approach, we can verify whether the fuel optimal gear selection is valuable or not. Figure 5.5 shows an example of this concept. The blue line using shift up control shows the cost difference compared to the current shift

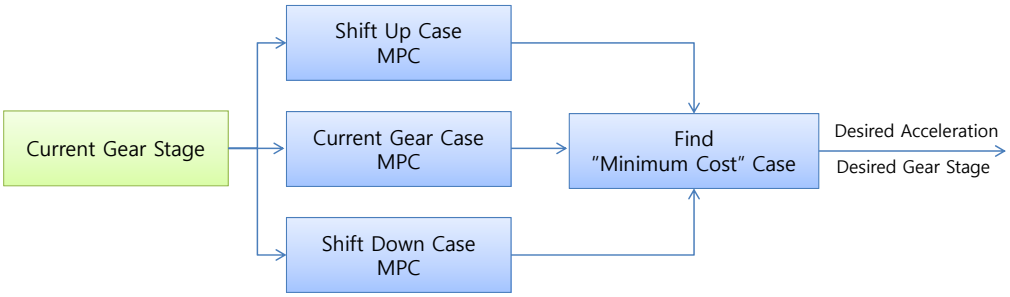

Figure 5.4: Framework of Optimal Gear Selection

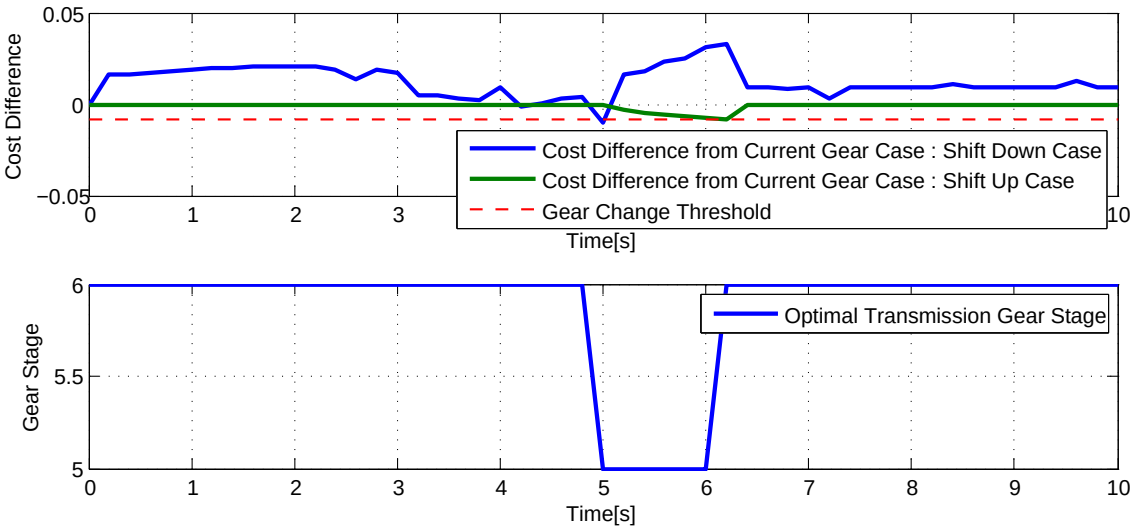

Figure 5.5: Example of Optimal Gear Selection

case. Also, the red line indicates the shift down case. In order to avoid frequent gear change, a gear change threshold (in dashed red line) was applied. Also, another constraint for gear change was applied. For shift-down case, the engine RPM should be lower than 4000RPM in order to avoid engine overload. For the shift-up case, to avoid engine stall, the engine RPM should be larger than 800RPM. Using this concept, the optimal gear change can be conducted as shown in the bottom graph in Figure 5.5.

5.4 Simulation Results Using Real Traffic Data

In this section, three types of simulation results are presented. First, in order to validate the distance controller, very basic scenarios were chosen. After that, associated with the front vehicle's future movement estimator, the Nonlinear Model Predictive Control Logic, without consideration of optimal gear change is verified with real traffic data of the front vehicles. Finally, the optimal gear selection was taken into account for Mixed Integer Nonlinear Model Predictive Control of fuel efficiency ACC.
Simulations were performed using MATLAB based m-file and simulink files. For the vehicle plant, engine dynamics model, torque converter model, transmission gear model and longitudinal vehicle force model without tire dynamics were used. The sampling time is 0.2 seconds. YALMIP was used for MPC formulation and IPOPT was used as an optimization solver. In the receding horizon logic, 10 steps prediction and sampling time with 0.2 second were used.

5.4.1 Distance Controller Validation under Normal Scenarios

Three simple scenarios are suggested for validation of the controller. For the first scenario, Table 5.1 shows the simulation settings and the results are shown in Figure 5.6. This is a very normal scenario of the ACC system. When the ego vehicle follows a front vehicle, the front vehicle makes a lane change, then the ego vehicle meets a new front vehicle at a further distance. As we expect, the ego vehicle accelerates and decelerates to converge to the desired goal very smoothly, as shown in the Figure 5.6.

Table 5.1: Simulation Setting of Scenario 1

Set Speed	$100km/h$
Initial Speed	$80km/h$
Initial Distance	$42m$
Initial Distance Error	$17m$
Scenario	1. following 80km/h vehicle and the front vehicle is cut-out 2. meet another 80km/h vehicle at 59m

The next scenario is another basic traffic condition as shown in Table 5.2. When the front vehicle accelerates and then decelerates, the ego vehicle keeps safe distance as shown in Figure 5.7. The ego vehicle follows the front vehicle very smoothly while maintaining a safe distance.

The last scenario is described in Table 5.3. The ego vehicle suddenly finds a slow moving vehicle in the forward direction. Since the front vehicle is located at a further distance than the desired distance, the ego vehicle keeps going and then decelerates to keep safe distance, as shown in Figure 5.8.

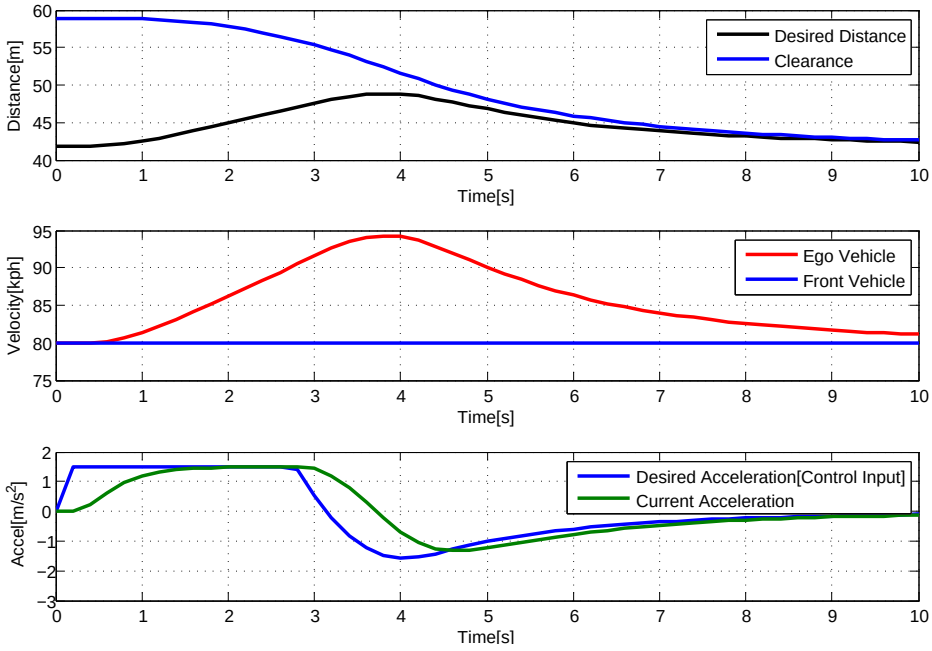

Figure 5.6: Scenario 1 - Positive Distance Error

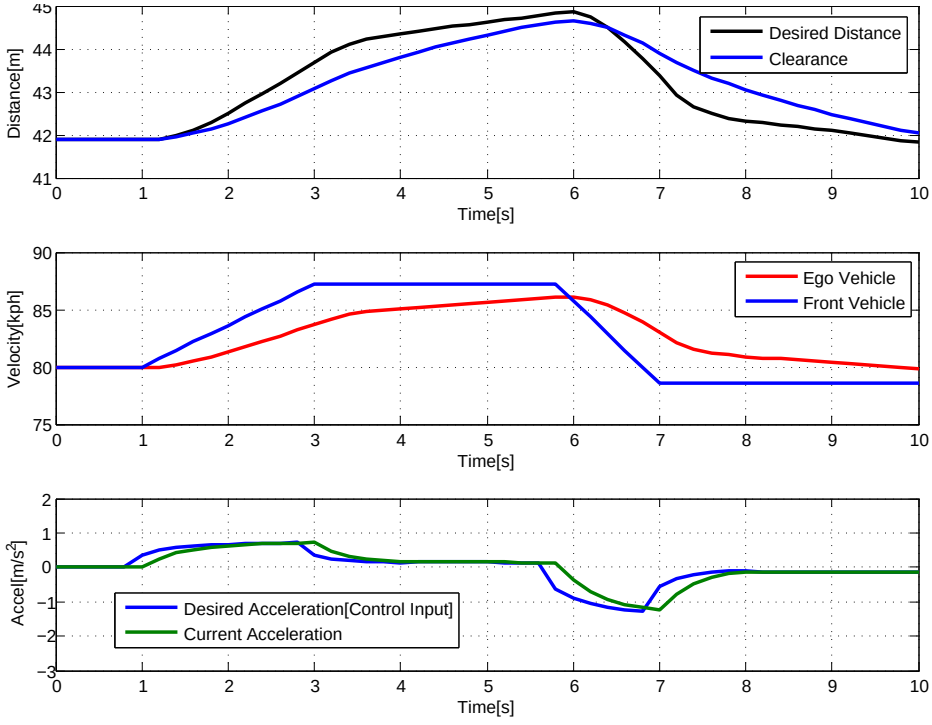

Figure 5.7: Scenario 2 - Accelerating and Braking

Table 5.2: Simulation Setting of Scenario 2

Set Speed	$100km/h$
Initial Speed	$80km/h$
Initial Distance	$42m$
Initial Distance Error	$0m$
Scenario	1. front vehicle's accelerating with 1 m/s^2 and keeping speed 2. front vehicle's braking with -2 m/s^2 and keeping speed

Table 5.3: Simulation Setting of Scenario 3

Set Speed	$80km/h$
Initial Speed	$80km/h$
Initial Distance	$50m$
Initial Distance Error	$18m$
Scenario	front slow moving vehicle cuts-in at 70km/h

From three basic examples, we can conclude that the control logic has good and stable performance as a distance controller.

5.4.2 Distance Controller without Optimal Gear Selection Using Real Traffic Data

The front vehicle's future motion using real traffic data was fed in the NMPC logic during the prediction horizon. Also, during the prediction horizon (2 seconds), we assume that the gear stage has been kept at the current gear stage.
In order to compare the performance of the suggested logic, a Linear-Quadratic based optimal controller was chosen as a reference controller. However, the LQ controller uses only current information, such as relative velocity and distance. Figure 5.9 shows the control results. The ego vehicle follows the front vehicle very smoothly as shown in the distance and velocity graphs. Also, during simulation, instant fuel consumption rate, which is a function of engine speed and engine torque, was calculated using a fuel consumption map. The results are shown in the bottom graph of the figure.
Figure 5.10 shows simulation results using the MPC approach. When the front vehicle moves, the ego vehicle tracks the front vehicle's velocity and desired distance. The third graph shows the calculated optimal control input (desired acceleration) and the vehicle's current acceleration. The control performance looks very similar to that of the LQ controller. However, focusing on the velocity profile shown in Figure 5.11 and 5.12, we can find two differentiating characteristics. The first advantage of the MPC controller is that considering

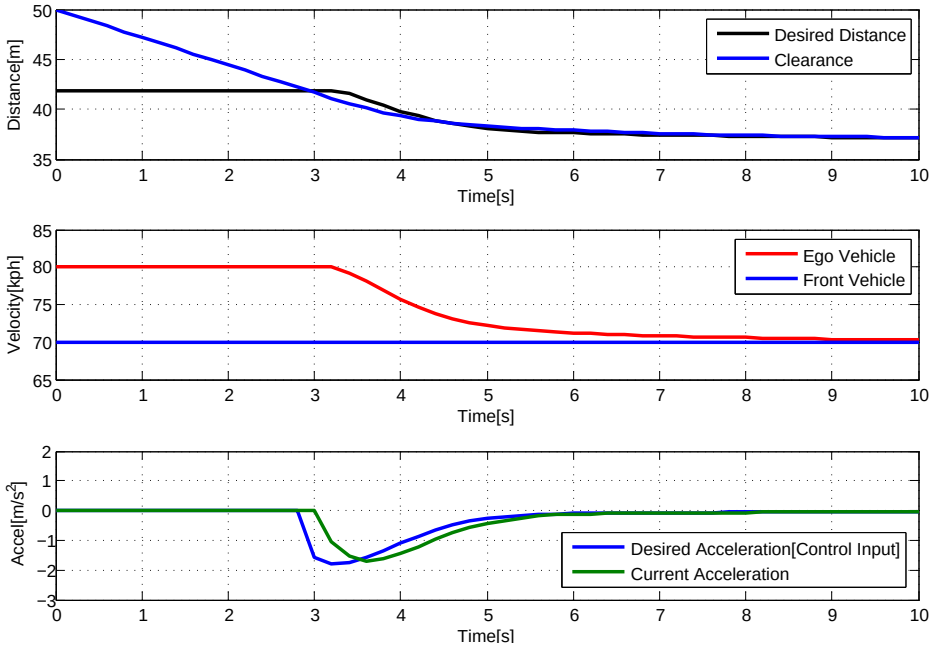

Figure 5.8: Scenario 3 - Slow Moving Front Vehicle

the front vehicle's future motion has a safer reaction than when the front vehicle starts to brake. As shown in Figure 5.11, the MPC controller decelerates earlier than the LQ controller at 1.8 seconds in advance. If we consider platoon control, this feature can guarantee the string stability of the system. The other important feature is the amplitude of velocity fluctuation. As shown in Figure 5.12, the velocity change amplitude of the MPC controller is smaller that the amplitude of the LQ controller. For example, as shown in the figure, the MPC controller has 3.5km/h velocity fluctuation amplitude, and the LQ controller has 6.1km/h velocity fluctuation amplitude. Therefore, the MPC controller has smoother response and the ego vehicle does not have to accelerate or decelerate more than the LQ controller based vehicle. As a result, this smooth response has the potential to improve fuel efficiency. These two advantages come from the prediction of the front vehicle's motion.
Focusing on fuel consumption, fuel consumption related results are shown in Figure 5.13. Engine speed of the MPC controller has a smoother response than the LQ controller. Also, in the engine torque graph, under braking, negative engine torque due to engine friction torque was observed. The torque graph using the MPC controller has a faster response than the LQ controller due to the prediction of the front vehicle's movement. Depending on engine speed and engine torque, the fuel consumption rate can be gathered as shown in the third graph. During the simulation time(30 seconds), the total fuel consumption was gathered from the fuel consumption map. Table 5.4 shows the fuel consumption results using both approaches. The MPC approach can improve fuel consumption by 3.67 % compared with

the LQ approach.

Table 5.4: Fuel Consumption Improvement of MPC Controller

Control Approach	Fuel Consumption	Fuel Efficiency Improvement
LQ	24.79g for 30 seconds	-
MPC	23.98g for 30 seconds	3.67%

5.4.3 Basic Distance Controller with Optimal Gear Selection Using Real Traffic Data

In addition to the MPC logic considering the future motion of the front vehicle, the controlled vehicle's optimal gear selection was considered. The same traffic data and simulation settings used in section 5.3.3 were applied. Control results, as shown in Figure 5.14, are very close to the results when optimal gear selection was neglected, as shown in Figure 5.10. However, as shown on the last graph in Figure 5.15, the fuel optimal gear stage is different from the normal gear stage. Engine speed and engine torque show different aspects while fuel rate is almost the same. This is because we need to place more weight on a basic goal of the controller (converging relative velocity and distance error to zero) than the fuel consumption part. Therefore, the velocity profile of fuel efficient ACC considering optimal gear stage has a very similar trajectory to that of a normal fuel efficiency ACC, as shown in Figure 5.16. As a result, as shown in Table 5.5, the fuel optimal gear selection logic can only improve 0.4 % for 30 seconds. Although the suggested logic does not show good performance for fuel economy, the controller to select fuel optimal gear stage may increase fuel efficiency by adjusting weighting gain under different traffic scenarios. Furthermore, although the conventional gear selection is not perfectly optimal in terms of fuel consumption, it is tuned for power and fuel optimality.

Table 5.5: Fuel Consumption Improvement of MPC Controller with Optimal Gear Selection

Control Approach	Fuel Consumption	Fuel Efficiency Improvement
MPC	23.98g for 30 seconds	-
MPC+Optimal Gear	23.90g for 30 seconds	0.4%

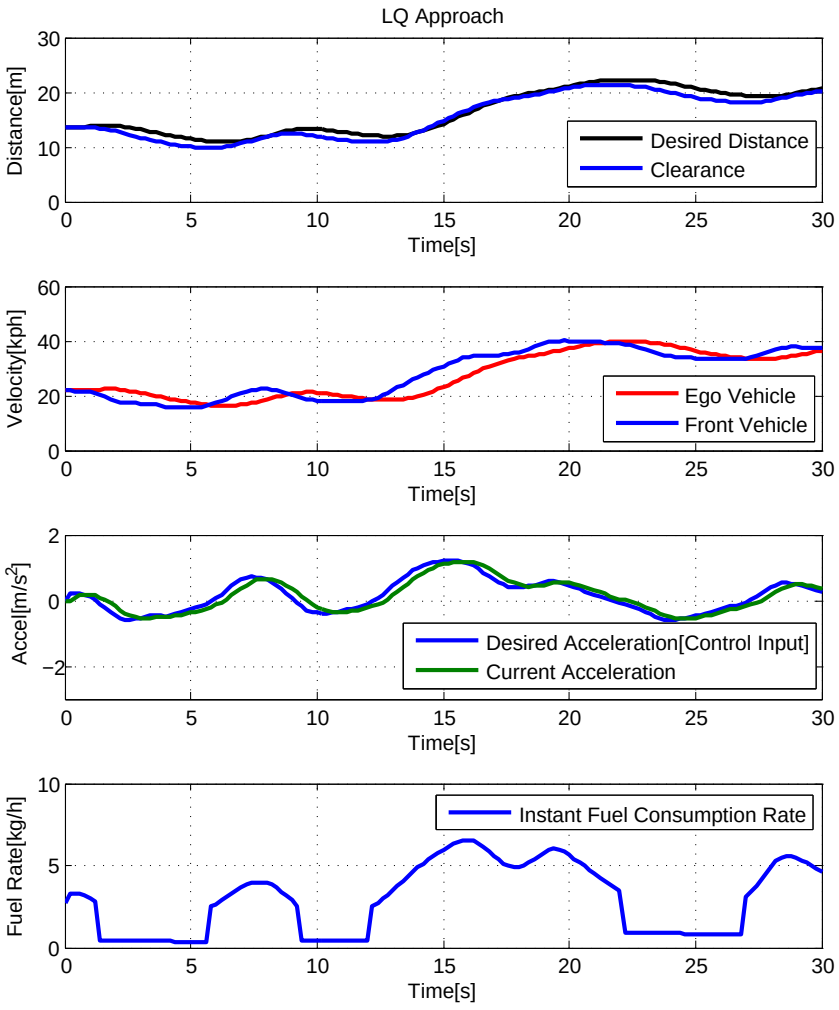

Figure 5.9: Distance Control Using LQ Controller

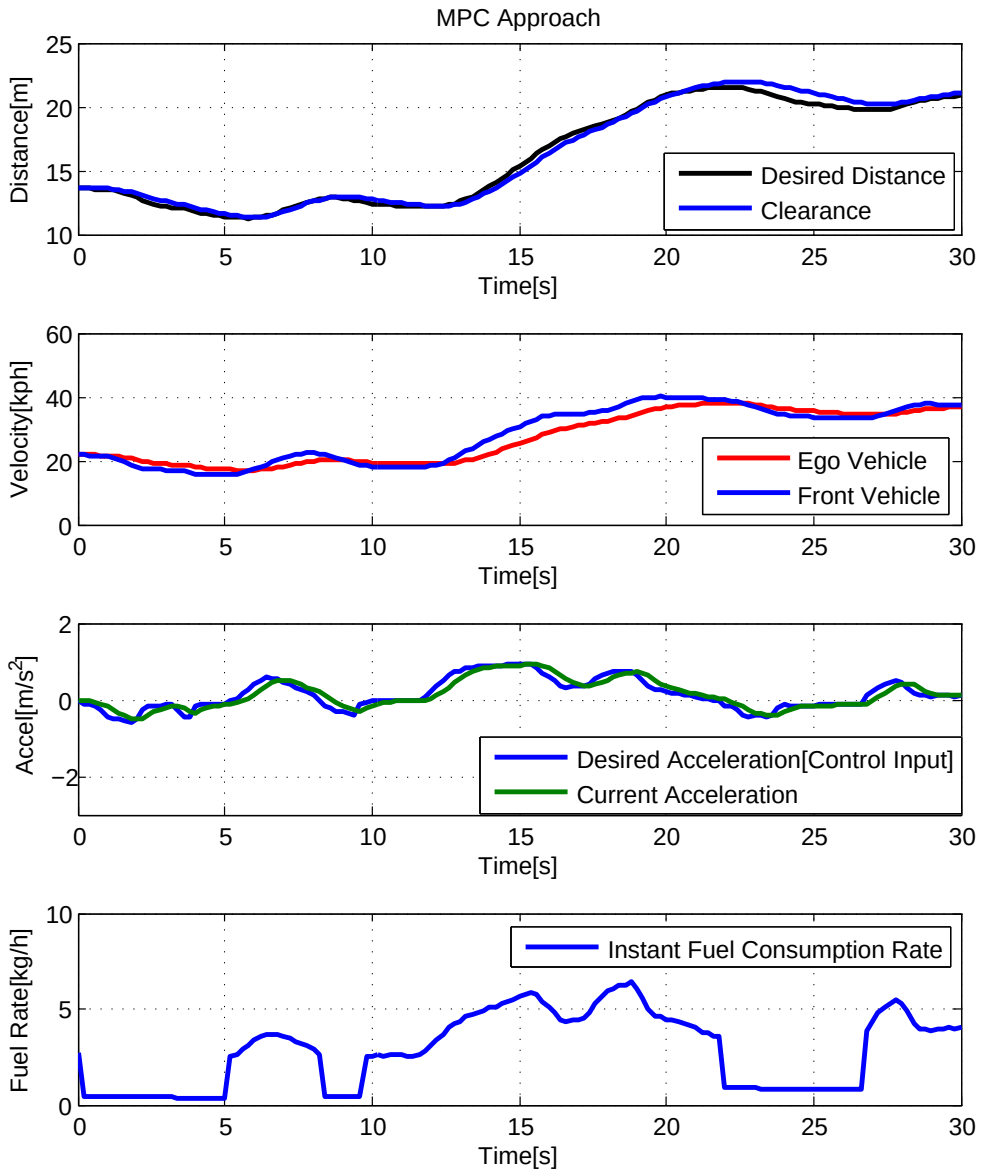

Figure 5.10: Distance Control Using MPC Controller

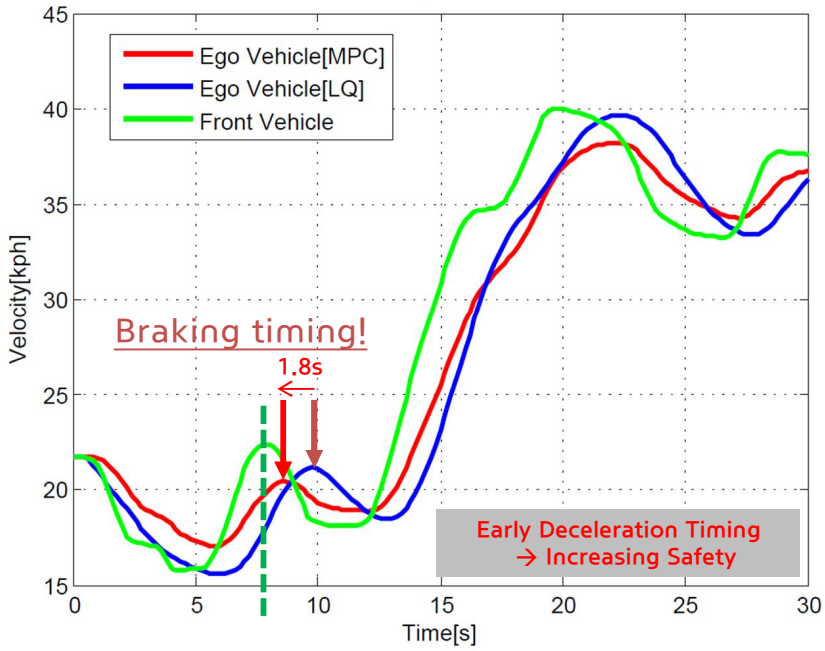

Figure 5.11: Distance Control Results Comparison - Velocity Profile for Braking Timing

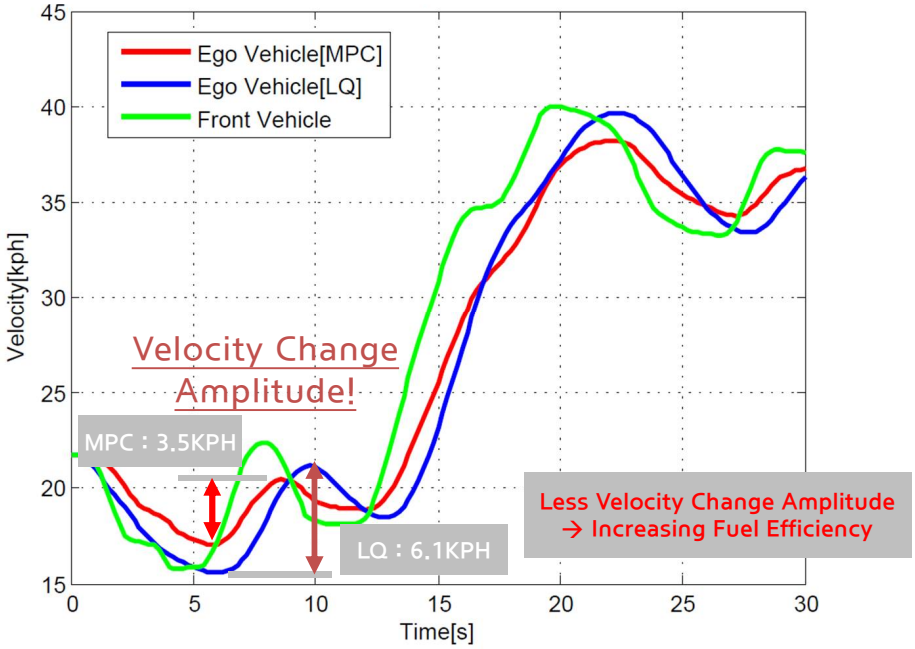

Figure 5.12: Distance Control Results Comparison - Velocity Profile for Fuel Saving

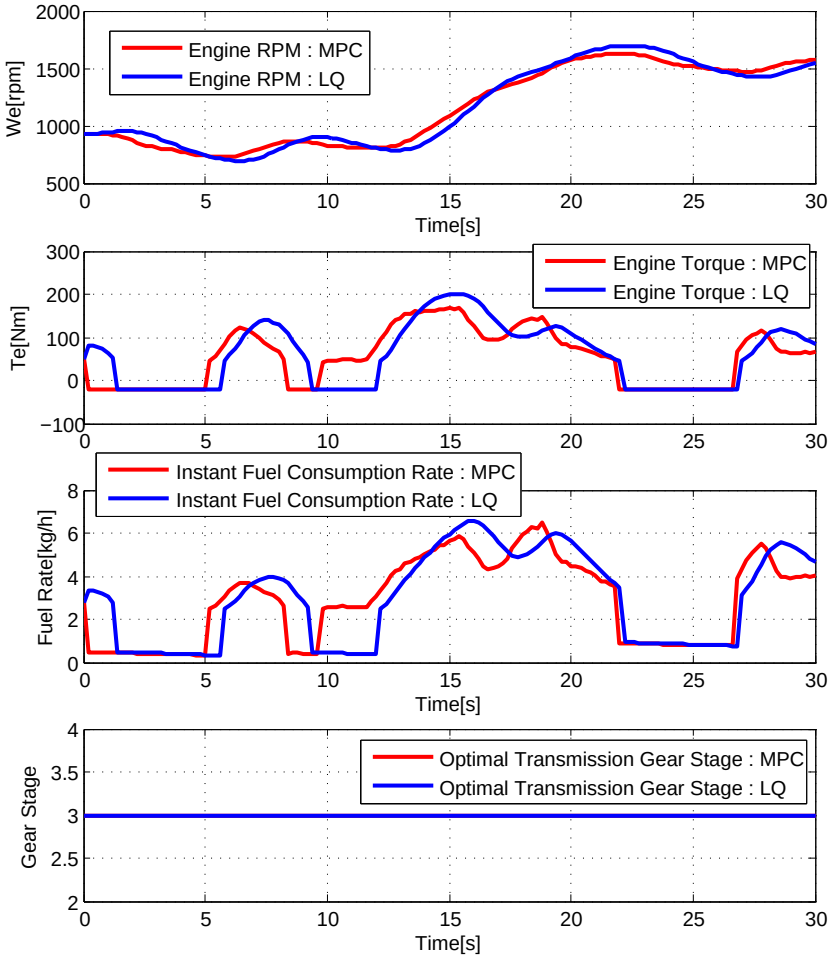

Figure 5.13: Distance Control Results Comparison - Fuel Consumption

5.5 Conclusion

In this chapter, a basic distance controller was proposed using the Nonlinear MPC approach. But, in order to improve fuel efficiency, a fuel consumption model was included in the optimization problem. The fuel consumption model was derived from a real vehicle's fuel consumption map. Through basic simulations, the control logic was validated.
In the previous chapter, the front vehicle's future motion estimator was suggested. From this module, a sequence of the future motion was fed to the distance controller. Considering the future motion in the optimization problem, the fuel efficiency ACC logic improved fuel economy by 3.67% under real traffic data. This is because the controller makes the ego vehicle's velocity profile very smooth to prevent abrupt acceleration and deceleration. Consequently, this approach is meaningful for real vehicle implementation to improve fuel efficiency for a distance controller.

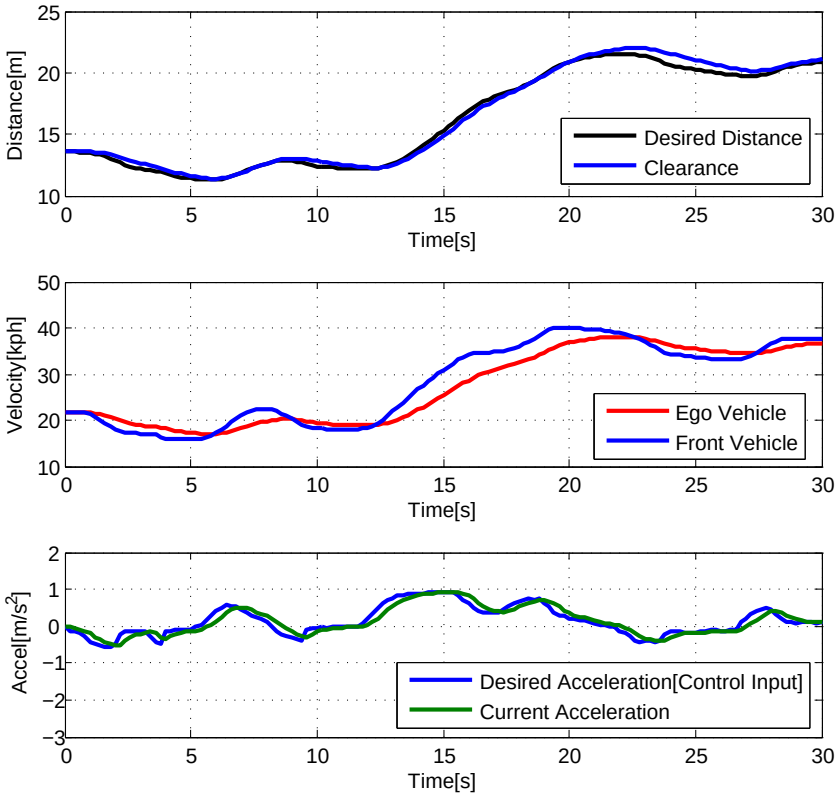

Figure 5.14: Distance Control Considering Optimal Gear Selection

Lastly, simple optimal gear selection logic was suggested. Although the optimal solution could not improve the fuel economy as anticipated, the suggested concept can be tuned for other traffic scenarios.

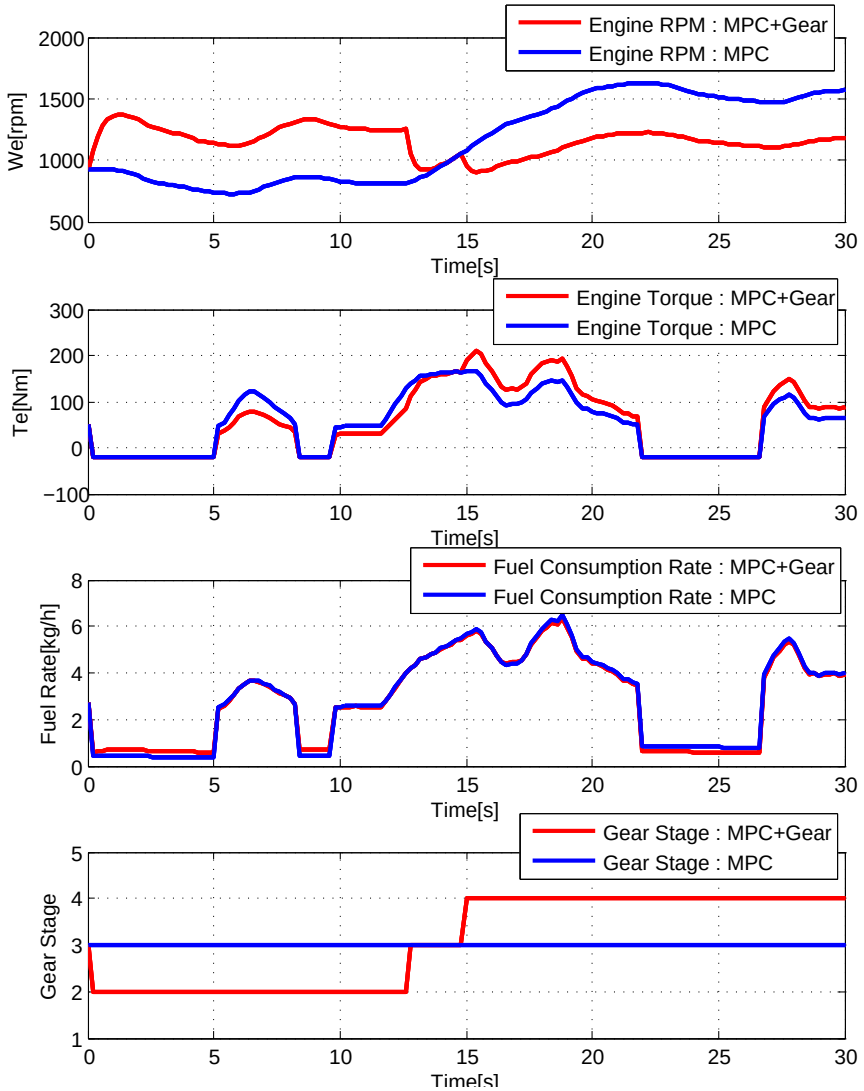

Figure 5.15: Distance Control Considering Optimal Gear Selection - Gear Stage

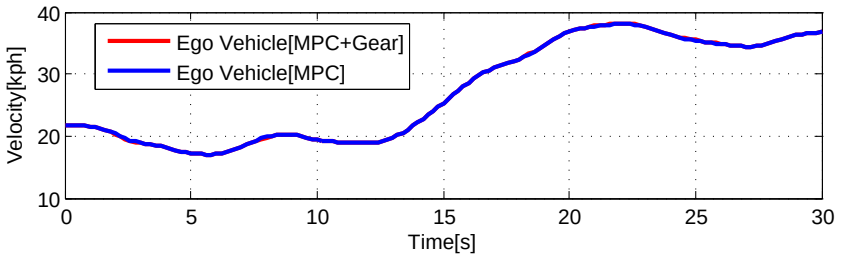

Figure 5.16: Distance Control Considering Optimal Gear Selection - Velocity Profile

Chapter 6

Conclusions and Future Work

This thesis presented disturbance estimators and controllers associated with the disturbances for an autonomous vehicle, such as a longitudinal distance controller and a lateral lane keeping controller.

6.1 Conclusions

- Lateral Disturbance Estimation
  In order to estimate road bank angle as a disturbance term for the lane keeping controller, in chapter 2, a kinematic relationship between the road shape and sensor measurements was proposed. All measurements were gathered at the vehicle body using only conventional vehicle sensors. Also, through longitudinal and lateral vehicle dynamics, the longitudinal road gradient and the lateral road bank angle were estimated simultaneously. In order to keep nonlinearity of the kinematics and dynamics, a dual-UKF approach was used. The proposed estimation approach was verified on a real vehicle at a special proving ground. After that, we observed that the estimator was able to extract longitudinal road gradient and bank angle simultaneously on public roads in real-time. The main contribution of this research is that a dual-UKF algorithm was suggested to estimate the longitudinal road gradient, the lateral road bank angle, and the vehicle body's roll angle simultaneously using only conventional vehicle sensors. As a result from real vehicle tests on public roads, the estimation error mean of the road bank angle was 0.08 degree.

- Lateral Motion Controller
  In chapter 3, a lane keeping controller associated with the road bank angle estimator was proposed. First, a steady state dynamic model to describe lateral vehicle dynamics over all speed ranges was derived. It was also useful to consider the bank angle effect. Through simulation and real vehicle tests, it was found that the model was reasonable and accurate. The model was also used to derive error dynamics for lateral offset and heading errors for lane keeping and path following situations. From the steady

state dynamic model and error dynamics, a lane keeping controller using the RHSC approach was designed. The control approach was simple to formulate and easy to add constraints to the receding horizon technique based on a system dynamics model. Through simulation, the controller and dynamics models were verified. After that, real vehicle tests were performed on public roads. Simultaneously, road angle estimation results were fed to the lane keeping controller to compensate for the lateral force disturbance effect. The proposed control logic was very good in keeping the vehicle to follow the lane. The main contribution of this research is the derivation of a steady state vehicle dynamics model for lateral vehicular motion to be utilized for a lane keeping controller over all vehicle speed ranges. Furthermore, the model includes road bank angle and tire side-slip effects.

- Longitudinal Disturbance Estimation
  In chapter 4, the front vehicle's future motion was considered as a disturbance term for the longitudinal distance controller. First, a new car-following model was proposed, that was deterministic and parametric, based on a well-tuned ACC system. After that, in order to extract the driver's driving style, a driver aggressivity factor was derived. Using the UKF approach, and comparing measurements with newly updated system states, the aggressivity factor was extracted in real-time. By adopting a base car-following model and an aggressivity factor estimator on the front vehicle, we could propagate the front vehicle's future motion. Also, through real vehicle tests on public roads, the performance of the proposed approach was verified. Therefore, another important contribution of this research is a new car-following model to describe the front vehicle's longitudinal speed control motion with an aggressivity factor estimator.

- Longitudinal Motion Controller
  In chapter 5, a Fuel Efficiency Adaptive Cruise Control as a distance controller associated with the front vehicle's future motion was introduced. First, a basic distance controller was proposed using the Nonlinear MPC approach. And then, in order to improve fuel efficiency, a fuel consumption model was included in the optimization problem. The fuel consumption model was derived from a real vehicle's fuel consumption map. Through basic simulations, the control logic was validated. From the work in chapter 4, a sequence of the front vehicle's future motion was acquired, and used by the distance controller. By considering the future motion in the optimization problem, the fuel efficiency ACC logic improved fuel economy by 3.67% under real traffic data. This was due to the controller making the ego vehicle's velocity profile very smooth to prevent abrupt acceleration and deceleration. Consequently, the approach in this thesis was meaningful for real vehicle implementation. Lastly, simple optimal gear selection logic was suggested. However, the optimal solution could not improve the fuel economy as anticipated. Although the suggested logic does not show good performance for fuel economy, the controller to select fuel optimal gear stage may increase fuel efficiency by adjusting weighting gain under different traffic scenarios. Furthermore, although

the conventional gear selection is not perfect for optimal fuel consumption, it is tuned for power and fuel optimality. A contribution of this research is the derivation and simulation of an algorithm for ACC with a new fuel consumption model.

From this research, disturbances for each longitudinal and lateral vehicle controller were estimated as deterministic values. These values were effectively included in the formulations of controllers and consequently, control performance improved.

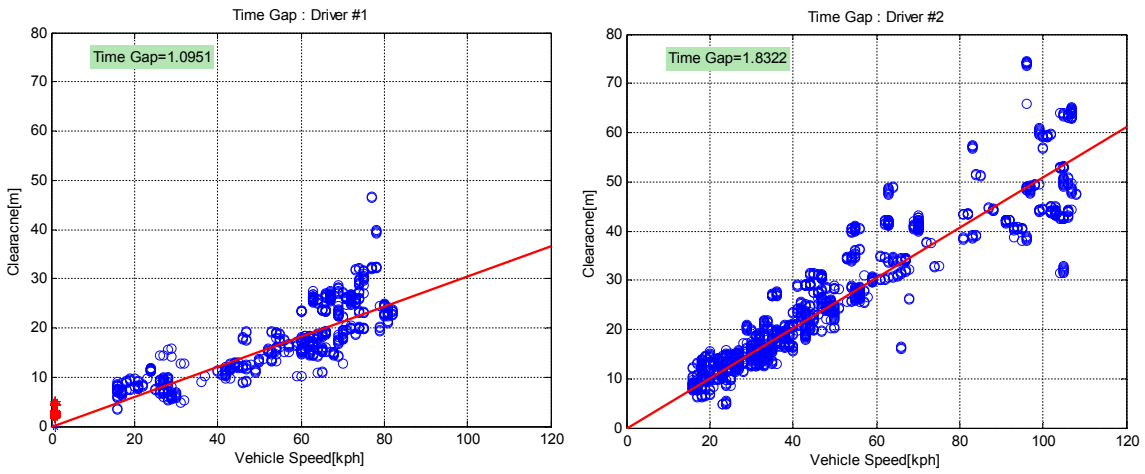

Figure 6.1: Timegap Variation

6.2 Future Work

In this research, some models and approaches were suggested and validated. To prove generality of the results, further work may be needed.

- Car-Following Model
  In chapter 2, a car-following model extracted from a well-tuned ACC system was suggested. It consists of some nonlinear equations. However, we cannot guarantee that the equations alway represent the driver's car following motion. It was only used for suggesting a method to predict the following vehicle's future motion. Therefore, as a future work, we can gather a large data set of different driver's car-following data and extract a representative car-following equation to describe the behavior. It may require significant effort, but it would allow us to derive a more generalized car-following model. In addition to that, in this research, it is assumed that all vehicle drivers have the same timegap tendency in following a front vehicle despite the fact that each vehicle driver has a different timegap. Preliminary research is conducted to verify this assumption. Figure 6.1 shows comparison of timegap of two vehicle drivers. Data was acquired on highways using a radar to detect the clearance to the front vehicle. As shown in the graphs, one driver's timegap is 1.09s and the other's is 1.83s. Therefore, as a future work, a generalized car-following model including timegap tendency should be generated using real vehicle test data.

- Fuel Efficiency Improvement Test
  In chapter 5, a Fuel Efficiency ACC system was proposed. However, the performance was only validated under simulations. Therefore, real vehicle tests under various scenarios may be conducted in the future.

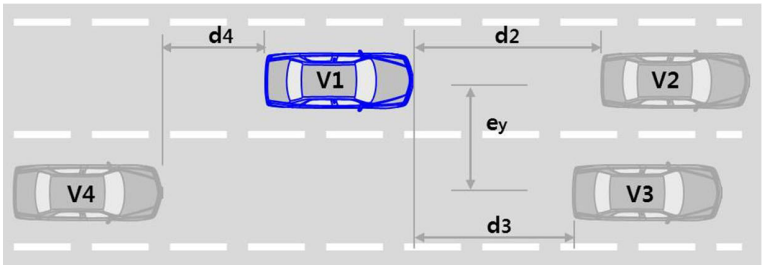

Figure 6.2: Interested Vehicles for Lane Change

- Improving an Automatic Lane Change Algorithm
  An automatic lane change function is an important feature of autonomous vehicles. However, if the controller considers only the current situation of the ego vehicle and surrounding traffic, it is sometimes impossible to make a lane change, although a human driver can. Therefore, if a car-following model is adopted on the surrounding vehicles, we can predict their motions, and the ego vehicle has better chances for lane change maneuver. This can be a further extended topic of disturbance estimation research. As preliminary research, a simple logic is derived to consider lateral offset(e_y) and relative distances(d_2, d_3, d_4) to the surrounding vehicles as shown in Figure 6.2. System state can be defined as follows:

$$x_1 = v_1 \quad : \text{Ego Vehicle Velocity} \tag{6.1}$$
$$x_2 = a_1 \quad : \text{Ego Vehicle Acceleration} \tag{6.2}$$
$$x_3 = j_1 \quad : \text{Ego Vehicle Jerk} \tag{6.3}$$
$$x_4 = d_2 \quad : \text{Distance to V2} \tag{6.4}$$
$$x_5 = v_2 - v_1 \quad : \text{Relative Velocity to V2} \tag{6.5}$$
$$x_6 = d_3 \quad : \text{Distance to V3} \tag{6.6}$$
$$x_7 = v_3 - v_1 \quad : \text{Relative Velocity to V3} \tag{6.7}$$
$$x_8 = d_4 \quad : \text{Distance to V4} \tag{6.8}$$
$$x_9 = v_4 - v_1 \quad : \text{Relative Velocity to V4} \tag{6.9}$$
$$x_{10} = e_y \quad : \text{Distance to the Adjacent Lane Center} \tag{6.10}$$
$$x_{11} = \dot{e}_y \quad : \text{Lateral Velocity} \tag{6.11}$$
$$x_{12} = \ddot{e}_y \quad : \text{Lateral Acceleration} \tag{6.12}$$

Discretized system dynamics can be defined as follows:

$$
\begin{aligned}
x_1(k+1) &= x_1(k) + T_s x_2(k) && (6.13)\\
x_2(k+1) &= (1 - \frac{T_s}{\tau_x})x_2(k) + \frac{T_s}{\tau_x}u_x(k) && (6.14)\\
x_3(k+1) &= -\frac{1}{\tau_x}x_2(k) + \frac{1}{\tau_x}u_x(k) && (6.15)\\
x_4(k+1) &= x_4(k) + T_s x_5(k) - \frac{1}{2}{T_s}^2 x_2(k) + \frac{1}{2}{T_s}^2 a_2(k) && (6.16)\\
x_5(k+1) &= x_5(k) - T_s x_2(k) + T_s a_2(k) && (6.17)\\
x_6(k+1) &= x_6(k) + T_s x_7(k) - \frac{1}{2}{T_s}^2 x_2(k) + \frac{1}{2}{T_s}^2 a_3(k) && (6.18)\\
x_7(k+1) &= x_7(k) - T_s x_2(k) + T_s a_3(k) && (6.19)\\
x_8(k+1) &= x_8(k) + T_s x_9(k) + \frac{1}{2}{T_s}^2 x_2(k) - \frac{1}{2}{T_s}^2 a_4(k) && (6.20)\\
x_9(k+1) &= x_9(k) + T_s x_2(k) - T_s a_4(k) && (6.21)\\
x_{10}(k+1) &= x_{10}(k) + T_s x_{11}(k) + \frac{1}{2}{T_s}^2 x_{12}(k) && (6.22)\\
x_{11}(k+1) &= x_{11}(k) + T_s x_{12}(k) && (6.23)\\
x_{12}(k+1) &= (1 - \frac{T_s}{\tau_y})x_{11}(k) + \frac{1}{\tau_y}u_y(k) && (6.24)
\end{aligned}
$$

If a MPC logic is constructed, acceleration terms of surrounding vehicles(a_2, a_3, a_4) are needed for future state propagation. For example, when as a distance controller associated with the front vehicle's future motion, ego vehicle(V_1) changes lanes, the future acceleration(a_4) of the behind vehicle in as a distance controller associated with the front vehicle's future motion, adjacent lane(V_4) can be predicted using a car-following model on the vehicle.

Bibliography

[1] *Highway Design Manual*. California Department of Transportation, 2006.

[2] H. Peng A. Y. Ungoren and H. E. Tseng. Experimental verificatiion of lateral speed estimation methods. In *Proceedings of AVEC 2002 6th Int.Symp. on Advanced Vehicle Control*, Hiroshima, Japan, 2002.

[3] P. S. addison and D. J. Low. A novel nonlinear car-following model. *Chaos*, 8(4):791–799, 1998.

[4] Behrang Asadi and Ardalan Vahidi. Predictive use of traffic signal state for fuel saving. In *12th IFAC Symposium on Control in Transportation Systems*, 2009.

[5] M. A. Brackstone B. Sultan and M. Macdonald. Drivers' use of deceleration and acceleration information in car-following process. *Transportation Research Record*, (1883):31–39, 2004.

[6] Seung-Hi Lee Chang Mook Kang and Chung Choo Chung. Comparative evaluation of dynamic and kinematic vehicle models. In *53rd IEEE Conference on Decision and Control*, LA, USA, 2014. IEEE.

[7] John Andrews Cunjia Liu, Wen-Hua Chen. Tracking control of small-scale helicopters using explicit nonlinear mpc augmented with disturbance observers. *Control Engineering Practive*, 20:258–268, 2012.

[8] R. Herman D. C. Gazis and R. W. Rothery. Nonlinear follow-the-leader models of traffic flow. In *Operational Research*, 1961.

[9] A. Nishio et al. Development of vehicle stability control system based on vehicle sideslip angle estimation. *SAE*, (2001-01-0137), 2001.

[10] Ashwin Carvalho et al. Predictive control of an autonomous ground vehicle using an iterative linearization approach. In *16th International IEEE Annual Conference on Intelligent Transportation Systems*, Hague, Netherlands, 2013.

[11] Changchun Liu et al. Nonlinear stochastic predictive control with unscented transformation for semi-autonomous vehicles. In *American Control Conference*, Portland, Oregon, USA, 2014.

[12] El-Shaimaa Nada et al. Modified duel unscented kalman filter approach for measuring vehicle states and vehicle parameters. *International Journal of Engineering Research and Technology*, 3(8):1423–1430, 2014.

[13] Erik Hellstrm et al. Look-ahead control for heavy trucks to minimize trip time and fuel consumption. *Control Engineering Practice*, 17(2):245–254, 2008.

[14] Guenther et al. Lateral stiffnes, cornering stiffness and relaxation length of the pneumatic tire. *SAE Technical Paper Series*, (900129), 1990.

[15] H. E. Tseng et al. Development of vehicle stability control at ford. *IEEE/ASME Transactions on Mechatronics*, 4(3):223–234, 1999.

[16] J. Hahn et al. Road bank angle estimation using disturbance observer. In *Proceedings of AVEC 2002 6th Int.Symp. on Advanced Vehicle Control*, Hiroshima, Japan, 2002.

[17] J. Ryu et al. Vehicle sidelsip and roll parameter estimation using gps. In *Proceedings of AVEC 2002 6th Int.Symp. on Advanced Vehicle Control*, Hiroshima, Japan, 2002.

[18] Jihan Ryu et al. Estimation of vehicle roll and road bank angle. In *Proceedings of 2004 American Control Conference*, Boston, USA, 2004.

[19] Norimitsu Ikami et al. Online parameter estimation of driving behavior using probability-weighted arx models. In *14th International IEEE Conference on Intelligent Transportation Systems*, Washington, DC, USA, 2011.

[20] T. A. Wenzel et al. Duel extended kalman filter for vehicle state and parameter estimation. *Vehicle System Dynamics*, 44(2):153–171, 2006.

[21] Valerio et al. Linear model predictive control for lane keeping and obstacle avoidance on low curvature roads. In *16th International IEEE Annual Conference on Intelligent Transportation Systems*, Hague, Netherlands, 2013.

[22] Yiqi Gao et al. A tube-based robust nonlinear predictive control approach to semiautonomous ground vehicles. *Vehicle System Dynamics: International Journal of Vehicle Mechanics and Mobility*, 2014.

[23] Jan P. Huissoon Steven L. Waslander Feyyaz Emre Sancar, Baris Fidan. Mpc based collaborative adaptive cruise control with rear end collision avoidance. In *IEEE Intelligent Vehicles Symposium Proceedings*, Dearborn, Michigan, USA, 2014.

[24] A. Bemporad Francisco Borrelli and M. Morari. *Predictive Control for linear and hybrid systems*. 2014.

[25] Hellstrm E. Frberg, A. and L Nielsen. Explicit fuel optimal speed profiles for heavy trucks on a set of topographic road profiles. *SAE Technical Paper*, (2006-01-1071), 2006.

[26] F. Gunawan. Two-vehicle dynamics of the car-following models on realistic driving condition. *Journal of Transportation Systems Engineering and Information Technology*, 12(2):67–75, 2012.

[27] Andreas Hansen and J. Karl Hedrick. Receding horizon sliding control for linear and nonlinear systems. In *American Control Conference*, Chicago, USA, 2015.

[28] W. Helly. Simulation of bottlenecks in single lane traffic flow. In *Proceedings of the Symposium on Theory of Traffic Flow*, New York, 1959.

[29] Robert Herman and Siamak Ardekani. The influence of stops on vehicle fuel consumption in urban traffic. *Transportation Science*, 19(1), 1985.

[30] R. Hermann and Arthur J. Krener. Nonlinear controllability and observability. *IEEE Transactions on Automatic Control*, 22(5):728, 1977.

[31] Kevin Moran Bart Saerens Hesham Rakha, Kyongho Ahn and Eric Van den Bulck. Simple comprehensive fuel consumption and co2 emission model based on instantaneous vehicle power. In *Transportation Research Board 90th Meeting*, 2011.

[32] Riley G. W. Heydinger, G. J. and J. P. Chrstos. Importance of tire lag on simulated vehicle response. *SAE Technical Paper Series*, (910135), 1991.

[33] H. Kim I. Kim and K. Huh. Development of estimation algorithms for vehicle's mass and road grade. *International Journal of Automotive Technology*, 14(6):889–895, 2013.

[34] M. Innoocenti and M. Falorni. State constrained sliding model controllers. In *American Control Conference*, 1998.

[35] B. G. Cao J. Y. Cao and Z. Liu. Driving resistance estimation based on unknown input observer. *Journal Appl. Sciences*, 6(4):888–891, 2006.

[36] Z. Liu J. Zhou and R. Pei. Sliding mode model predictive control with terminal constraints. In *Proceedings of the 3rd World Congress on Intelligent Control and Automation*, Hefei, China, 2000.

[37] Georg Schildbach Jason Kong, Mark Pfeiffer and Francesco Borrelli. Kinematic and dynamic vehicle models for autonomous driving control design. In *IEEE Intelligent Vehicles Symposium*, Seoul, Korea, 2015. IEEE.

[38] Gianantonio Bortolinb Jiali Fua. Gear shift optimization for off-road construction vehicles. *Social and Behavioral Sciences*, 54, 2012.

[39] Xinghuo Yu Jun Yang, Shihua Li. Sliding model control for systems with mismatched uncertainties via a disturbance observer. *IEEE Transactions on Industrial Electronics*, 60(1):160–169, 2013.

[40] Nicholas J. Kohut. Integrating traffic data and model predictive control to improve fuel economy. *Master's thesis, University of California, Berkeley*, 2009.

[41] Bart De Schutter Lakshmi Dhevi Baskar and Hans Hellendoorn. Model predictive control for intelligent speed adaptation in intelligent vehicle highway systems. In *17th IEEE International Conference on Control Applications, Part of 2008 IEEE Multi-conference on Systems and Control*, San Antonio, Texas, USA, 2008.

[42] Schmied R. Lang, D. and L Del Re. Prediction of preceding driver behavior for fuel efficient cooperative adaptive cruise control. *SAE Int. J. Engines*, 7(1):14–20, 2014.

[43] D. G. Luenberger. An introduction to observers. *IEEE/ASME Transactions on Automatic Control*, 47(12), 1971.

[44] Masakazu Mukai M. A. S. Kamal. Ecological vehicle control on roads with up-down slopes. *IEEE TRANSACTIONS ON INTELLIGENT TRANSPORTATION SYSTEMS*, 12(3):783–794, 2011.

[45] A. Hennecke M. Treiber and D. Helbing. Congested traffic states in empirical observations and microscopic simulations. *Physical Review E*, 62(2):1805–1824, 2000.

[46] Xiaoliang Ma and Magnus Jansson. Model estimation for car-following dynamics based on adaptive filtering approach. In *Proceedings of the 2007 IEEE Intelligent Transportation Systems Conference*, Seattle, WA, USA, 2007.

[47] Mattias Dagen Mark Wielitzka and Tobias Ortmaier. State estimation of vehicle's lateral dynamics using unscented kalman filter. In *53rd IEEE Conference on Decision and Control*, LA, USA, 2014. IEEE.

[48] H. Nijmeijer. Observability of autonomous discrete time non-linear systems: a geometric approach. *International Journal of Control*, 36(5):867, 1982.

[49] U.S. Department of Transportation. *TRAFFIC SAFETY FACTS 2013*.

[50] T. Wakita K. Takeda C. Miyajima P. Angkititrakul, T. Ryuta and T. Suzuki. Evaluation of driver-behavior models in real-world carfollowing task. In *Proc. IEEE International Conference on Vehicular Electronics and Safety*, 2009.

[51] M. Saunders P. Gill, W. Murray and M. Wright. *User's guide for NPSOL (version 4.0)*. Systems Optimization Laboratory, Stanford University, Stanford, CA.

[52] T. Nakatsuji P. Ranjitkar and A. Kawamua. Car-following models: an experiment based benchmarking. *Journal of the Eastern Asia Society for Transportation Studies*, 6:1582–1596, 2005.

[53] S. Panwai and H. Dia. Comparative evaluation of microscopic carfollowing behavior. *IEEE Transactions on Intelligent Transportation Systems*, 6(3):314–325, 2005.

[54] S. Panwai and H. Dia. Neural agent car-following models. *IEEE Transactions on Intelligent Transportation Systems*, 8(1):60–70, 2007.

[55] Rajesh Rajamani. *Vehicle Dynamics and Control*. Springer.

[56] Ilya Kolmanovsky Reza Ghaemi, Jing Sun. Computationally efficient model predictive control with explicit disturbance mitigation and constraint enforcement. In *45th IEEE Conference on Decision & Control*, San Diego, CA, USA, 2006.

[57] J. K. Uhlmann S. J. Julier and H. Durrant-Whyte. A new approach for filtering nonlinear systems. In *American Control Conference*, 1995.

[58] Francesco Borrelli Sanghyun Hong, Chankyu Lee and J. Karl Hedrick. A novel approach for vehicle inertial parameter identification using a dual kalman filter. *IEEE TRANSACTIONS ON INTELLIGENT TRANSPORTATION SYSTEMS*, 16(1):151–161, 2015.

[59] Y. Sebsadji. Vehicle roll and road bank angles estimation. In *Proceedings of the 17th World Congress The International Federation of Automatic Control*, Seoul, Korea, 2008.

[60] Rajesh Rajamani Shengbo Li, Keqiang Li and Jianqiang Wang. Model predictive multi-objective vehicular adaptive cruise control. *IEEE TRANSACTIONS ON CONTROL SYSTEMS TECHNOLOGY*, 19(3):556–566, 2011.

[61] Kanok Boriboonsomsin Sindhura Mandava and Matthew Barth. Arterial velocity planning based on traffic signal information under light traffic conditions. In *Proceedings of the 12th International IEEE Conference on Intelligent Transportation Systems*, 2009.

[62] Jonathan Seth Stichter. Investigation of vehicle and driver aggressivity and relation to fuel economy testing. *Master's thesis, Univerity of Iowa*, 2012.

[63] Ruzena Bajcsy Stphanie Lefvre, Chao Sun and Christian Laugier. Comparison of parametric and non-parametric approaches for vehicle speed prediction. In *American Control Conference*, Portland, Oregon, USA, 2014.

[64] Y. Luo T. Chen and K. Li. Multi-objective adaptive cruise control based on nonlinear model predictive algorithm. In *2011 IEEE International Conference on Vehicular Electronics and Safety (ICVES)*, Beijing, China, 2011.

[65] L. Nielsen U. Kiencke. *Automotive Control Systems for Engine, Driveline, and Vehicle*. Springer.

[66] William L. Garrard Vibhor L. Bageshwar and Rajesh Rajamani. Model predictive control of transitional maneuvers for adaptive cruise control vehicles. *IEEE TRANSACTIONS ON VEHICULAR TECHNOLOGY*, 53(5):1573–1585, 2004.

[67] E. A. Wan and R. Van der Merwe. The unscented kalman filter for nonlinear estimation. In *Adaptive Systems for Signal Processing, Communications, and Control Symposium*. IEEE, 2000.

[68] Jianlong Zhang and Petros A. Ioannou. Longitudinal control of heavy trucks in mixed traffic: Environmental and fuel economy considerations. *IEEE TRANSACTIONS ON INTELLIGENT TRANSPORTATION SYSTEMS*, 7(1):92–104, 2006.